

## ABSTRACT

LICHTY, JAMES D. Model and Tool Development for Studying Alzheimer's Disease in the Organism *C. elegans*. (Under the direction of Dr. Adriana San Miguel Delgadillo)

Alzheimer's Disease (AD) is a neurodegenerative disease which affects a large portion of the world's population. AD is characterized by progressive loss of neurological and motor function, protein deposition and aggregation of amyloid  $\beta$  ( $A\beta$ ) and microtubule-associated protein tau (MAPT), and widespread, neuronal oxidative stress, immune activation, and degeneration. Most AD study in humans must be done post-mortem to prevent danger to the patient, limiting information that can be gained from human studies alone. To that end, we use the model organism *C. elegans*, a microscopic nematode, to act as a host for the *in vivo* study of AD. *C. elegans* has many traits that make it a prime candidate for this purpose: it is transparent, allowing for neuronal imaging without needing to sacrifice the animal, it has a high homology with the human genome, and it shares neuron structure and types with humans. This work focuses on using this animal to study the  $A\beta$  peptide and how it interacts with the organism as whole, to further improve *C. elegans*' usefulness in studying AD. Our multifaceted approach highlights several ways in which *C. elegans* shines as a model for AD, but also raises a few concerns that must be considered when using this organism.

In **Chapter 2**, we attempt to generate a new *C. elegans* strain which expresses  $A\beta$  both intracellularly and extracellularly, to recapitulate an aspect of AD in humans not currently reflected in *C. elegans* models. We use a novel method of  $A\beta$  expression in *C. elegans* using a combination of pan-neuronal promoter, signal peptide, protector sequence to prevent incorrect cleavage of  $A\beta$  during processing, and the C99 fragment of the human amyloid precursor protein (APP), which contains  $A\beta$ . This method takes advantage of the fact that *C. elegans* has a functional  $\gamma$ -secretase, which cleaves  $A\beta$  from C99. While C99 DNA and RNA can be detected

within the strain, A $\beta$ -specific dyes and antibody staining were unsuccessful at A $\beta$  peptide detection. Additionally, the strains tested failed to show significant differences in expected health metrics, determined from existing literature.

In **Chapter 3**, we use existing *C. elegans* strains, which express human A $\beta$  pan-intra-neuronally, to study the interactions of A $\beta$  and environmental stressors. A $\beta$  has been previously shown to have a protective effect against pathogens, but little to no work examines other environmental stressors. We show that A $\beta$  provides selective resistance against specific stressors while lowering resistance to others. A $\beta$  does this in a hormetic-oxidative stress independent manner, activating several genes in the *hsp* family, and initiating a neuropeptide signaling cascade between neurons and other tissues. This effect is unique to A $\beta$ , having a much stronger effect than other control proteins tested.

In **Chapter 4**, we develop an injury device capable of targeted and consistent injury of *C. elegans* neurons to mimic traumatic brain injury (TBI). TBI is one of the biggest risk factors for AD, and it has been extensively associated with increased A $\beta$  production and aggregation in humans, but little is known about how A $\beta$  directly interacts with injury. We iteratively designed the injury device using microfluidics, 3D-printed, and finally a LEGO design that is modular and easy to replicate. Using a fluorescently labelled strain, we show the devices consistently injure head neurons, producing dendritic blebbing and breakage, measured using fluorescent imaging.

In **Chapter 5**, we describe a system for labeling and tracking within an AD drug screen. Drug screens typically require a population of worms to be split into treatment groups, each receiving a unique drug. To track which drug was administered, these treatments need to be kept separate for any subsequent assays and data collection, dramatically increasing labor, time, and resource costs. To help address drug screen challenges, we developed a novel method of labeling

group of worms using a fluorescently labeled *E. coli* food source library. This library would be fed to a population of worms, with each treatment group receiving a different fluorescent tag through colonization of their gut. These treatment groups can then be pooled back together, preventing the need to run an assay for each treatment group individually. The fluorescent tag is then read during data collection using fluorescent techniques to associate each data point with the respective treatment group.

© Copyright 2024 by James D. Lichy

All Rights Reserved

Model and Tool Development for Studying Alzheimer's Disease in the Organism *C. elegans*

by  
James Lichty

A dissertation submitted to the Graduate Faculty of  
North Carolina State University  
in partial fulfillment of the  
requirements for the degree of  
Doctor of Philosophy

Chemical Engineering

Raleigh, North Carolina  
2023

APPROVED BY:

---

Dr. Adriana San Miguel  
Committee Chair

---

Dr. Albert Keung

---

Dr. Nathan Crook

---

Dr. Troy Ghashghaei

## BIOGRAPHY

James Daniel Lichty was born in Waterloo, Iowa, in 1996 to two wonderful parents: Dan and Kristy. As a child, James was an avid reader, fascinated with the fantasy and sci-fi genres. He was especially interested in how those books handled biology and what was possible using science. As he grew up, his tastes for literature and understanding of the world developed and matured, causing him to want to pursue a degree in science, settling on chemical engineering as a good balance between practicality and versatility.

After graduating from high school, James began his studies at Iowa State University, joined by his future husband Brandon Fecht, an avid mathematician. During his sophomore year, he joined the brand-new Mansell Lab in the Chemical and Biological Engineering Department, focusing on studying the pathogen *C. difficile* and its quorum sensing system. Once he had finished his undergraduate work, he accepted an offer to complete a doctoral degree in Chemical and Biomolecular Engineering at North Carolina State University starting in the Fall of 2018. The following spring, he joined Dr. Adriana San Miguel in her lab to study Alzheimer's Disease using the model organism *C. elegans*.

## ACKNOWLEDGEMENTS

I would first like to thank my amazing husband, Brandon Fecht, for his continuous support and for being willing to move so far for me to complete this degree. He has been my rock when it came to dealing with the stress and trials of obtaining this degree. Without him, I would not have made it here today. I would also like to thank my parents, Dan and Kristy, who supported and fostered my love of learning and science, and everything they did for me. I would also like to thank my brothers, Jake and John, and the many other family members cheering me on during the completion of this degree.

I next want to thank my advisor, Dr. Adriana San Miguel, for her keen insights, willingness to support my ideas, even when they didn't work out, and encouragement when I needed it. I would like to thank Sandra Bailey, who always ensures the department runs smoothly. I would like to thank my committee members for their help with the development of this research: Dr. Nathan Crook, Dr. Albert Keung, and Dr. Troy Ghashghaei. I would also like to thank my lab members, both past and present, for their support, camaraderie, and general willingness to collaborate: Dr. Sahand Saberi-Bosari, Dr. Daniel Midkiff, Dr. Javier Huayta, Dr. Andrew Clark, Rita Tejada, Karthik Suresh Arulalan, Zach Kalmanson, Kin Gomez, Victoria Yarmey, Kaleb Decker, Joey Crapster, Sreevansh Mareddy, Sydne Tison, Joshua Currens, Mariam Shah, Daisy Aguilar, Morgan Stephens, Ori Soker, Rodrigo Mayorga, Jaelyn Kenzel, and Noah Torreyson.

## TABLE OF CONTENTS

<b>LIST OF TABLES .....</b>	<b>viii</b>
<b>LIST OF FIGURES .....</b>	<b>ix</b>
<b>CHAPTER 1: Introduction and Motivation.....</b>	<b>1</b>
1.1 Introduction and motivation for studying Alzheimer’s disease .....	1
1.2 <i>C. elegans</i> as a model for Alzheimer’s disease and amyloid $\beta$ .....	2
1.3 Current challenges and limitations with modeling Alzheimer’s disease in <i>C. elegans</i> .....	3
1.4 Dissertation overview and broader impacts .....	5
1.5 References .....	8
<b>CHAPTER 2: Generating an extracellular A<math>\beta</math> expression system for <i>C. elegans</i> .....</b>	<b>15</b>
2.1 Abstract .....	15
2.2 Introduction .....	15
2.3 Results and discussion.....	18
2.3.1 Design considerations for expressing A $\beta$ extracellularly in <i>C. elegans</i> .....	18
2.3.2 PCR and RT-qPCR analysis to detect C99 .....	22
2.3.3 Failure to detect C99 or A $\beta$ peptides .....	23
2.4 Materials and methods .....	28
2.4.1 Strains, media, and culture.....	28
2.4.2 Generation of constructs and transgenic lines .....	28
2.4.3 PCR and RT-qPCR for C99 detection .....	30
2.4.4 X-34 dye staining.....	31
2.4.5 Immunohistochemistry .....	31
2.5 References .....	32

## CHAPTER 3: A $\beta$ induces hormetic-like effects in *C. elegans* models of Alzheimer's Disease

.....	37
3.1 Abstract .....	37
3.2 Introduction .....	37
3.3 Results and discussion.....	40
3.3.1 A $\beta$ induces selective stress resistance in <i>C. elegans</i> .....	40
3.3.2 A $\beta$ -induce stress resistance is dependent on A $\beta$ levels and localization .....	42
3.3.3 Foreign protein expression only partially accounts for increased stress resistance..	44
3.3.4 Antioxidant exposure does not suppress the protective effect of A $\beta$ .....	45
3.3.5 A $\beta$ upregulates several stress response pathways .....	46
3.3.6 A $\beta$ -induced stress resistance requires neuropeptide signaling .....	47
3.3.7 Conclusions.....	51
3.4 Materials and methods .....	53
3.4.1 Strains .....	53
3.4.2 <i>C. elegans</i> growth and maintenance .....	53
3.4.3 <i>C. elegans</i> crossing .....	54
3.4.4 Oxidative stress assay .....	54
3.4.5 Heat stress assay .....	55
3.4.6 Hypoxia assay .....	55
3.4.7 RNA extraction and gene expression profiling.....	55
3.4.8 RNAi plate preparation and suppression assay.....	56
3.4.9 Statistical analysis.....	56
3.5 References .....	57

<b>CHAPTER 4: Mimicking traumatic brain injury in <i>C. elegans</i> using custom made devices</b>	<b>65</b>
4.1 Abstract	65
4.2 Introduction	65
4.3 Results and discussion	67
4.3.1 Manual trauma results in inconsistent injury and difficult to control force	67
4.3.2 Microfluidic trauma device fails to produce sufficient injury	67
4.3.3 3D-Printed and LEGO injury devices induce severe neuronal damage in dopaminergic head neurons	73
4.4 Material and methods	79
4.4.1 Strains, media, and culture	79
4.4.2 Microfluidic device design, assembly, and use	79
4.4.3 3D-printed device design and use	79
4.4.4 LEGO device design and use	80
4.5 References	81
<b>CHAPTER 5: Gutbow: Labeling <i>C. elegans</i> for pooled screens</b>	<b>84</b>
5.1 Abstract	84
5.2 Introduction	85
5.3 Results and discussion	89
5.3.1 Gutbow overview	89
5.3.2 Gutbow Design and Considerations	90
5.4 Materials and methods	99
5.4.1 Strains, media, and culture	99

5.4.2 Library construct design and assembly .....	99
5.4.3 Fluorescent <i>E. coli</i> longevity in the worm gut.....	100
5.5 References .....	101
<b>CHAPTER 6: Conclusions</b> .....	<b>106</b>
6.1 Summary and overview of projects.....	106
6.1.1 Extracellular A $\beta$ expression in <i>C. elegans</i> .....	107
6.1.2 Interactions between A $\beta$ and external stressors .....	110
6.1.3 Devices for mimicking TBI .....	112
6.1.4 Gutbow labeling for drug screens .....	114
6.2 Applications beyond the scope of this dissertation .....	116
6.2.1 Extracellular A $\beta$ expression in <i>C. elegans</i> .....	116
6.2.2 Interactions between A $\beta$ and external stressors .....	117
6.2.3 Devices for mimicking TBI .....	118
6.2.4 Gutbow labeling for drug screens .....	118
6.3 References .....	120

## LIST OF TABLES

Table 2.1	Plasmid constructs generated in this work.....	23
Table 2.2	<i>C. elegans</i> strains generated in this work.....	29
Table 3.1	<i>C. elegans</i> strains used in this work.....	53
Table 5.1	DNA primers used in this work .....	96

## LIST OF FIGURES

- Figure 2.1 Human Amyloidogenic APP and *C. elegans* APL-1 Processing Pathways. A) Human APP is included into the membrane during processing after translation. APP is then sequentially cleaved by a human  $\beta$ -secretase and  $\gamma$ -secretase. This releases the A $\beta$  peptide extracellularly where it forms oligomers, fibrils, and the characteristic aggregates. B) *C. elegans* APL-1 is similarly included into the membrane during post-translational processing. There APL-1 is sequentially cleaved by a worm  $\alpha$ -secretase and  $\gamma$ -secretase to release an A $\beta$ -like peptide, which doesn't fulfill the same roles as A $\beta$ . .....18
- Figure 2.2 Proposed processing pathway utilizing the described method. Human C99 is expressed pan-neuronally and included into the neuronal cell membrane during post-translational processing. There C99 is cleaved by the worm  $\gamma$ -secretase to release A $\beta$  extracellularly, mimicking its expression in humans. ....19
- Figure 2.3 Signal peptide screening and selection process. A pool of candidate proteins was determined using the online GExplore database. The candidate pool was limited to neuronally expressed proteins that are directed to either the cell membrane or extracellular space during processing. Each candidate protein was run through SignalP 5.0 to determine cleavage sites for the protein's signal peptide. Signal peptides that were very large or contained multiple cleavage sites were rejected from the pool for simplicity. Signal peptides from accepted candidates were isolated based on the cleavage site and added to the 5' end of the C99 construct to create a test construct. Each test construct was rerun through SignalP 5.0 to recheck the cleavage sites. A final 15 signal peptide pool was generated from

successful test constructs. The depicted SignalP 5.0 graph is an example output from the software, where the red line corresponds to the signal peptide sequence, the yellow line to the rest of sequence, and the green line to the predicted cleavage sites. ....20

Figure 2.4 Construct design for extracellular A $\beta$  expression. The construct consists of the rab-3 promoter, a signal peptide from the library of 15 signal peptides determined using SignalP 5.0, a two AA protector sequence necessary for prevent A $\beta$  cleavage, the C99 fragment of human APP, and the universal unc-54 3' UTR. ....22

Figure 2.5 PCR and RT-qPCR results from the ASM15 C. elegans strain. A) PCR amplification of the C99 gene from ASM15 lysis. C99 is 300bp. Each lane is a repeat to confirm accuracy. B) Amplification plots from RT-qPCR for C99 mRNA in ASM15 strain. C99 mRNA was consistent across all three samples and had higher amplification when compared to negative controls, indicating successful detection. C) Melt Curve Plot from RT-qPCR for C99 mRNA in ASM15 strain. A detectable peak in the negative controls indicate possible contamination of the samples with genomic DNA. Regardless, each set of peaks represent a different product, as the melt temperatures are different. Green lines indicates negative controls and purple lines indicate C99 mRNA. ....24

Figure 2.6 C. elegans heads stained with the dye X-34. The dotted line indicates head location. A) Wild-type C. elegans showing no clear aggregates. B) ASM15 C. elegans with suspected aggregates indicated with arrows. These aggregates were later confirmed to be indistinguishable from the pharyngeal marker and off-target stained of X-34. It is unclear if the highlighted clumps are A $\beta$  aggregates. ....25

Figure 3.1  $A\beta$  provides selective resistance to severe heat and hypoxic stress, but not paraquat-induced oxidative stress. (A) Overview of experimental setup. Animals were age-synchronized to L4 larvae and then allowed to grow for another 24 hrs. before exposure to stressors. (B) Survival rate after 24 hr. exposure to 50mM paraquat stress. (C) Survival rate after 4 hrs. 37 °C heat stress exposure and overnight recovery at 20 °C. (D) Survival rate after 48 hrs. hypoxia (< 0.1 % O<sub>2</sub>) exposure and overnight recovery. WT is wild-type N2 Bristol,  $A\beta^+$  is JKM2,  $A\beta^-$  is JKM3. N = 9 (12 for hypoxia stress) replicates per strain. Each dot represents a replicate of approx. 30 worms. Statistical analysis was performed using ANOVA. \* is p-value < 0.05, \*\* is p-value < 0.01, \*\*\* is p-value < 0.005.....41

Figure 3.2  $A\beta$ -induced heat stress resistance is dependent on  $A\beta$  expression levels and neuronal localization. (A) Overview of experimental setup. Temperature upshift to 25 °C was staggered such that stress exposure occurred at the same time for each condition. (B) Survival rate after 5.5 hr. 37 °C heat stress exposure and overnight recovery at 20 °C. Time at 25 °C correlates to levels of  $A\beta$  in the neurons in n $A\beta$  strain. (C) Survival rate after 5.5 hr. 37 °C heat stress exposure and overnight recovery at 20 °C. Time at 25 °C correlates to levels of  $A\beta$  in the neurons in n $A\beta$  strain and in muscles in m $A\beta$  strain. WT is wild-type N2 Bristol, n $A\beta$  is CL2355, m $A\beta$  is CL4176. N=9 replicates per condition. Each dot represents a replicate of approx. 30 worms. Statistical analysis was performed using two-sample t-test and two-way ANOVA. \* is p-value < 0.05, \*\* is p-value < 0.01, \*\*\* is p-value < 0.005.....43

Figure 3.3 Heat stress resistance is partially replicated with other neuronally expressed proteins and is not eliminated with NAC treatment. A) Survival rate after 4 hr. 37 °C heat stress exposure and overnight 20 °C recovery in pan-neuronal GFP strain. (B) Survival rate after 4 hr. 37 °C heat stress exposure and overnight recovery in worms grown on control and 5 mM NAC plates for 24 hrs. before heat stress exposure. WT is wild-type N2 Bristol, nGFP is OH438, A $\beta$ <sup>+</sup> is JKM2, A $\beta$ <sup>-</sup> is JKM3. N=9 replicates per condition. Each dot represents a replicate of approx. 30 worms. Statistical analysis was performed using two-sample t-test and two-way ANOVA. \* is p-value < 0.05, \*\* is p-value < 0.01, \*\*\* is p-value < 0.005. ....45

Figure 3.4 Nanostring analysis indicates several resistance genes upregulated in both stressed and unstressed worms and RNAi suppression suggests resistance is communicated through neuropeptide signaling. (A-C) Nanostring analysis on unstressed (A), heat stressed (B), and hypoxic stressed (C) worms. Genes are grouped by type and box color indicates expression changes. 3 biological replicates were pooled per sample. (D) Survival rate after 4 hr. 37 °C heat stress exposure in RNAi suppressed worms. RNAi control was HT115 with empty vector. WT is wild-type N2 Bristol, A $\beta$ <sup>+</sup> is JKM2, A $\beta$ <sup>-</sup> is JKM3, rrf-3(-) is RNAi-sensitive strain NL2099, A $\beta$ <sup>+</sup>rrf-3(-) is ASM35, a cross between JKM2 and NL2099. N=9 replicates per condition. Each dot represents a replicate of approx. 30 worms. Statistical analysis was performed using two-sample t-test and two-way ANOVA. \* is p-value < 0.05, \*\* is p-value < 0.01, \*\*\* is p-value < 0.005. .49

Figure 4.1 Microfluidic device designs for mechanical injury to mimic TBI. Flow channels are cyan, valves are yellow, injury features are maroon, and example worms are

gray. A) Device Y design and layout. Worms enter the device through the loading chamber (LC) and into the injury channel (IC). There they are held in place by the hold valve (HV) and the injury feature valves (IFV) are actuated to injure the worm. This design requires that worms enter the IC tail-first. After injury, the worm is flushed into either outlet channel (OC1 and OC2). The flush channel (FC) is used to move worms through the device. B) Device V design and layout. This device contains a single outlet channel (OC) and pseudo flush channel (pFC). The IFVs are split to allow separate control, eliminating the need for tail-first worms. The HV was lengthened to improve its ability to hold the worm in place. The IC is separated from the pFC by a channel restriction instead of a valve, and this restriction is either square-cut or tapered. C) Device V2 design and layout, similar to Device V with a few changes. Valves on the LC and OC were lengthened to improve flow control. The channel restriction in the IC was replaced with a series of smaller flush channels, to prevent worms from escaping into the pFC and reduce clogging during operation. Shown is the final 10  $\mu\text{m}$  design. ....68

Figure 4.2 3D printed and LEGO Nematine designs and injury. A) wDrop design overview. (Left) Agar pad that was imprinted onto a music record to generate lanes for aligning worms during injury. Each lane is wide enough for 1-2 worms to be aligned in. Worms were paralyzed with 2 mM tetramisole to assist in positioning. (Middle) wDrop base brick, with a slot on top for dropping the coverslip into for injury. Underneath is a slot to position the coverslip containing the agar pad and worms during injury. (Right) Stackable wDrop brick, used to increase height and

thus severity of the injury. B) Guillotine-based 3D-printed Nematine design. The blade and tracks are indicated with arrows. C) Preliminary images collected from BY200 worms with the 3D-printed Nematine. Uninjured worms show little to no defects in the dendrites. Injured worms show significant blebbing (cyan arrows) or complete severing (yellow arrows) of the dendrites. Neuronal cell bodies are indicated with green stars. D) LEGO Nematine design. The blade and tracks are indicated with arrows. E) Preliminary image collected from BY200 worms with the LEGO Nematine. Injured worms show similar blebbing (cyan arrows) injury patterns as worms injured with the 3D-printed Nematine. Neuronal cell bodies are indicated with green stars.....74

Figure 5.1 Proposed Gutbow method for labeling worms during a drug screen. The Gutbow library is combined with a drug library to associate each drug with a specific Gutbow label. This drug-color library is then exposed to worms, allowing for the drug to take effect and for the Gutbow label to colonize the worm gut. These worms can then be combined into a single population for assaying. During or after data collection, the Gutbow label can be reread for each worm to connect the worm's results with the drug treatment it received. ....90

Figure 5.2 Proposed label identification method for Gutbow. Fluorescent readings are collected from each construct in the library for RFP, YFP, GFP, and eBFP. The ratios of each are associated with a randomly assigned label, visualized here using randomized colors. The library is identified by these labels. After assaying and data collection, fluorescent readings are collected for each animal and characterized in a similar manner to identify the label. ....94

## CHAPTER 1: Introduction and Motivation

### 1.1 Introduction and motivation for studying Alzheimer's disease

Alzheimer's Disease (AD) is a neurodegenerative disorder in which patients progressively lose neurological and motor functions typically beginning around age 80. AD affects a large portion of the world's population, either through being directly afflicted or by relationship to those with the disease<sup>1-3</sup>. Rates of AD are predicted to increase in the coming years, foretelling not only a large medical burden on the world's population but also a large financial burden in the form of medical costs and the unpaid labor of family members to care for the patients<sup>1-3</sup>. Thus, AD presents a large risk for the world's future. AD is characterized by immune system activation, oxidative stress, inflammation, neurodegeneration, and accumulation of two proteins, amyloid  $\beta$  ( $A\beta$ ) and microtubule-associated protein tau ( $\tau$ )<sup>1-3</sup>. There is currently no cure for AD, due largely to the amount of unknown information there is regarding the disease. While many genetic mutations have become associated with AD, these only explain cases of familial-AD, which account for approximately 5% of cases<sup>1-3</sup>. For the remaining cases, there isn't a clear, defined cause or causes that can explain them. There are many biological explanations that have been proposed for the disease, the most prominent of which is the amyloid cascade hypothesis<sup>4-11</sup>. This hypothesis proposes that  $A\beta$  triggers a cascade of effects in the brain over time that eventually leads to AD. An opposing hypothesis is the pathogen hypothesis, which connects AD to recurrent infections throughout a person's life that slowly build up damage in the brain, causing AD late in life<sup>4-11</sup>. Other external factors have also been associated with increased rates of AD, especially traumatic brain injury (TBI)<sup>12,13</sup>. AD research is limited by the fact that it is a human disease, and most human studies must be done post-mortem. Thus, powerful and well-characterized models are needed to fully understand the disease.

## 1.2 *C. elegans* as a model for Alzheimer's disease and amyloid $\beta$

*C. elegans* is a microscopic, hermaphroditic, soil-living nematode with a short lifespan of approximately 3 weeks<sup>14-16</sup>. Many of *C. elegans*' characteristics make it an attractive model for studying AD. It shares many neuron subtypes with humans, such as dopaminergic neurons, and is optically transparent, permitting for monitoring of those neurons while the animal is still alive<sup>14-16</sup>. Each animal has the same number of neurons, and in the same positioning and orientation<sup>14-16</sup>. Additionally, *C. elegans* has many orthologs for human genes and proteins, allowing for translation of effects seen in the animal to possible effects in humans<sup>14-16</sup>. There are many useful tools developed for use in *C. elegans* as well that can be used in AD research: RNAi suppression for targeted knock-down of AD-relevant genes, fluorescent labeling, and imaging for assessing neuron health, and calcium imaging for quantifying neuronal activity<sup>17,18</sup>. Additionally, *C. elegans* has many well-established, low-cost protocols for genetic and drug screening, making it a prime candidate for testing AD drugs<sup>16,17,19,20</sup>. The characteristics of *C. elegans* and the variety of specialized tools developed for use with it, along with the low labor and monetary costs of managing large populations of animals make it a great candidate for a model of AD.

There are many *C. elegans* AD models currently in use that have been used extensively for AD research. Models that focus on A $\beta$  are typically one of two varieties: either pan-neuronal or pan-muscular expression of A $\beta$ <sup>21-23</sup>. These models are characterized by several deficits, such as paralysis, neuron loss, mitochondrial dysfunction, decreased lifespan, and increased oxidative stress, many of which are shared with AD in humans<sup>21-28</sup>. Interestingly, A $\beta$  expression has been associated with some positive effects in *C. elegans* as well, specifically that it can protect against pathogens<sup>29</sup>. This matches some theories about how A $\beta$  may act in humans, as there is some evidence based on A $\beta$ 's structure and behavior that it can act as an antimicrobial peptide<sup>29,30</sup>. *C.*

*elegans*' simplicity while still being able to capture all of these AD-relevant characteristics highlights its ability to function as a model for AD.

### **1.3 Current challenges and limitations with modeling Alzheimer's disease in *C. elegans***

While there is much research on A $\beta$  using *C. elegans*, there are still a few key areas that need to be explored. One such area is the localization of A $\beta$  within *C. elegans*. Current models utilizing A $\beta$  in *C. elegans* are limited to intracellular expression of the peptide<sup>21-23</sup>. While intracellular A $\beta$  is relevant for AD, extracellular A $\beta$  is also theorized to play a large role in AD progression<sup>31-35</sup>. Intracellular A $\beta$  in *C. elegans* is associated with several defects such as decreased lifespan, mitochondrial dysfunction, and membrane disruption<sup>21-23</sup>. While these effects are similar to those seen in AD, there are many aspects of AD not replicated in *C. elegans* that could be due to the localization of A $\beta$ . Extracellular A $\beta$  contributes to loss of calcium homeostasis, membrane depolarization, and membrane pore formation<sup>34-36</sup>. Including both intracellular and extracellular A $\beta$  in a *C. elegans* model could improve the model's ability to replicate these aspects of the AD or increase the severity of the effects already seen in current models. Understanding the effects of extracellular A $\beta$  are necessary to generate a clearer picture of AD, and thus needed for *C. elegans* models to reflect the disease more accurately.

Developing AD is heavily associated with several environmental risk factors, such as TBI, chemical exposure, and other stressors<sup>1-3,12,13</sup>. Despite this, there is little research on how environmental stressors impact *C. elegans* AD models. While A $\beta$ 's interaction with pathogens in *C. elegans* has been explored, how A $\beta$  interacts with other environmental stressors is largely unknown. *C. elegans* may not experience some of the stressors humans do, but there are several common worm stressors that could produce similar effects such as heat stress, oxidative stress, or hypoxia. Additionally, fully characterizing how expressing A $\beta$  affects the worm's ability to

respond to different stressors can give insight into different genetic pathways  $A\beta$  is influencing. Due to AD's association with environmental stressors, not characterizing these interactions could lead to possible mistranslation of results when drawing connections between *C. elegans* and humans<sup>13</sup>.

Despite TBI being one of the biggest external predictors of developing AD<sup>1-3,12,13</sup>, there is currently no tool capable of mimicking blunt force trauma in *C. elegans* consistently. While manually inflicting trauma, such as with a pipette tip or similar object, could be used to injure the animals, humans lack the accuracy and control necessary for reproducible results. To produce consistent results, a researcher would need to accurately control the force they apply at a scale less than 1 mm, while also ensuring they injure the same location on each animal. There is a microfluidic device capable of reproducing some effects of TBI, which uses acoustic waves to injure the whole worm<sup>37</sup>. This method has two major drawbacks: it lacks the ability to target specific parts of worm and it doesn't produce an impact such as seen in several TBIs. Additionally, it is unclear if that device can induce neuronal damage markers such as dendrite blebbing and breakage, as only behavioral effects were reported<sup>37</sup>. As TBI is a significant risk factor for AD, a tool capable of reproducing mechanical trauma in *C. elegans* would be invaluable for researching AD.

There is currently no cure or effective treatment for AD<sup>1-3</sup>. To solve this issue there are wide variety of drugs designed and being tested in clinical trials to target different aspects of AD<sup>38</sup>. Despite this, few drugs have shown success in clinical trials for treating AD, regardless of any initial benefits observed during development<sup>38</sup>. Drugs that have been successful are limited in effectiveness to only early-stage AD or to treating the symptoms but not the cause<sup>38</sup>. The high failure rate of these drugs, combined with the typical costs of developing a drug produce a

prohibitively high barrier to creating a successful treatment<sup>1-3,38</sup>. To help reduce costs and determine a drug's initial effectiveness against AD, several researchers use *C. elegans* models of AD. The ability to produce large populations of worms for wide-scope drug screens is an attractive attribute of *C. elegans*. However, costs can remain high, in part due to the inability to distinguish each worm from animals in the same group. To keep track of which drug each worm received, each drug treatment group within a screen must be kept separate during the entire screen, necessitating that an assay for drug effectiveness be repeated for each group<sup>39-43</sup>. Thus, the material, labor, and time costs for an effectiveness assay are multiplied by the number of treatment groups there are, restricting the scope of a screen based on resources available. However, limiting the scope for a screen with a low success rate, such as for AD drugs, significantly reduces the chances of a successful hit. To address this, there are several methods for improving chances in *C. elegans* drug screens, in particular microfluidic devices for increasing throughput during the assay portion<sup>39-43</sup>. While these devices increase throughput by several orders of magnitude through automation when compared to manually assaying for drug effectiveness, treatment groups still need to be kept physically separate from each other. This doesn't solve the central issue, highlighting the need for more methods to reduce the costs associated with drug screens.

#### **1.4 Dissertation overview and broader impacts**

In this work, we sought to address the above-mentioned difficulties associated with utilizing *C. elegans* as a model for AD. Extracellular A $\beta$ , while relevant to AD, has yet to be captured in a worm strain expressing the peptide. In the first project, we developed a method for expressing A $\beta$  extracellularly utilizing a combination of endogenous signal peptide and innate *C. elegans* machinery capable of cleaving human APP. By expressing the C99 fragment of APP

preceded by a neuronal worm signal peptide, we theorized C99 would be included into the neuronal membrane and cleaved by the worm  $\gamma$ -secretase to release A $\beta$  extracellularly. C99 transcription and translation was confirmed by PCR and RT-qPCR, respectively, but neither dye nor antibody staining were successful in producing a detectable signal. Antibody staining is considered the gold-standard for protein detection and visualization, but a literature search confirmed little success for neuronal A $\beta$ . This indicated that there are likely larger issues with A $\beta$  visualization methods in *C. elegans* that need to be addressed before the success of this project can be determined.

To characterize A $\beta$  interactions with environmental stressors, we exposed A $\beta$ -expressing worms to oxidative, heat, and hypoxia stresses. AD worms exhibited a decreased resistance to oxidative stress, but an increased resistance to heat and hypoxia stressors, indicating a possible hormesis-like effect. The stress resistance was dependent on both A $\beta$  levels and localization and was not alleviated by antioxidant exposure. While expression of other foreign proteins mimicked A $\beta$ -induced resistance, they were not able to fully recapitulate the effects. Gene expression analysis indicated the *hsp* family genes as mediators for this resistance. Since stress resistance is typically a cell non-autonomous response, we examined communication between different tissues and determined that neuropeptide signaling is necessary for A $\beta$ -induced stress resistance. This work highlights several previously unexplored interactions in *C. elegans* AD models. While it is not immediately apparent how these interactions may connect to AD in humans, they must be further characterized to prevent mistranslation of results in *C. elegans* models. Additionally, the *hsp* family of genes falls under control of the *C. elegans* *daf-16*, *hsf-1*, *hif-1*, and *skn-1* pathways, the human orthologs of which have been implicated in AD. These interactions may give some insight into how A $\beta$  influences those pathways in humans.

In the third project, we describe a series of devices designed for recreating TBI in *C. elegans*. The first series of designs were microfluidic devices which injured worms through actuation of an injury valve. While these devices simplified animal handling and allowed for precise control of worm position and trauma severity, the device could not withstand pressures necessary to produce an observable injury phenotype. The next set of devices utilized 3D printing to produce a guillotine-based design, the Nematine. The Nematine was capable of consistent and severe injury, exhibited by dendritic blebbing and severing in worms, but was limited by the roughness of 3D printing. The final design replicated the 3D-printed Nematine, but with LEGOs instead, which maintained injury patterns while eliminating flaws. The accessibility of our design's materials and its simplicity make it an easily adaptable tool readily available to *C. elegans* researchers. Additionally, while intended for use with *C. elegans* AD models, the LEGO Nematine can be altered for use with other neurodegenerative diseases.

In the final project, we detail a novel method for labeling groups of worms during a drug assay, Gutbow. Gutbow utilizes a library of fluorescent *E. coli* tags, that are fed to worms to colonize their gut. Each tag can be associated with a different drug treatment group within a screen, allowing for tracking of which treatment each worm received. This allows treatment groups to be pooled during drug effectiveness assays and then identified during data collection. As treatment groups are pooled, fewer replicates of the effectiveness assay are needed, reducing the time, labor, and material costs of the assay. While this method was designed for use with AD drug screens, it can be easily adapted to not only other drug screens, but also other types of screens, such as genetic screens. This greatly increases Gutbow's applications beyond our intended use.

## 1.5 References

- 1) Alzheimer's Association (2020). *2020 Alzheimer's Disease Facts and Figures. On the Front Lines: Primary Care Physicians and Alzheimer's Care in America.*
- 2) *Alzheimer's Disease Fact Sheet* | National Institute on Aging. (n.d.). Retrieved November 23, 2020, from <https://www.nia.nih.gov/health/alzheimers-disease-fact-sheet>
- 3) *What is Alzheimer's Disease?* | CDC. (n.d.). Retrieved November 23, 2020, from <https://www.cdc.gov/aging/aginginfo/alzheimers.htm>
- 4) Pimplikar, S. W. (2009). Reassessing the amyloid cascade hypothesis of Alzheimer's disease. In *International Journal of Biochemistry and Cell Biology* (Vol. 41, Issue 6, pp. 1261–1268). NIH Public Access. <https://doi.org/10.1016/j.biocel.2008.12.015>
- 5) Honjo, K., van Reekum, R., & Verhoeff, N. P. L. G. (2009). Alzheimer's disease and infection: Do infectious agents contribute to progression of Alzheimer's disease? In *Alzheimer's and Dementia* (Vol. 5, Issue 4, pp. 348–360). *Alzheimers Dement.* <https://doi.org/10.1016/j.jalz.2008.12.001>
- 6) Dominy, S. S., Lynch, C., Ermini, F., Benedyk, M., Marczyk, A., Konradi, A., Nguyen, M., Haditsch, U., Raha, D., Griffin, C., Holsinger, L. J., Arastu-Kapur, S., Kaba, S., Lee, A., Ryder, M. I., Potempa, B., Mydel, P., Hellvard, A., Adamowicz, K., ... Potempa, J. (2019). *Porphyromonas gingivalis* in Alzheimer's disease brains: Evidence for disease causation and treatment with small-molecule inhibitors. *Science Advances*, 5(1), eaau3333. <https://doi.org/10.1126/sciadv.aau3333>
- 7) Holmes, C., El-Okl, M., Williams, A. L., Cunningham, C., Wilcockson, D., & Perry, V. H. (2003). Systemic infection, interleukin 1 $\beta$ , and cognitive decline in Alzheimer's disease.

*Journal of Neurology Neurosurgery and Psychiatry*, 74(6), 788–789.

<https://doi.org/10.1136/jnnp.74.6.788>

- 8) Eimer, W. A., Vijaya Kumar, D. K., Navalpur Shanmugam, N. K., Rodriguez, A. S., Mitchell, T., Washicosky, K. J., György, B., Breakefield, X. O., Tanzi, R. E., & Moir, R. D. (2018). Alzheimer's Disease-Associated  $\beta$ -Amyloid Is Rapidly Seeded by Herpesviridae to Protect against Brain Infection. *Neuron*, 99(1), 56-63.e3.  
<https://doi.org/10.1016/j.neuron.2018.06.030>
- 9) Maheshwari, P., & Eslick, G. D. (2015). Bacterial infection and Alzheimer's disease: A meta-analysis. *Journal of Alzheimer's Disease*, 43(3), 957–966.  
<https://doi.org/10.3233/JAD-140621>
- 10) Fulop, T., Witkowski, J. M., Bourgade, K., Khalil, A., Zerif, E., Larbi, A., Hirokawa, K., Pawelec, G., Bocti, C., Lacombe, G., Dupuis, G., & Frost, E. H. (2018). Can an Infection Hypothesis Explain the Beta Amyloid Hypothesis of Alzheimer's Disease? *Frontiers in Aging Neuroscience*, 10. <https://doi.org/10.3389/fnagi.2018.00224>
- 11) Lim, S. L., Rodriguez-Ortiz, C. J., & Kitazawa, M. (2015). Infection, systemic inflammation, and Alzheimer's disease. In *Microbes and Infection* (Vol. 17, Issue 8, pp. 549–556). Elsevier Masson SAS. <https://doi.org/10.1016/j.micinf.2015.04.004>
- 12) Ramos-Cejudo J, Wisniewski T, Marmar C, Zetterberg H, Blennow K, de Leon MJ, Fossati S. Traumatic Brain Injury and Alzheimer's Disease: The Cerebrovascular Link. *EBioMedicine*. 2018 Feb;28:21-30. doi: 10.1016/j.ebiom.2018.01.021. Epub 2018 Jan 31. PMID: 29396300; PMCID: PMC5835563.
- 13) Elonheimo HM, Andersen HR, Katsonouri A, Tolonen H. Environmental Substances Associated with Alzheimer's Disease—A Scoping Review. *International Journal of*

*Environmental Research and Public Health*. 2021; 18(22):11839.

<https://doi.org/10.3390/ijerph182211839>

- 14) Corsi, A. K., Wightman, B. & Chalfie, M. A transparent window into biology: A primer on *Caenorhabditis elegans*. *Genetics* 200, 387–407 (2015).
- 15) Kim, W., Underwood, R. S., Greenwald, I., & Shaye, D. D. (2018). Ortholist 2: A new comparative genomic analysis of human and *caenorhabditis elegans* genes. *Genetics*, 210(2), 445–461. <https://doi.org/10.1534/genetics.118.301307>
- 16) Hodgkin J. Introduction to genetics and genomics (September 6, 2005), *WormBook*, ed. The *C. elegans* Research Community, WormBook, doi/10.1895/wormbook.1.17.1, <http://www.wormbook.org>.
- 17) Zugasti, O., Thakur, N., Belougne, J., Squiban, B., Kurz, C. L., Soulé, J., Omi, S., Tichit, L., Pujol, N., & Ewbank, J. J. (2016). A quantitative genome-wide RNAi screen in *C. elegans* for antifungal innate immunity genes. *BMC Biology*, 14(1). <https://doi.org/10.1186/s12915-016-0256-3>
- 18) Kerr, R.A. Imaging the activity of neurons and muscles (June 2, 2006), *WormBook*, ed. The *C. elegans* Research Community, WormBook, doi/10.1895/wormbook.1.113.1, <http://www.wormbook.org>.
- 19) Artal-Sanz, M., de Jong, L., & Tavernarakis, N. (2006). *Caenorhabditis elegans*: A versatile platform for drug discovery. In *Biotechnology Journal* (Vol. 1, Issue 12, pp. 1405–1418). *Biotechnol J*. <https://doi.org/10.1002/biot.200600176>
- 20) Ewbank, J. J., & Zugasti, O. (2011). *C. elegans*: Model host and tool for antimicrobial drug discovery. In *DMM Disease Models and Mechanisms* (Vol. 4, Issue 3, pp. 300–304). The Company of Biologists Ltd. <https://doi.org/10.1242/dmm.006684>

- 21) Wu, Y.; Wu, Z.; Butko, P.; Christen, Y.; Lambert, M. P.; Klein, W. L.; Link, C. D.; Luo, Y., Amyloid-beta-induced pathological behaviors are suppressed by Ginkgo biloba extract EGb 761 and ginkgolides in transgenic *Caenorhabditis elegans*. *J Neurosci* 2006, 26 (50), 13102–13.
- 22) Link, C. D. (1995). Expression of human  $\beta$ -amyloid peptide in transgenic *Caenorhabditis elegans*. *Proceedings of the National Academy of Sciences of the United States of America*, 92(20), 9368–9372. <https://doi.org/10.1073/pnas.92.20.9368>
- 23) Gallrein, C., Iburg, M., Michelberger, T., Kocak, A., Puchkov, D., Liu, F., Mariscal, S., Nayak, T., Schierle, G., Kirstein, J. (2021). Novel amyloid-beta pathology *C. elegans* model reveals distinct neurons as seeds of pathogenicity. *Progress in Neurobiology*, 198. <https://doi.org/10.1016/j.pneurobio.2020.101907>.
- 24) Fong, S., Teo, E., Ng, L. F., Chen, C. B., Lakshmanan, L. N., Tsoi, S. Y., Moore, P. K., Inoue, T., Halliwell, B., & Gruber, J. (2016). Energy crisis precedes global metabolic failure in a novel *Caenorhabditis elegans* Alzheimer Disease model. *Scientific Reports*, 6(1), 1–9. <https://doi.org/10.1038/srep33781>
- 25) Guha, S., Fischer, S., Johnson, G. V., & Nehrke, K. (2020). Alzheimer’s disease-relevant tau modifications selectively impact neurodegeneration and mitophagy in a novel *C. elegans* single-copy transgenic model. *BioRxiv*, 2020.02.12.946004. <https://doi.org/10.1101/2020.02.12.946004>
- 26) Dimitriadi, M., & Hart, A. C. (2010). Neurodegenerative disorders: Insights from the nematode *Caenorhabditis elegans*. In *Neurobiology of Disease* (Vol. 40, Issue 1, pp. 4–11). NIH Public Access. <https://doi.org/10.1016/j.nbd.2010.05.012>

- 27) Teo, E., Ravi, S., Barardo, D., Kim, H. S., Fong, S., Gassiot, A. C., Tan, T. Y., Ching, J., Kovalik, J. P., Wenk, M. R., Gunawan, R., Moore, P. K., Halliwell, B., Tolwinski, N., & Gruber, J. (2019). Metabolic stress is a primary pathogenic event in transgenic *Caenorhabditis elegans* expressing pan-neuronal human amyloid beta. *ELife*, 8. <https://doi.org/10.7554/eLife.50069>
- 28) Treusch, S., Hamamichi, S., Goodman, J. L., Matlack, K. E. S., Chung, C. Y., Baru, V., Shulman, J. M., Parrado, A., Bevis, B. J., Valastyan, J. S., Han, H., Lindhagen-Persson, M., Reiman, E. M., Evans, D. A., Bennett, D. A., Olofsson, A., DeJager, P. L., Tanzi, R. E., Caldwell, K. A., ... Lindquist, S. (2011). Functional links between A $\beta$  toxicity, endocytic trafficking, and Alzheimer's disease risk factors in yeast. *Science*, 334(6060), 1241–1245. <https://doi.org/10.1126/science.1213210>
- 29) Deepak Kumar Vijaya Kumar et al., Amyloid- $\beta$  peptide protects against microbial infection in mouse and worm models of Alzheimer's disease. *Sci. Transl. Med.* 8, 340ra72-340ra72 (2016). DOI: 10.1126/scitranslmed.aaf1059
- 30) Pastore, A., Raimondi, F., Rajendran, L. et al. Why does the A $\beta$  peptide of Alzheimer share structural similarity with antimicrobial peptides?. *Commun Biol* 3, 135 (2020). <https://doi.org/10.1038/s42003-020-0865-9>
- 31) Hartmann, T. (1999). Intracellular biology of Alzheimer's disease amyloid beta peptide. In *European Archives of Psychiatry and Clinical Neuroscience* (Vol. 249, Issue 6, pp. 291–298). Springer Verlag. <https://doi.org/10.1007/s004060050102>
- 32) Ferreira, I. L., Bajouco, L. M., Mota, S. I., Auberson, Y. P., Oliveira, C. R., & Rego, A. C. (2012). Amyloid beta peptide 1-42 disturbs intracellular calcium homeostasis through

- activation of GluN2B-containing N-methyl-d-aspartate receptors in cortical cultures. *Cell Calcium*, 51(2), 95–106. <https://doi.org/10.1016/j.ceca.2011.11.008>
- 33) Bayer, T. A., & Wirths, O. (2010). Intracellular accumulation of amyloid-beta - A predictor for synaptic dysfunction and neuron loss in Alzheimer's disease. *Frontiers in Aging Neuroscience*, 2(MAR). <https://doi.org/10.3389/fnagi.2010.00008>
- 34) Renner, M., Lacor, P. N., Velasco, P. T., Xu, J., Contractor, A., Klein, W. L., & Triller, A. (2010). Deleterious Effects of Amyloid  $\beta$  Oligomers Acting as an Extracellular Scaffold for mGluR5. *Neuron*, 66(5), 739–754. <https://doi.org/10.1016/j.neuron.2010.04.029>
- 35) Townsend, M., Shankar, G. M., Mehta, T., Walsh, D. M., & Selkoe, D. J. (2006). Effects of secreted oligomers of amyloid  $\beta$ -protein on hippocampal synaptic plasticity: A potent role for trimers. *Journal of Physiology*, 572(2), 477–492. <https://doi.org/10.1113/jphysiol.2005.103754>
- 36) Rajasekhar, K., Chakrabarti, M., & Govindaraju, T. (2015). Function and toxicity of amyloid beta and recent therapeutic interventions targeting amyloid beta in Alzheimer's disease. In *Chemical Communications* (Vol. 51, Issue 70, pp. 13434–13450). Royal Society of Chemistry. <https://doi.org/10.1039/c5cc05264e>
- 37) Miansari, M., Mehta, M.D., Schilling, J.M. *et al.* Inducing Mild Traumatic Brain Injury in *C. elegans* via Cavitation-Free Surface Acoustic Wave-Driven Ultrasonic Irradiation. *Sci Rep* 9, 12775 (2019). <https://doi.org/10.1038/s41598-019-47295-1>
- 38) Huang LK, Kuan YC, Lin HW, Hu CJ. Clinical trials of new drugs for Alzheimer disease: a 2020-2023 update. *J Biomed Sci.* 2023 Oct 2;30(1):83. doi: 10.1186/s12929-023-00976-6. PMID: 37784171; PMCID: PMC10544555.

- 39) Mondal, S., Hegarty, E., Martin, C. *et al.* Large-scale microfluidics providing high-resolution and high-throughput screening of *Caenorhabditis elegans* poly-glutamine aggregation model. *Nat Commun* **7**, 13023 (2016). <https://doi.org/10.1038/ncomms13023>
- 40) Chung, K., Crane, M. M. & Lu, H. Automated on-chip rapid microscopy, phenotyping and sorting of *C. elegans*. *Nat. Methods* **5**, 637–643 (2008).  
<https://doi.org/10.1038/nmeth.1227>
- 41) Hulme, S. E., Shevkoplyas, S. S., Apfeld, J., Fontana, W. & Whitesides, G. M. A microfabricated array of clamps for immobilizing and imaging *C. elegans*. *Lab. Chip* **7**, 1515–1523 (2007). <https://doi.org/10.1039/B707861G>
- 42) Lee, H, Kim S, Coakley S, Mugno P, Hammarlund M, Hilliard M, Lu H. A multi-channel device for high-density target-selective stimulation and long-term monitoring of cells and subcellular features in *C. elegans*. *Lab on a Chip*. 2014;23.  
<https://doi.org/10.1039/C4LC00789A>
- 43) Caceres Ide, C., Valmas, N., Hilliard, M. A. & Lu, H. Laterally orienting *C. elegans* using geometry at microscale for high-throughput visual screens in neurodegeneration and neuronal development studies. *PloS ONE* **7**, e35037 (2012).  
<https://doi.org/10.1371/journal.pone.0035037>

## **CHAPTER 2: Generating an extracellular A $\beta$ expression system for *C. elegans***

### **2.1 Abstract**

While current amyloid  $\beta$  (A $\beta$ ) expressing *C. elegans* models can mimic several aspects of Alzheimer's disease, one key characteristic that has yet to be generated is extracellular expression of A $\beta$ . In this chapter, we describe a novel method for attempting to achieve this. Using endogenous components of the homologous *C. elegans* A $\beta$ -like processing pathway, we attempt to generate a strain capable of expressing human A $\beta$  extracellularly. We express the C99 fragment of the human amyloid precursor protein (APP), preceded by a signaling peptide and protector peptide sequence under a pan-neuronal *C. elegans* promoter. By detecting the C99 DNA and RNA with PCR and RT-qPCR respectively, we show that our strain both incorporated the construct into an extrachromosomal array and can transcribe C99 off that array. Neither dye nor antibody staining were able to detect A $\beta$  within the animals though, suggesting either an issue with those staining methods for detecting A $\beta$  or a more complex trafficking issue than our method could solve.

### **2.2 Introduction**

A $\beta$  localization in neurons, whether intracellular or extracellular, has a profound impact on the effects it causes to those neurons<sup>1-6</sup>. Intracellular A $\beta$  has been connected to mitochondrial dysfunction, synaptic dysfunction and loss, disruption of telomere maintenance, and loss of calcium homeostasis<sup>1-4</sup>. Alternatively, while extracellular A $\beta$  is also associated with loss of calcium homeostasis, it additionally contributes to membrane depolarization, membrane pore formation, and immune activation<sup>4-6</sup>. The effects of both localizations vary significantly, thus highlighting a need for animal models to be able to replicate both. Current models utilizing A $\beta$  in *C. elegans* lack the ability to generate extracellular A $\beta$ , possibly leaving a blind spot in AD

research<sup>7-9</sup>. Previous attempts at generating a strain capable of producing extracellular A $\beta$  are theorized to have failed due to rerouting of the A $\beta$  peptide during processing (Christopher Link, Personal Communication, June 2020), despite using an artificially designed signal peptide meant for extracellular expression<sup>8</sup>. C. Link theorized that this rerouting may be due to either the size of the signal peptide-A $\beta$  construct<sup>8</sup> or that it was recognized as a foreign protein by *C. elegans* (Christopher Link, Personal Communication, June 2020), and thus rerouted to remain intracellular for sequestration, breakdown, and disposal. While some strains have shown that A $\beta$  can migrate from neurons to surrounding tissues, this only occurred later in life and in conjunction with significant damage to the neuronal membrane<sup>9</sup>. Gallrein C., et al. theorized that A $\beta$  causes this damage to the cell membrane, which allows for leaking into the surrounding tissue<sup>9</sup>. Thus, a strain designed to express A $\beta$  extracellularly early in life must attempt to address these challenges.

In humans, A $\beta$  is produced through a multistep process beginning with the APP<sup>10-12</sup> (Fig 2.1A). APP is expressed in neurons, where it is processed through the endoplasmic reticulum and golgi apparatus before being released in a vesicle that is integrated into the cell membrane<sup>10-12</sup>. APP is oriented such that the N-terminus is in the extracellular space and the C-terminus is in the cytoplasm<sup>10-12</sup>. There are two pathways through which APP can be further processed: amyloidogenic and non-amyloidogenic. The pathway is determined by which enzyme cleaves APP first. Cleavage by the  $\alpha$ -secretase protein initiates the non-amyloidogenic pathway, as the enzyme cleaves APP within the A $\beta$  residue<sup>10-12</sup>. The  $\beta$ -secretase instead cleaves APP such that the 99 amino acid C99 fragment containing A $\beta$  remains membrane bound, and the N-terminus of APP is released extracellularly<sup>10-12</sup>. C99 is then cleaved by the  $\gamma$ -secretase to release A $\beta$  extracellularly. From there A $\beta$  self-assembles and aggregates to form the characteristic

extracellular oligomers and aggregates seen in AD<sup>10-12</sup>. Accumulation of intracellular A $\beta$  is theorized to come from two sources: amyloidogenic APP cleavage not localized to the cell membrane and reuptake of A $\beta$  after its release from membrane bound APP<sup>1-3</sup>. It is currently unclear how APP cleavage would occur when not membrane bound, indicating that A $\beta$  reuptake is the more likely culprit. Regardless, both intracellular and extracellular A $\beta$  play integral roles in AD progression<sup>1-6</sup>.

*C. elegans* contains an APL-1 processing pathway, homologous to the human APP pathway with a few key differences<sup>13-16</sup> (Fig 2.1B). APL-1 processing occurs much in the same way as APP processing in humans. APL-1 is integrated into the membrane and sequentially cleaved by a worm  $\alpha$ -secretase followed by a worm  $\gamma$ -secretase, much like APP and the  $\beta$ - and  $\gamma$ -secretases. The first difference is that *C. elegans* lacks its own A $\beta$  peptide as the APL-1 sequence does not contain an equivalent peptide that gets cleaved and released during processing that behaves like A $\beta$ . Additionally, *C. elegans* doesn't have a  $\beta$ -secretase, although it does have the worm  $\alpha$ - and  $\gamma$ -secretases<sup>13-16</sup>. Link, C. observed that the *C. elegans*  $\gamma$ -secretase was able to cleave human APP at the correct residue but failed to see any  $\beta$ -secretase activity in the organism (Christopher Link, Personal Communication, June 2020).

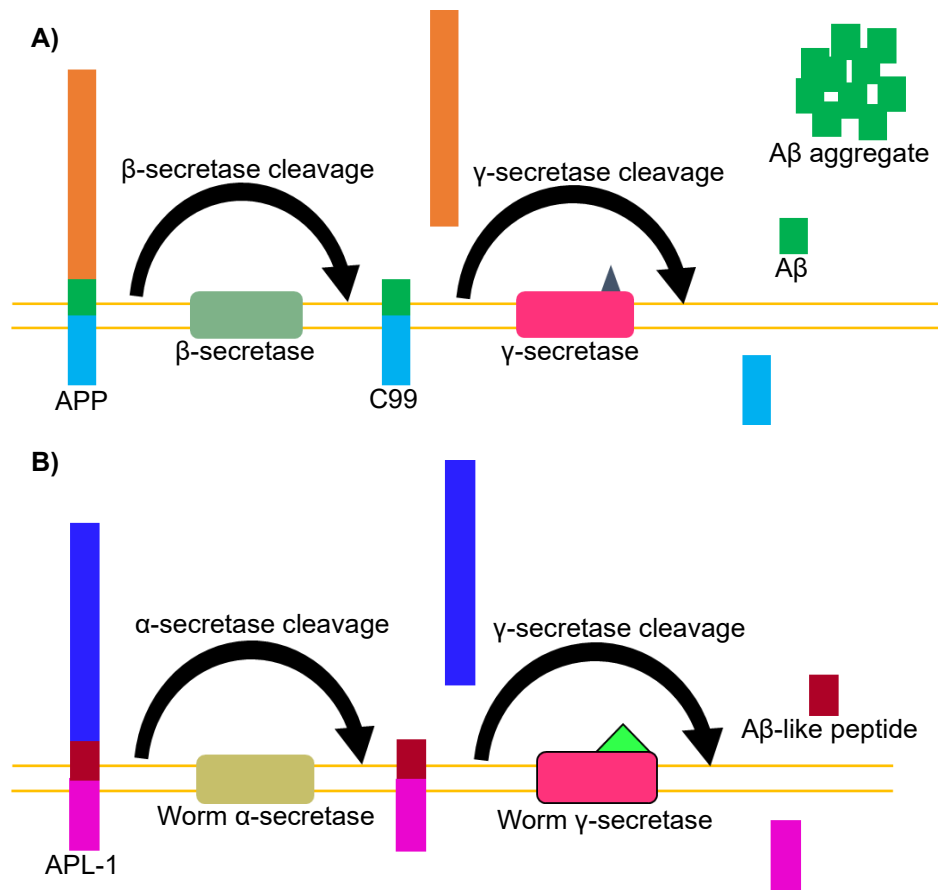


**Figure 2.1: Human Amyloidogenic APP and *C. elegans* APL-1 Processing Pathways.** A) Human APP is included into the membrane during processing after translation. APP is then sequentially cleaved by a human  $\beta$ -secretase and  $\gamma$ -secretase. This releases the A $\beta$  peptide extracellularly where it forms oligomers, fibrils, and the characteristic aggregates. B) *C. elegans* APL-1 is similarly included into the membrane during post-translational processing. There APL-1 is sequentially cleaved by a worm  $\alpha$ -secretase and  $\gamma$ -secretase to release an A $\beta$ -like peptide, which doesn't fulfill the same roles as A $\beta$ .

## 2.3 Results and Discussion

### 2.3.1 Design considerations for expressing A $\beta$ extracellularly in *C. elegans*

To address the main two problems with previous attempts at extracellular expression of A $\beta$ , we designed a construct meant to handle them separately. Firstly, for the issue of A $\beta$  size during processing, instead of expressing just the A $\beta$  peptide, we expressed the entire C99 human fragment. We theorized that, while *C. elegans* doesn't have  $\beta$ -secretase activity, its  $\gamma$ -secretase activity should be sufficient to release A $\beta$  from C99. Additionally, C99 contains the full

transmembrane domain from APP, improving its chances at successful inclusion into the cell membrane during processing. After inclusion into the membrane, C99 would be cleaved by the worm  $\gamma$ -secretase, like its processing in humans, to release A $\beta$  extracellularly. And since C99 cleavage doesn't occur until after inclusion in the neuron membrane, the theorized redirection based on A $\beta$  size should be prevented. This would protect our construct from the first of the theorized problems.

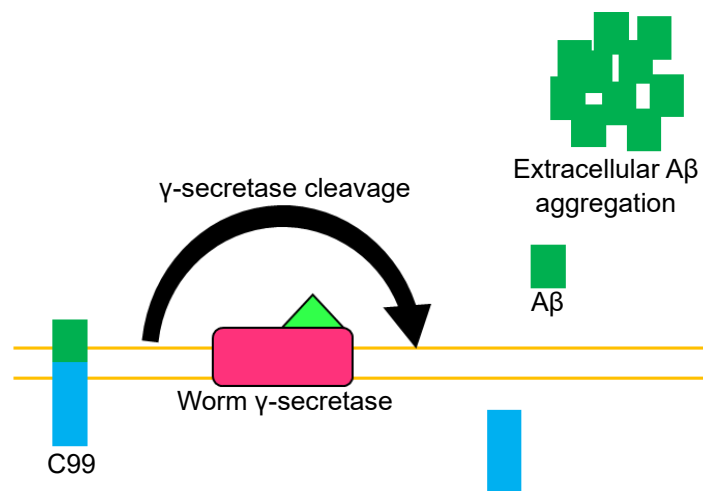


**Figure 2.2:** Proposed processing pathway utilizing the described method. Human C99 is expressed pan-neuronally and included into the neuronal cell membrane during post-translational processing. There C99 is cleaved by the worm  $\gamma$ -secretase to release A $\beta$  extracellularly, mimicking its expression in humans.

For the second theorized problem, recognition as a foreign protein, we decided to use a different signal peptide. Previous attempts at expressing A $\beta$  extracellularly have used artificial signal peptides to direct A $\beta$ <sup>8</sup>, which were designed for extracellular expression in *C. elegans* but were not taken from *C. elegans* proteins. We hypothesized that using an endogenous signal peptide would help to disguise C99 from the host cell, improving its chances of integrating into the membrane. To direct C99 to the membrane, we used an endogenous *C. elegans* signal peptide selected from a library of 15 we extracted from proteins that are directed to either the membrane or extracellular space of neurons during their processing (Fig 2.3). The signal peptides were

taken directly from *C. elegans* proteins using the online database GExplore<sup>17</sup>. Signal peptide candidates were extracted from target proteins using SignalP 5.0, an online resource for the prediction of signal peptide cleavage sites<sup>18</sup>. SignalP 5.0 utilizes a neural network trained on known signal peptide sequences to predict all eukaryotic cleavage sites within a fed sequence and estimates the likelihood of cleavage at each residue. We fed candidate protein sequences to SignalP 5.0 to first filter for signal peptides with only one cleavage site and that were small enough to be easily inserted into our construct, ideally less than 100bp. This size restriction was

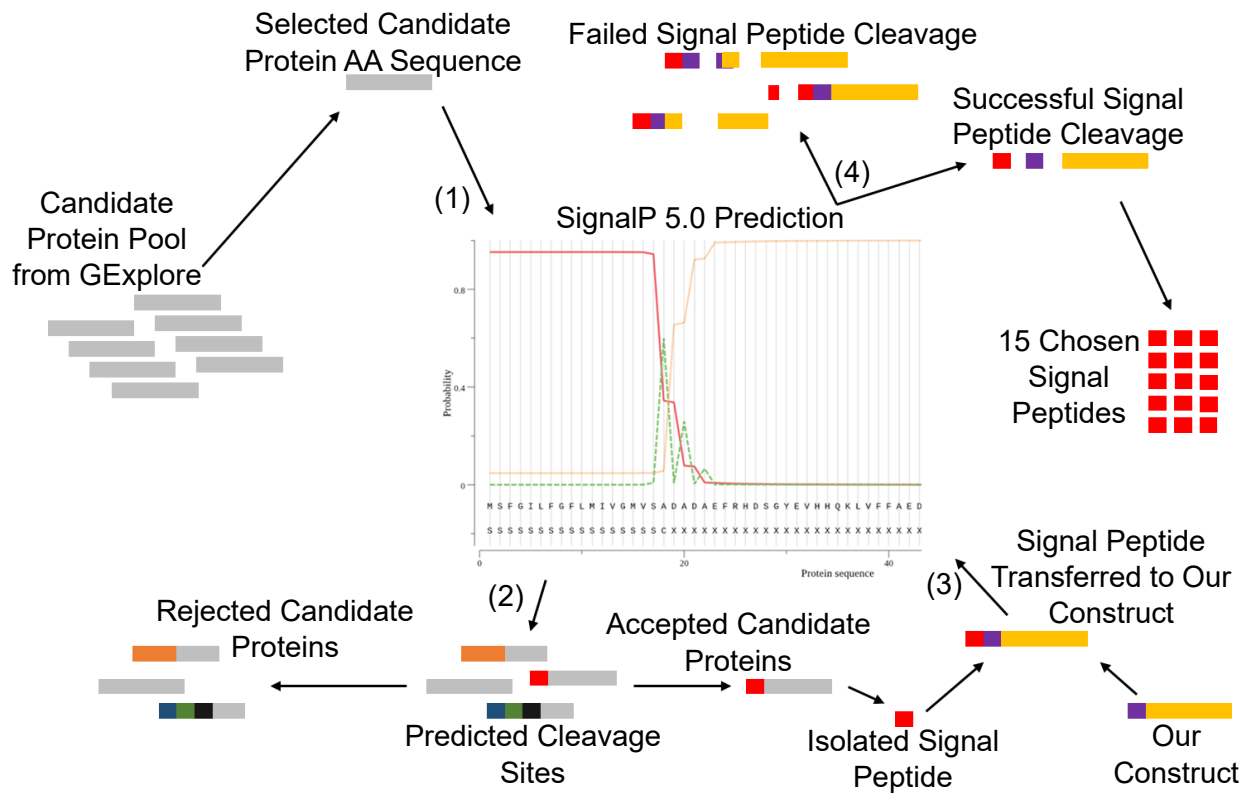


**Figure 2.3:** Signal peptide screening and selection process. A pool of candidate proteins was determined using the online GExplore database. The candidate pool was limited to neuronally expressed proteins that are directed to either the cell membrane or extracellular space during processing. Each candidate protein was run through SignalP 5.0 to determine cleavage sites for the protein’s signal peptide. Signal peptides that were very large or contained multiple cleavage sites were rejected from the pool for simplicity. Signal peptides from accepted candidates were isolated based on the cleavage site and added to the 5’ end of the C99 construct to create a test construct. Each test construct was rerun through SignalP 5.0 to recheck the cleavage sites. A final 15 signal peptide pool was generated from successful test constructs. The depicted SignalP 5.0 graph is an example output from the software, where the red line corresponds to the signal peptide sequence, the yellow line to the rest of sequence, and the green line to the predicted cleavage sites.

put into place to simplify generating the final plasmid constructs. By limiting the signal peptide size to 100bp, each signal peptide could be inserted into a backbone construct, containing each other piece necessary for C99 expression, using site-directed mutagenesis. This process was simpler than generating 15 individual constructs, saving both time and labor, and reducing the chances for errors. Once a signal peptide passed that step, we isolated it from the candidate protein and put it on the N-terminus of our construct and reran it through SignalP 5.0. If the signal peptide-construct combination was successfully cleaved in SignalP 5.0, we kept it for our library, which resulted in 15 successful hits.

In addition to these two considerations, we also decided to use the *rab-3* promoter because it has been well established for pan-neuronal expression in *C. elegans* and the *unc-54* 3'UTR as a universal 3'UTR<sup>19,20</sup>. Lastly, McColl et al. showed that many of the current *C. elegans* models actually express A $\beta$  with the first two amino acids cleaved off (A $\beta$ <sub>3-42</sub>)<sup>21</sup>. This form of A $\beta$  is less toxic and thus represents a problem when trying to mimic AD. We included in our construct a two amino acid protector sequence, designed to protect against this erroneous cleavage and ensure that full-length A $\beta$  was expressed<sup>21</sup>. The complete construct was the *rab-3p:SignalPeptide:ProtectorPeptide:C99:unc-54* 3'UTR (Fig 2.4A, Table 2.1). A plasmid without the signal and protector peptides was also constructed to act as a control. Initially, the control plasmid was microinjected with an mCherry pharyngeal marker to generate ASM16, but during preliminary testing with that strain, mCherry interfered with A $\beta$  visualization, requiring a replacement marker<sup>22-23</sup>. Instead, each of the 16 constructs were microinjected into *C. elegans* along with a hybrid roller and hygromycin, chosen as it can self-excise upon temperature upshift, resulting in strains ASM17-32<sup>22-24</sup> (Table 2.1). Utilizing a self-excising cassette allows for



**Figure 2.4:** Construct design for extracellular A $\beta$  expression. The construct consists of the *rab-3* promoter, a signal peptide from the library of 15 signal peptides determined using SignalP 5.0, a two AA protector sequence necessary for prevent A $\beta$  cleavage, the C99 fragment of human APP, and the universal *unc-54* 3' UTR.

insertion of a marker to confirm the success of microinjection and then removal of that marker before experiments to prevent interference.

### 2.3.2 PCR and RT-qPCR analysis to detect C99

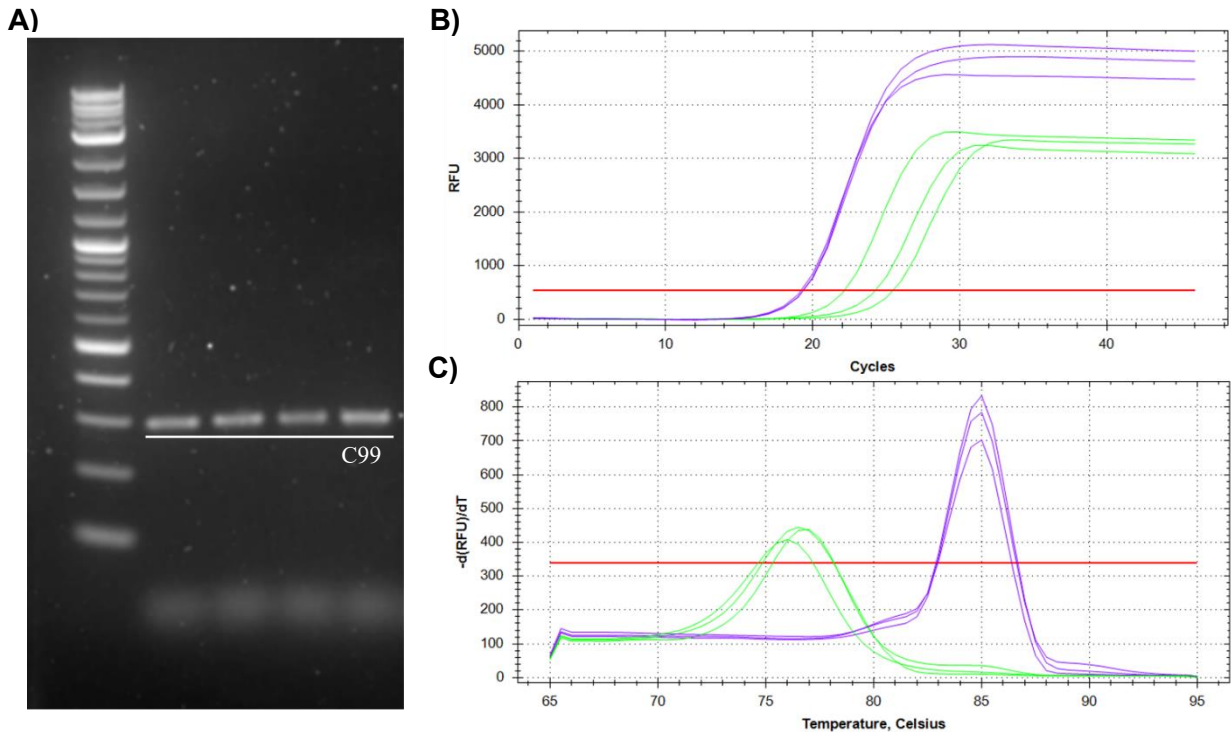
To confirm that each construct had successfully been integrated into an extrachromosomal array, PCR was used to extract and amplify C99 DNA. Rather than test all 16 strains at once, we narrowed our initial scope to just ASM15, as it contained the *apl-1* signal peptide, which we theorized had the best chance of mimicking A $\beta$  expression. Apl-1 is the homolog to human APP, and thus would have the closest expression pattern to human APP of the chosen proteins<sup>13-16</sup>. In the PCR electrophoresis gel, the C99 specific primers produced a band at approximately 300bp. The C99 DNA fragment used to generate the extrachromosomal array was also approximately 300bp, indicating that C99 DNA had been successfully inserted (Fig. 2.5A). We next sought to confirm that C99 was being transcribed from the extrachromosomal array using RT-qPCR. By looking at C99 mRNA, we confirmed that our construct was successfully transcribed (Fig 2.5B). This was further supported by a singular peak on the melt curve, showing a single product in our sample (Fig 2.5C). With these two assays, we successfully showed the C99 was incorporated into the strain and was being transcribed.

Table 2.1. Plasmid constructs generated in this work

Name	Genotype
JDLSP1	<i>Prab-3_ida-1</i> -SP_ArtificialSP_C99_ <i>unc-54-3'</i> UTR
JDLSP2	<i>Prab-3_nlp-11</i> -SP_ArtificialSP_C99_ <i>unc-54-3'</i> UTR
JDLSP3	<i>Prab-3_nlg-1e</i> -SP_ArtificialSP_C99_ <i>unc-54-3'</i> UTR
JDLSP4	<i>Prab-3_glr-4a</i> -SP_ArtificialSP_C99_ <i>unc-54-3'</i> UTR
JDLSP5	<i>Prab-3_crm-1b</i> -SP_ArtificialSP_C99_ <i>unc-54-3'</i> UTR
JDLSP6	<i>Prab-3_lat-1a</i> -SP_ArtificialSP_C99_ <i>unc-54-3'</i> UTR
JDLSP7	<i>Prab-3_old-1</i> -SP_ArtificialSP_C99_ <i>unc-54-3'</i> UTR
JDLSP8	<i>Prab-3_dyf-7</i> -SP_ArtificialSP_C99_ <i>unc-54-3'</i> UTR
JDLSP9	<i>Prab-3_aff-1</i> -SP_ArtificialSP_C99_ <i>unc-54-3'</i> UTR
JDLSP10	<i>Prab-3_hot-7</i> -SP_ArtificialSP_C99_ <i>unc-54-3'</i> UTR
JDLSP11	<i>Prab-3_apl-1a</i> -SP_ArtificialSP_C99_ <i>unc-54-3'</i> UTR
JDLSP12	<i>Prab-3_des-2b</i> -SP_ArtificialSP_C99_ <i>unc-54-3'</i> UTR
JDLSP13	<i>Prab-3_fmi-1a</i> -SP_ArtificialSP_C99_ <i>unc-54-3'</i> UTR
JDLSP14	<i>Prab-3_tol-1</i> -SP_ArtificialSP_C99_ <i>unc-54-3'</i> UTR
JDLSP15	<i>Prab-3_deg-3</i> -SP_ArtificialSP_C99_ <i>unc-54-3'</i> UTR
JDLSP0	<i>Prab-3_C99_ unc-54-3'</i> UTR

### 2.3.3 Failure to detect C99 or A $\beta$ peptides

In order to verify the translation of the C99 sequence into protein and cleavage of C99, we first stained the ASM15 strain with the A $\beta$ -specific dye, 1,4-bis(3-carboxy-4-hydroxyphenylethenyl)-benzene (X-34). X-34 selectively binds A $\beta$  fibrils and aggregates<sup>25,26</sup>. We



**Figure 2.5:** PCR and RT-qPCR results from the ASM15 *C. elegans* strain. A) PCR amplification of the C99 gene from ASM15 lysis. C99 is 300bp. Each lane is a repeat to confirm accuracy. B) Amplification plots from RT-qPCR for C99 mRNA in ASM15 strain. C99 mRNA was consistent across all three samples and had higher amplification when compared to negative controls, indicating successful detection. C) Melt Curve Plot from RT-qPCR for C99 mRNA in ASM15 strain. A detectable peak in the negative controls indicate possible contamination of the samples with genomic DNA. Regardless, each set of peaks represent a different product, as the melt temperatures are different. Green lines indicate negative controls and purple lines indicate C99 mRNA.

theorized that if  $A\beta$  is being successfully cleaved from C99, it should form its characteristic fibrils and aggregates. Therefore, if X-34 staining indicates aggregates, C99 translation and cleavage are verified. Our initial assay showed promising results, with  $A\beta$  aggregates appearing around the pharynx, where the highest concentration of neurons is in the worm (Fig 2.6). Unfortunately, after imaging unstained ASM15, we realized that we could not reliably differentiate between mCherry in the pharynx and any stained  $A\beta$ , as mCherry and X-34 have significant overlap in their spectra<sup>23,25,26</sup>. Moreover, there appeared to be X-34 staining outside of the head in both AD and non-AD worms, despite the lack of  $A\beta$ , calling into question the specificity of X-34. Additionally, there was significant variability in the observed fluorescence

levels, likely due to mosaicism with the extrachromosomal array<sup>27</sup>. Mosaicism occurs due to the extrachromosomal array not transmitting to every cell during animal development, resulting in only a fraction of the animal's cells containing the array<sup>27</sup>. Typically, integration into the genome can address this problem, but can also prove to be a time intensive process which didn't seem worth pursuing if C99 translation and cleavage had yet to be confirmed.

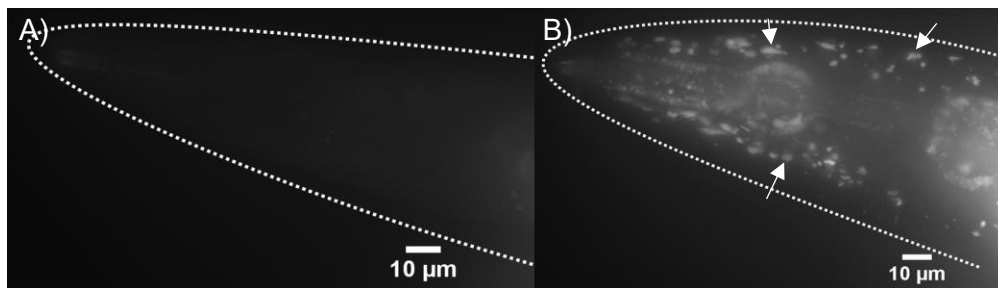


**Figure 2.6:** *C. elegans* heads stained with the dye X-34. The dotted line indicates head location. A) Wild-type *C. elegans* showing no clear aggregates. B) ASM15 *C. elegans* with suspected aggregates indicated with arrows. These aggregates were later confirmed to be indistinguishable from the pharyngeal marker and off-target stained of X-34. It is unclear if the highlighted clumps are A $\beta$  aggregates.

To solve the issue regarding the X-34 dye, we alternated to antibody staining with an antibody that had significantly less overlap with the mCherry pharyngeal marker. Additionally, antibodies could be chosen to target any form of A $\beta$  rather than just fibrils and aggregates. We also changed the co-injection marker to the hybrid roller-hygromycin marker mentioned above, eliminating concerns with spectral overlap. To test the effectiveness of the alternative staining method, day 1 adults were stained using an anti-A $\beta$  primary antibody targeting the 17-24 residue, followed by a secondary antibody targeting the primary antibody and conjugated with Texas Red. The primary antibody was selected for its ability to bind both C99 and A $\beta$  in any form if the 17-24 residue of A $\beta$  was intact. A primary and secondary antibody were used to produce a stronger signal, as this would likely detect even low levels of C99 translation. To improve the penetration of the antibody into the animal's tissues, two attempts were made using freeze-crack and

collagenase methods for disrupting the cuticle<sup>28</sup>. Despite this, antibody staining failed to detect any A $\beta$  or C99, suggesting that there was a problem with either the staining method, or with the expression method for C99. Additionally, we repeated this experiment with a control that expresses A $\beta$  pan-neuronally but only intracellularly. This intracellular-A $\beta$  control experiment also failed to detect any A $\beta$ , indicating that the issue was likely in the staining method. We hypothesized three possible errors, in order of likelihood, that could be causing this problem:

1. Antibody staining failed, as our control failed to show A $\beta$  and there aren't many examples of successful detection of neuronal A $\beta$  in *C. elegans* literature using dyes or antibody staining.
2. Antibody staining is working, but A $\beta$  levels are below the resolution threshold of antibody staining. This is possible, as while there's little evidence for antibody staining to detect neuronal A $\beta$  in *C. elegans* literature, there is evidence that Elisa and Western Blot assays can<sup>7-8</sup>. These assays analyze concentrated protein from the whole animal or multiple animals, whereas antibody staining relies on detection of diffuse protein spread throughout a single animal.
3. A $\beta$  isn't being produced at all, due to an error in the expression method, either in the translation of mRNA to protein, the localization of C99 to the membrane, or in the cleavage of C99 to release A $\beta$ .

In addition to testing for the presence of C99 and A $\beta$ , we ran preliminary assays for detrimental health effects in our strain. We examined lifespan, brood size, and behavioral patterns for any differences from wild-type worms. These preliminary assays were chosen as A $\beta$  expression has been associated with changes in these health metrics in *C. elegans*<sup>8-9</sup>. Animals expressing C99 seemed to exhibit a slight grouping phenotype, characterized by animals

remaining in the edge of the bacterial food lawn and avoiding the center of the lawn. Despite this, no quantifiable difference was observed between the C99 expressing strain and wild-type worms. The grouping phenotype was too inconsistent and minor to properly quantify. This indicated that although there may have been issues with antibody staining, C99 production and cleavage into A $\beta$  may not be occurring as well. It was expected that if C99 was properly translated and cleaved to produce A $\beta$ , a detrimental phenotype would exist. The lack of a phenotype suggests that either A $\beta$  is not being produced, or if it is, it does not induce any detrimental effects. Although an Elisa or Western Blot assay could have confirmed C99 translation and cleavage, antibody staining, or similar visualization method, is necessary to confirm project success, as determining the location of A $\beta$  within the organism is necessary for determining intracellular versus extracellular localization. If A $\beta$  remained intracellular or its reuptake rate by the cell was greater than its export rate, then our model wouldn't recapitulate that aspect of AD. Due to lack of successful antibody staining and no appreciable change of health metrics, it is likely that this method for C99 expression and cleavage to produce extracellular A $\beta$  was unsuccessful. Although unclear at which step in this process the error occurs, it is likely during or after translation, as C99 DNA and RNA are detectable. While endogenous signal peptides were used to direct the peptide to the cell membrane, it possible that these were not sufficient for redirecting a foreign protein; increasing the scope to include signal peptides from proteins other than the 15 chosen may possibly improve success. Additionally, although C99 contains the transmembrane domain of APP, it is unclear if full length APP is necessary for membrane inclusion. An alternative method of expressing full length APP with an edited  $\beta$ -secretase site may prove more successful, if that  $\beta$ -secretase site were changed to allow cleavage by another *C. elegans* enzyme. Though, selection of an appropriate cleavage site

alternative would require careful consideration, as cleavage of an altered APP would compete with endogenous targets of the chosen enzyme. Utilizing unaltered human APP would require introducing  $\beta$ -secretase activity into the worms. This would generate new enzymatic activity in *C. elegans* neurons, as there is currently no equivalent protein, which could produce unforeseen effects. These effects could also convolute detrimental effects from extracellular A $\beta$ , interfering with results. While these alternatives to our method exist and could be tested, without a successful method for visualization of neuronal A $\beta$ , their success could not be determined. A $\beta$  staining and visualization in *C. elegans* is an area of research which needs much improvement as several of the current methods lack the ability and consistency required to be reliably applied in studying AD.

## **2.4 Materials and Methods**

### **2.4.1 Strains, media, and culture**

*C. elegans* was maintained on standard Nematode Growth Medium (NGM) plates seeded with OP50 *E. coli* bacteria and kept at 20 °C unless otherwise stated<sup>29</sup>. Age-synchronization for experiments was performed by washing plates with a 1 mL of a solution of M9 media supplemented with 0.01% v/v TX-100 (M9TX). Worms were allowed to settle, and supernatant was removed and replaced with 1 mL of 1:2:1 mixture of bleach, 1M NaOH, and water. Once eggs were released, they were washed 3 times with 1 mL M9TX, and transferred to fresh plates.

### **2.4.2 Generation of constructs and transgenic lines**

The base plasmid construct, pGH8-C99 was assembled using Gibson assembly (NEB #M5510). The pGH8 plasmid containing pRab-3 and the *unc-54* 3'UTR was used as the backbone<sup>30</sup>. pGH8-pRAB-3::mCherry::unc-54utr was a gift from Erik Jorgensen (Addgene plasmid # 19359 ; <http://n2t.net/addgene:19359> ; RRID:Addgene\_19359) The C99 fragment of

APP was amplified from pCAX-APP-C99<sup>31</sup>. pCAX-APP-C99 was a gift from Dennis Selkoe & Tracy Young-Pearse (Addgene plasmid # 30146 ; <http://n2t.net/addgene:30146> ; RRID:Addgene\_30146). These were then amplified again with primers designed to add homology regions necessary for Gibson assembly. To generate each of the signal peptide constructs, primers were designed containing the signal and protector peptide sequences. These primers were used in site-directed mutagenesis (NEB #E0554S) to insert into the pGH8-C99 plasmid, generating the remaining constructs (Table 2.2). Successful insertion of the peptide sequences was confirmed by Sanger sequencing. The pGH8-C99 construct was inserted into an extrachromosomal array along with the pharyngeal mCherry co-injection marker using standard microinjection procedures<sup>22-23</sup>. Once each construct was confirmed, they were inserted into an extrachromosomal array along with the dual roller-hygromycin co-injection marker using standard microinjection procedures into the Bristol N2 wild-type strain<sup>22-24</sup>. This generated the 17 strains used in this work (Table 2.1). Successful injection was confirmed using fluorescent microscopy looking for the co-injection marker.

Table 2.2. *C. elegans* strains generated in this work

Name	Genotype
ASM16	delEx3[ <i>myo-2p::mCherry</i> + <i>rab-3p::C99</i> ]
ASM17	delEx5[ <i>rab-3p::apl-1aSP::C99</i> + GFP::SEC::3xFlag]
ASM18	delEx6[ <i>rab-3p::hot-7SP::C99</i> + GFP::SEC::3xFlag]
ASM19	delEx7[ <i>rab-3p::C99</i> + GFP::SEC::3xFlag]
ASM20	delEx8[ <i>rab-3p::nlp-11SP::C99</i> + GFP::SEC::3xFlag]
ASM21	delEx9[ <i>rab-3p::nlg-1eSP::C99</i> + GFP::SEC::3xFlag]
ASM22	delEx10[ <i>rab-3p::dyf-7SP::C99</i> + GFP::SEC::3xFlag]
ASM23	delEx11[ <i>rab-3p::old-1SP::C99</i> + GFP::SEC::3xFlag]

Table 2.2 (continued)

ASM24	delEx12[ <i>rab-3p::lat-1aSP::C99 + GFP::SEC::3xFlag</i> ]
ASM25	delEx13[ <i>rab-3p::ida-1SP::C99 + GFP::SEC::3xFlag</i> ]
ASM26	delEx14[ <i>rab-3p::tol-1SP::C99 + GFP::SEC::3xFlag</i> ]
ASM27	delEx15[ <i>rab-3p::des-2bSP::C99 + GFP::SEC::3xFlag</i> ]
ASM28	delEx16[ <i>rab-3p::deg-3SP::C99 + GFP::SEC::3xFlag</i> ]
ASM29	delEx17[ <i>rab-3p::crm-1bSP::C99 + GFP::SEC::3xFlag</i> ]
ASM31	delEx18[ <i>rab-3p::fmi-1aSP::C99 + GFP::SEC::3xFlag</i> ]
ASM32	delEx19[ <i>rab-3p::glr-4aSP::C99 + GFP::SEC::3xFlag</i> ]

### 2.4.3 PCR and RT-qPCR for C99 detection

C99 presence in the ASM15 strain was confirmed using PCR (NEB #E0555S). DNA was extracted from worms by picking several of them into a solution of 100 µg/mL Proteinase K in worm lysis buffer (50 mM KCl, 10 mM Tris pH 8.3, 2.5 mM MgCl<sub>2</sub>, 0.45% NP-40, and 0.45% Tween-20). This was exposed to -80 °C for 10 min. followed by 65 °C for 60 min. and 95 °C for 15 min. This solution was used directly for PCR without further modification.

For RT-qPCR, worms were first age-synchronized by bleaching and cultured to adulthood at 20 °C. Worms were then washed from plates and rinsed several times with M9TX. RNA was extracted using the Direct-zol RNA Miniprep extraction kit (Cat# R2051). During the Tri Reagent step, a motorized pestle was used for 1 min to help break the worm cuticle. RNA from this was directly used in the Luna Universal One-Step RT-qPCR kit (NEB #E3005S) at a concentration of 50 ng/µL.

#### **2.4.4 X-34 Dye Staining**

For X-34 dye staining, worms were first age-synchronized by bleaching and cultured to adulthood at 20 °C. Worms were then stained according to the protocol from Link et al.<sup>24</sup> and imaged using fluorescent microscopy.

#### **2.4.5 Immunohistochemistry**

For immunohistochemistry, worms were first age-synchronized by bleaching and cultured to adulthood at 20 °C. Immunohistochemistry was then performed per standard protocols<sup>30</sup> and imaged using fluorescent microscopy. Antibodies used were an anti-A $\beta$  mouse primary antibody targeting the 17-24 residue of A $\beta$  (VWR 76302-456) and an anti-mouse donkey secondary antibody conjugated with Texas Red (VWR RL610-709-002).

## 2.5 References

1. Hartmann, T. (1999). Intracellular biology of Alzheimer's disease amyloid beta peptide. In *European Archives of Psychiatry and Clinical Neuroscience* (Vol. 249, Issue 6, pp. 291–298). Springer Verlag. <https://doi.org/10.1007/s004060050102>
2. Ferreira, I. L., Bajouco, L. M., Mota, S. I., Auberson, Y. P., Oliveira, C. R., & Rego, A. C. (2012). Amyloid beta peptide 1-42 disturbs intracellular calcium homeostasis through activation of GluN2B-containing N-methyl-d-aspartate receptors in cortical cultures. *Cell Calcium*, 51(2), 95–106. <https://doi.org/10.1016/j.ceca.2011.11.008>
3. Bayer, T. A., & Wirths, O. (2010). Intracellular accumulation of amyloid-beta - A predictor for synaptic dysfunction and neuron loss in Alzheimer's disease. *Frontiers in Aging Neuroscience*, 2(MAR). <https://doi.org/10.3389/fnagi.2010.00008>
4. Rajasekhar, K., Chakrabarti, M., & Govindaraju, T. (2015). Function and toxicity of amyloid beta and recent therapeutic interventions targeting amyloid beta in Alzheimer's disease. In *Chemical Communications* (Vol. 51, Issue 70, pp. 13434–13450). Royal Society of Chemistry. <https://doi.org/10.1039/c5cc05264e>
5. Renner, M., Lacor, P. N., Velasco, P. T., Xu, J., Contractor, A., Klein, W. L., & Triller, A. (2010). Deleterious Effects of Amyloid  $\beta$  Oligomers Acting as an Extracellular Scaffold for mGluR5. *Neuron*, 66(5), 739–754. <https://doi.org/10.1016/j.neuron.2010.04.029>
6. Townsend, M., Shankar, G. M., Mehta, T., Walsh, D. M., & Selkoe, D. J. (2006). Effects of secreted oligomers of amyloid  $\beta$ -protein on hippocampal synaptic plasticity: A potent role for trimers. *Journal of Physiology*, 572(2), 477–492. <https://doi.org/10.1113/jphysiol.2005.103754>

7. Wu, Y.; Wu, Z.; Butko, P.; Christen, Y.; Lambert, M. P.; Klein, W. L.; Link, C. D.; Luo, Y., Amyloid-beta-induced pathological behaviors are suppressed by Ginkgo biloba extract EGb 761 and ginkgolides in transgenic *Caenorhabditis elegans*. *J Neurosci* 2006, 26 (50), 13102–13.
8. Link, C. D. (1995). Expression of human  $\beta$ -amyloid peptide in transgenic *Caenorhabditis elegans*. *Proceedings of the National Academy of Sciences of the United States of America*, 92(20), 9368–9372. <https://doi.org/10.1073/pnas.92.20.9368>
9. Gallrein, C., Iburg, M., Michelberger, T., Kocak, A., Puchkov, D., Liu, F., Mariscal, S., Nayak, T., Schierle, G., Kirstein, J. (2021). Novel amyloid-beta pathology *C. elegans* model reveals distinct neurons as seeds of pathogenicity. *Progress in Neurobiology*, 198. <https://doi.org/10.1016/j.pneurobio.2020.101907>.
10. Shoji, M., Golde, T. E., Ghiso, J., Cheung, T. T., Estus, S., Shaffer, L. M., Cai, X. D., McKay, D. M., Tintner, R., Frangione, B., & Younkin, S. G. (1992). Production of the Alzheimer amyloid  $\beta$  protein by normal proteolytic processing. *Science*, 258(5079), 126–129. <https://doi.org/10.1126/science.1439760>
11. Vardy, E. R. L. C., Catto, A. J., & Hooper, N. M. (2005). Proteolytic mechanisms in amyloid- $\beta$  metabolism: Therapeutic implications for Alzheimer's disease. In *Trends in Molecular Medicine* (Vol. 11, Issue 10, pp. 464–472). Elsevier. <https://doi.org/10.1016/j.molmed.2005.08.004>
12. Storey, E., & Cappai, R. (1999). The amyloid precursor protein of Alzheimer's disease and the A $\beta$  peptide. In *Neuropathology and Applied Neurobiology* (Vol. 25, Issue 2, pp. 81–97). *Neuropathol Appl Neurobiol*. <https://doi.org/10.1046/j.1365-2990.1999.00164.x>

13. Link, C. D., Taft, A., Kapulkin, V., Duke, K., Kim, S., Fei, Q., Wood, D. E., & Sahagan, B. G. (2003). Gene expression analysis in a transgenic *Caenorhabditis elegans* Alzheimer's disease model. *Neurobiology of Aging*, 24(3), 397–413.  
[https://doi.org/10.1016/S0197-4580\(02\)00224-5](https://doi.org/10.1016/S0197-4580(02)00224-5)
14. Wiese, M., Antebi, A., & Zheng, H. (2010). Intracellular Trafficking and Synaptic Function of APL-1 in *Caenorhabditis elegans*. *PLoS ONE*, 5(9), e12790.  
<https://doi.org/10.1371/journal.pone.0012790>
15. Daigle, I., & Li, C. (1993). *apl-1*, a *Caenorhabditis elegans* gene encoding a protein related to the human  $\beta$ -amyloid protein precursor. *Proceedings of the National Academy of Sciences of the United States of America*, 90(24), 12045–12049.  
<https://doi.org/10.1073/pnas.90.24.12045>
16. Link, C. D. (2006). *C. elegans* models of age-associated neurodegenerative diseases: Lessons from transgenic worm models of Alzheimer's disease. *Experimental Gerontology*, 41(10), 1007–1013. <https://doi.org/10.1016/j.exger.2006.06.059>
17. Hutter H, Ng MP, Chen N. GExplore: a web server for integrated queries of protein domains, gene expression and mutant phenotypes. *BMC Genomics*. 2009 Nov 16;10:529.
18. SignalP 5.0 improves signal peptide predictions using deep neural networks. José Juan Almagro Armenteros, Konstantinos D. Tsirigos, Casper Kaae Sønderby, Thomas Nordahl Petersen, Ole Winther, Søren Brunak, Gunnar von Heijne and Henrik Nielsen. *Nature Biotechnology*, 37, 420-423, doi:10.1038/s41587-019-0036-z (2019)
19. Wormbase. *Rab-3*. [https://wormbase.org/species/c\\_elegans/gene/WBGene00004267#0-9f-10](https://wormbase.org/species/c_elegans/gene/WBGene00004267#0-9f-10)

20. Merritt, C., et al. Transgenic solutions for the germline (February 8, 2010), *WormBook*, ed. The *C. elegans* Research Community, WormBook, doi/10.1895/wormbook.1.148.1, <http://www.wormbook.org>.
21. Mccoll, G., Roberts, B. R., Pukala, T. L., Kenche, V. B., Roberts, C. M., Link, C. D., Ryan, T. M., Masters, C. L., Barnham, K. J., Bush, A. I., & Cherny, R. A. (2012). Utility of an improved model of amyloid-beta (A $\beta$ 1-42) toxicity in *Caenorhabditis elegans* for drug screening for Alzheimer's disease. *Molecular Neurodegeneration*, 7(1), 57. <https://doi.org/10.1186/1750-1326-7-57>
22. Single-copy insertion of transgenes in *Caenorhabditis elegans*. Christian Frøkjær-Jensen, M Wayne Davis, Christopher E Hopkins, Blake J Newman, Jason M Thumme, Søren-Peter Olesen, Morten Grunnet & Erik M Jorgensen. 10.1038/ng.248 [PubMed 18953339](https://pubmed.ncbi.nlm.nih.gov/18953339/)
23. Evans, T. C., ed. Transformation and microinjection (April 6, 2006), *WormBook*, ed. The *C. elegans* Research Community, WormBook, doi/10.1895/wormbook.1.108.1, <http://www.wormbook.org>.
24. Streamlined Genome Engineering with a Self-Excising Drug Selection Cassette. Dickinson DJ, Pani AM, Heppert JK, Higgins CD, Goldstein B. *Genetics*. 2015 Jun 3. pii: *genetics.115.178335*. 10.1534/genetics.115.178335 [PubMed 26044593](https://pubmed.ncbi.nlm.nih.gov/26044593/)
25. Link, C. D., Johnson, C. J., Fonte, V., Paupard, M. C., Hall, D. H., Styren, S., Mathis, C. A., & Klunk, W. E. (2001). Visualization of fibrillar amyloid deposits in living, transgenic *Caenorhabditis elegans* animals using the sensitive amyloid dye, X-34. *Neurobiology of Aging*, 22(2), 217–226. [https://doi.org/10.1016/S0197-4580\(00\)00237-2](https://doi.org/10.1016/S0197-4580(00)00237-2)
26. Styren, S. D., Hamilton, R. L., Styren, G. C., & Klunk, W. E. (2000). X-34, a fluorescent derivative of Congo red: A novel histochemical stain for Alzheimer's disease pathology.

*Journal of Histochemistry and Cytochemistry*, 48(9), 1223–1232.

<https://doi.org/10.1177/002215540004800906>

27. Yochem, J. and Herman, R. K. Genetic mosaics (December 27, 2005), *WormBook*, ed. The *C. elegans* Research Community, WormBook, doi/10.1895/wormbook.1.58.1, <http://www.wormbook.org>.
28. Duerr, J. S. Immunohistochemistry (June 19, 2006), *WormBook*, ed. The *C. elegans* Research Community, WormBook, doi/10.1895/wormbook.1.105.1, <http://www.wormbook.org>
29. Wood W. The nematode *Caenorhabditis elegans*. Cold Spring Harb Monogr Arch. 1988;17.
30. Single-copy insertion of transgenes in *Caenorhabditis elegans*. Christian Frøkjær-Jensen, M Wayne Davis, Christopher E Hopkins, Blake J Newman, Jason M Thumme, Søren-Peter Olesen, Morten Grunnet & Erik M Jorgensen. 10.1038/ng.248 [PubMed 18953339](https://pubmed.ncbi.nlm.nih.gov/18953339/)
31. A critical function for beta-amyloid precursor protein in neuronal migration revealed by in utero RNA interference. Young-Pearse TL, Bai J, Chang R, Zheng JB, LoTurco JJ, Selkoe DJ. *J Neurosci*. 2007 Dec 26. 27(52):14459-69. 10.1523/JNEUROSCI.4701-07.2007 [PubMed 18160654](https://pubmed.ncbi.nlm.nih.gov/18160654/)

## CHAPTER 3: A $\beta$ induces hormetic-like effects in *C. elegans* models of Alzheimer's Disease

### 3.1 Abstract

The amyloid  $\beta$  (A $\beta$ ) peptide is known for its characteristic aggregates in the disease and ability to cause a wide range of detrimental effects in the various models used to study it. Despite this, A $\beta$  has also been shown to induce some beneficial effects. In the organism *C. elegans*, A $\beta$  has exhibited antimicrobial properties against external pathogen stressors. Here we explore A $\beta$ 's ability to protect against other external stressors, to further characterize *C. elegans*' use as a model for Alzheimer's disease. We exposed A $\beta$ -expressing *C. elegans* to heat, oxidative, and hypoxia stressors and found that A $\beta$  selectively increased resistance to heat and hypoxia stresses but not oxidative stress. This effect was only partially mimicked by other foreign protein controls, implying A $\beta$  exerts some additional effect. Only A $\beta$  levels in the neurons, and not muscles, correlated with stress resistance levels. This selective stress resistance was mediated by the HSP family of genes and required neuropeptide signaling to function. These results highlight some possible effects of expressing A $\beta$  that must be considered when using *C. elegans* as a model for Alzheimer's disease.

### 3.2 Introduction

Alzheimer's disease (AD) is a progressive neurodegenerative disease that causes loss of cognitive function in patients, typically starting at advanced age. AD is characterized by several features: the formation of amyloid  $\beta$  (A $\beta$ ) aggregates and micro-tubule associated protein tau (tau) tangles, immune activation, inflammation, oxidative stress, and neuron loss<sup>1</sup>. In addition to forming plaques and aggregates, mutations in the A $\beta$  peptide are associated with higher rates of AD, while A $\beta$  expression also induces AD-like symptoms in cell and animal models<sup>2-4</sup>. These lines of evidence have made A $\beta$  a priority target in AD research. Interestingly, some studies have

also indicated that A $\beta$  can potentially act as an antimicrobial peptide, suggesting a protective role for A $\beta$ <sup>5,6</sup>. Extensive work seeking to identify how A $\beta$  becomes toxic in the brain has pointed to certain A $\beta$  isoforms, small oligomer intermediates, and A $\beta$  localization as key determinants in toxicity<sup>7-9</sup>. Despite these discoveries, A $\beta$ 's role in AD is still unclear, creating a need for well-characterized, robust models.

The nematode *C. elegans* has been previously used as a model for AD<sup>10-12</sup>. *C. elegans* boasts many benefits as a model for neurodegenerative diseases: it is transparent, allowing for in vivo imaging in live animals; has high homology with the human genome and proteome, including several stress-related pathways; and shares many neuron subtypes with humans<sup>13</sup>. Current models of AD in *C. elegans* focus on intracellular expression of human A $\beta$  either pan-neuronally or pan-muscularly<sup>10-12</sup>. These models exhibit several symptoms such as severe paralysis, behavioral and motor defects, and reduced lifespan<sup>10-12</sup>. A $\beta$  expression in worms has also been linked to loss of function and stability in mitochondria, leading to oxidative and metabolic stress<sup>14</sup>. Conversely, worms expressing A $\beta$  have also been shown to exhibit increased pathogen resistance, indicating a possible beneficial effect against environmental stressors<sup>5</sup>. A $\beta$  shares some characteristics and behaviors with antimicrobial peptides, such as pathogen cell surface adhesion and pore formation, which may be the cause of this interaction<sup>5-6</sup>. The relationships between A $\beta$  and other environmental stressors have yet to be examined despite several stressors, like oxidative stress, being associated with higher rates of AD<sup>15,16</sup>. Investigating these interactions may improve our understanding of AD and how A $\beta$  functions within it.

There is significant overlap between stress pathways in animals, including *C. elegans* and humans. The *C. elegans* gene *daf-16*, an ortholog for the human forkhead transcription factor (FOXO), has been highlighted for its ability to extend lifespan and increase stress resistance<sup>17</sup>.

Another *C. elegans* gene, *hsf-1*, is involved in the heat stress response and is an ortholog for the human HSF1<sup>18</sup>. The *hif-1* gene (ortholog of human HIF1A) controls hypoxia resistance by regulating many hypoxia response genes, including *vhl-1* and *egl-9*<sup>19</sup>. The *skn-1* gene acts as a master regulator of the oxidative stress response in worms and its human orthologs, the Nrf/CNC proteins, are also regulators of oxidative stress<sup>20</sup>. All four of these transcription factor pathways have important roles in aging and aging-related diseases in humans and have been implicated in AD<sup>21-24</sup>. Due to the substantial overlap between human and *C. elegans* stress response pathways, analysis of interactions between stress and A $\beta$  in *C. elegans* can shed light on the effects of A $\beta$  in humans.

In this work, we use several *C. elegans* models of AD to examine whether interactions exist between the effects of environmental stressors and A $\beta$  expression and elucidate the underlying pathways behind any changes in A $\beta$ -driven resistance to stress. We assessed the resistance of A $\beta$ -expressing worms to oxidative stress, heat stress, and hypoxia. Our results indicate that A $\beta$  expression selectively increases resistance to heat stress and hypoxia while reducing resistance to oxidative stress. When supplemented with an antioxidant, n-acetyl cysteine (NAC) and heat stressed, A $\beta$ -induced stress resistance was unchanged, indicating that hormesis driven by ROS (reactive oxygen species) was not the source. A $\beta$ , despite causing oxidative stress, likely directly induces stress resistance independent of hormesis. Neuronal expression of A $\beta$  affected stress resistance in a dose-dependent manner, while muscular levels of A $\beta$  had no correlation with stress resistance. Using nCounter gene expression analysis, we identified several stress genes upregulated by A $\beta$  in both unstressed and stressed worms. Several of these genes act downstream of the major stress response pathways, *daf-16*, *hif-1*, *hsf-1*, and *skn-1*, suggesting A $\beta$  activates these transcription factors either directly or by inducing cellular

stress. Since stress response genes are mainly activated in the intestine, we sought to determine how neuronal A $\beta$  was influencing other tissues to induce stress resistance. Using RNAi to knockdown two well-known genes required for neuropeptide signaling, *unc-31* and *egl-3*<sup>25,26</sup>, stress resistance returned to WT levels, pointing to neuropeptide signaling as the source of communication from neurons to other tissues for A $\beta$ -induced stress resistance. These factors taken together highlight the complex effects of A $\beta$  in cells and at the organismal level. A $\beta$  expression has some beneficial effect for the animals in some contexts and thus results of studies of A $\beta$  in *C. elegans* should consider possible interactions with environmental conditions. These results suggest that A $\beta$  may play a substantial role in stress response, either through directly activating stress pathways or acting as a hormetic stressor.

### **3.3 Results and discussion**

#### **3.3.1 A $\beta$ induces selective stress resistance in *C. elegans*.**

To determine whether A $\beta$  modulates responses to environmental stress, we analyzed the resistance of worms expressing A $\beta$  to various stressors. We chose three strains for exposure: a wild-type N2 (WT), JKM2 (A $\beta$ +), which co-expresses A $\beta$  and A $\beta$  tagged with wrmScarlet pan-neuronally, and JKM3 (A $\beta$ -), which expresses wrmScarlet pan-neuronally<sup>10</sup>. The A $\beta$ + strain expresses the tagged A $\beta$  sub-stoichiometrically to limit wrmScarlet's impact on A $\beta$  aggregation, resulting in an aggregation pattern driven by A $\beta$ <sup>10</sup>. To assess worms' resistance to oxidative stress, we exposed them to a 50 mM paraquat solution for 24 hrs. (Fig 3.1A). As expected, this toxic dose of paraquat<sup>27</sup> resulted in reduced survival in the A $\beta$ + strain (37 %) as compared to the N2 wildtype (92 %) and the A $\beta$ - strain (69 %) (Fig 3.1B). As shown by Gallrein et al.<sup>10</sup>, the A $\beta$ + strain exhibits elevated levels of internal oxidative stress from A $\beta$  expression, possibly increasing their susceptibility to external oxidative stress and thus reduced resistance to paraquat. The A $\beta$ -

strain exhibited a less severe decrease in survival, possibly due to expression of neuronal wrmScarlet. Although the A $\beta$ <sup>+</sup> strain also expresses wrmScarlet, it does so at much lower levels than the A $\beta$ <sup>-</sup> strain, and this does not completely account for the discrepancy in survival between the two strains.

We next expanded our assay to include two additional common environmental stressors: heat stress and hypoxia. We exposed the worms to a severe heat stress of 37 °C for 4 hrs. and then allowed them to recover overnight at 20 °C (Fig 3.1A). Unexpectedly, the A $\beta$ <sup>+</sup> strain exhibited increased heat stress resistance, surviving at an average rate of 90 %, compared to 42 % and 62 % in WT and A $\beta$ <sup>-</sup>, respectively (Fig 3.1C). Similarly, when exposed to severe hypoxic conditions (<0.1 % O<sub>2</sub>) for 48 hrs. followed by overnight recovery (Fig 3.1A), the A $\beta$ <sup>+</sup> strain had

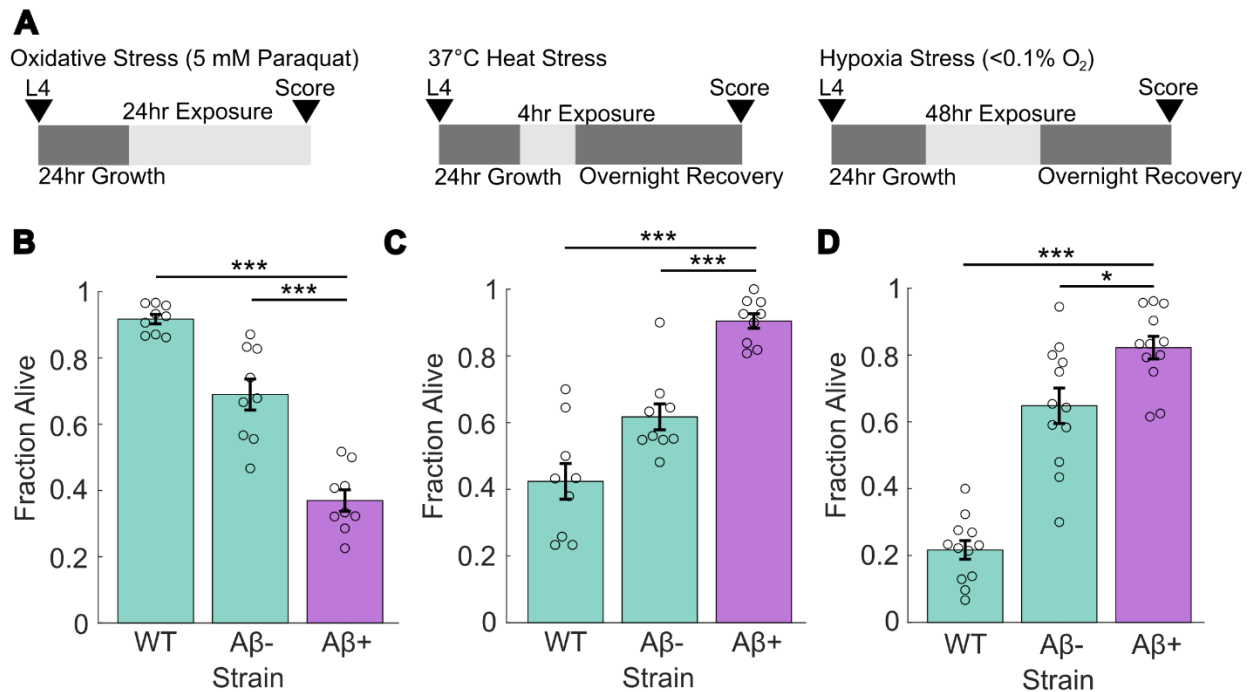


**Figure 3.1:** A $\beta$  provides selective resistance to severe heat and hypoxic stress, but not paraquat-induced oxidative stress. (A) Overview of experimental setup. Animals were age-synchronized to L4 larvae and then allowed to grow for another 24 hrs. before exposure to stressors. (B) Survival rate after 24 hr. exposure to 50mM paraquat stress. (C) Survival rate after 4 hrs. 37 °C heat stress exposure and overnight recovery at 20 °C. (D) Survival rate after 48 hrs. hypoxia (< 0.1 % O<sub>2</sub>) exposure and overnight recovery. WT is wild-type N2 Bristol, A $\beta$ <sup>+</sup> is JKM2, A $\beta$ <sup>-</sup> is JKM3. N = 9 (12 for hypoxia stress) replicates per strain. Each dot represents a replicate of approx. 30 worms. Statistical analysis was performed using ANOVA. \* is p-value < 0.05, \*\* is p-value < 0.01, \*\*\* is p-value < 0.005.

increased hypoxia resistance, with an average survival rate of 82 %, compared to 22 % and 65 % in WT and A $\beta$ -, respectively (Fig 3.1D). We attributed this increased resistance to a possible hormesis-like effect. Notably, the A $\beta$ + strain does not display increased lifespan, which is often a hallmark of hormesis<sup>10</sup>. The A $\beta$ - control strain also demonstrated a higher tolerance to these two stressors when compared to WT, although not as high as the A $\beta$ + strain. This effect could stem from the wrmScarlet protein, like in the oxidative stress assay (Fig 3.1B). However, the substantial survival difference between the A $\beta$ + and the A $\beta$ - indicate that wrmScarlet alone is not driving these differences. A $\beta$  and wrmScarlet could induce similar protective effects, but the A $\beta$ - strain lacks several other physiological deficits shown in the A $\beta$ + strain such as decreased lifespan, brood size, and movement<sup>10</sup>.

### **3.3.2 A $\beta$ -induced stress resistance is dependent on A $\beta$ levels and localization.**

To validate that A $\beta$  induces heat stress resistance, we tested the effects of increasing doses of A $\beta$  in strain CL2355, referred to as the nA $\beta$  strain here. The nA $\beta$  strain expresses A $\beta$  pan-neuronally upon upshift to 25 °C<sup>12</sup>, and thus A $\beta$  abundance is expected to be influenced by the time spent at 25 °C. We upshifted the nA $\beta$  strain to 25 °C for increasing amounts of time and then exposed it to heat stress (37 °C for 5.5 hrs.) followed by overnight recovery at 20 °C (Fig 3.2A-B) to test heat stress resistance. The nA $\beta$  strain exhibited increased heat stress resistance when compared to the WT strain, which increased with time at 25 °C. Notably, the 12 hr. timepoint showed the greatest difference in resistance between strains, with the nA $\beta$  strain exhibiting an average survival rate of 60 % compared to the WT strain's 33 % average survival rate. We also noted that upshift to 25 °C produces an increase in heat stress resistance in the WT strain, which results in insignificant survival rate differences between strains at 24 and 48 hrs. The trend of 25 °C-induced heat stress resistance in wildtype animals is consistent with prior

reports<sup>28,29</sup>. Despite this effect, our results suggest that A $\beta$  expression induces an additional protective effect, since a significant difference in heat stress survival is observed between the two strains at 12hrs.

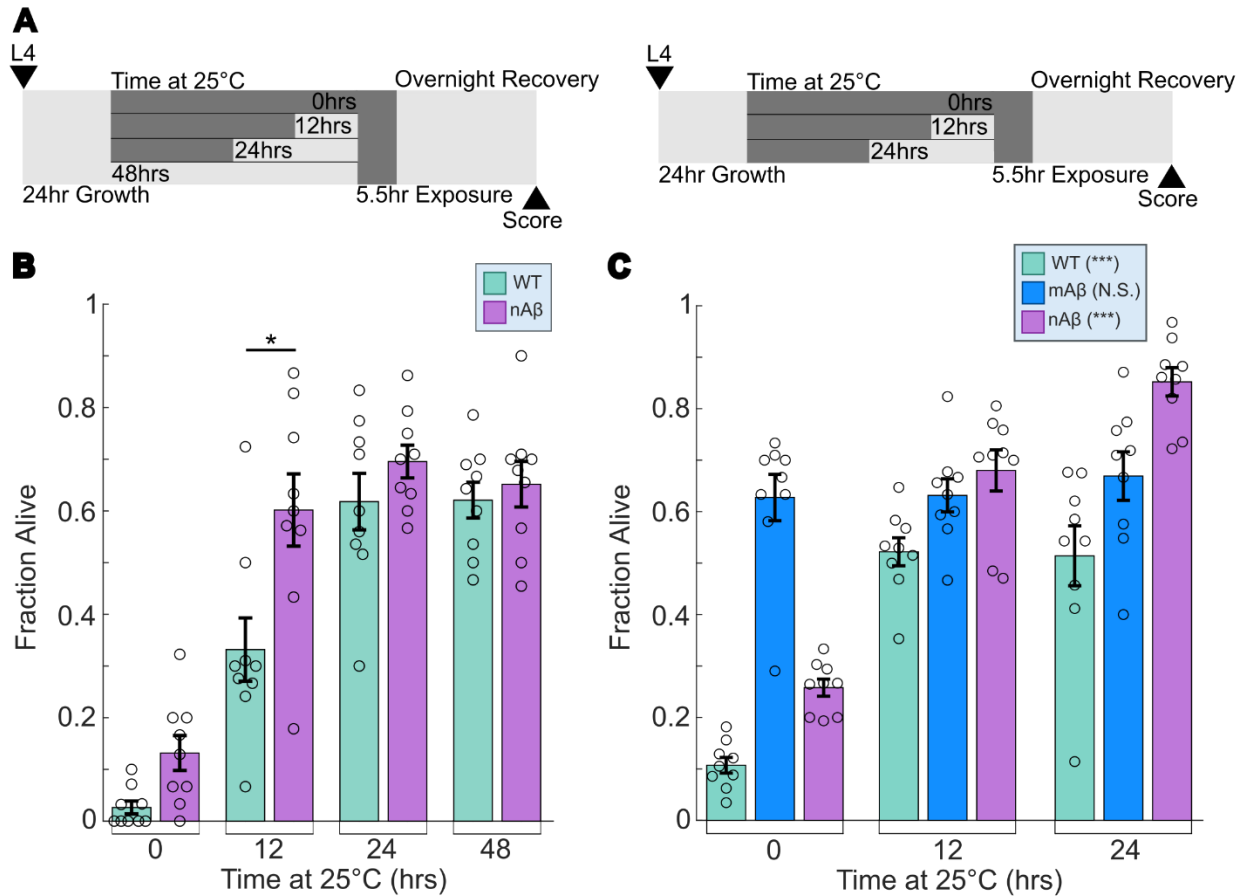


**Figure 3.2:** A $\beta$ -induced heat stress resistance is dependent on A $\beta$  expression levels and neuronal localization. (A) Overview of experimental setup. Temperature upshift to 25 °C was staggered such that stress exposure occurred at the same time for each condition. (B) Survival rate after 5.5 hr. 37 °C heat stress exposure and overnight recovery at 20 °C. Time at 25 °C correlates to levels of A $\beta$  in the neurons in nA $\beta$  strain. (C) Survival rate after 5.5 hr. 37 °C heat stress exposure and overnight recovery at 20 °C. Time at 25 °C correlates to levels of A $\beta$  in the neurons in nA $\beta$  strain and in muscles in mA $\beta$  strain. WT is wild-type N2 Bristol, nA $\beta$  is CL2355, mA $\beta$  is CL4176. N=9 replicates per condition. Each dot represents a replicate of approx. 30 worms. Statistical analysis was performed using two-sample t-test and two-way ANOVA. \* is p-value < 0.05, \*\* is p-value < 0.01, \*\*\* is p-value < 0.005.

Since both the A $\beta$ <sup>+</sup> and the nA $\beta$  strains express A $\beta$  in neurons, we next tested whether the increased stress resistance is specific to A $\beta$  expression in this tissue. We expanded this heat stress assay to include strain CL4176 (referred to as mA $\beta$ ) (Fig 3.2C). The mA $\beta$  strain also expresses

A $\beta$  upon upshift to 25 °C<sup>11</sup>, but in muscles instead of neurons. Rather than showing a dose-dependent heat stress resistance as we expected, the mA $\beta$  strain maintained a survival rate of approximately 64 % regardless of the time spent at 25°C (Fig 3.2C). This result indicates that the resistance in the mA $\beta$  strain is not a result of A $\beta$  levels. While the nA $\beta$  strain contains a fluorescence marker, the mA $\beta$  has a rol-6(su1006) marker that deforms the cuticle and results in a roller phenotype<sup>30</sup>, which possibly explains this. In addition, the efficiency of A $\beta$  production as a function of time at 25 °C likely differs in these two tissues. Since the mA $\beta$  strain's resistance did not vary, while the nA $\beta$  strain's resistance did vary and reached higher levels than the mA $\beta$  strain, we conclude that A $\beta$  in neurons is a driver of heat stress resistance. It is unclear what aspect of the mA $\beta$  strain contributes to increased heat stress resistance, but previous work has shown that A $\beta$  is undetectable when uninduced in this strain<sup>11</sup>, indicating that A $\beta$  levels in muscles likely have little effect on resistance.

### **3.3.3 Foreign protein expression only partially accounts for increased stress resistance.**

As noted in our initial stress assays, wrmScarlet in the A $\beta$ - strain induces some level of stress resistance. To test if foreign protein expression drives this effect, we sought to replicate the effect with another strain expressing GFP pan-neuronally, OH438 (referred to as nGFP) (Fig 3.3A)<sup>31</sup>. The nGFP strain exhibited increased heat stress resistance similar to the A $\beta$ - strain, with an average survival rate of 53 %. This result strengthens the idea that the hormesis-like effect stems at least partially from foreign protein expression in the neurons. Yet, the A $\beta$ + strain had significantly higher survival than the A $\beta$ - strain (Fig 3.1), implying that foreign protein

expression alone does not completely account for the effect and that A $\beta$  induces protective effects against stress.

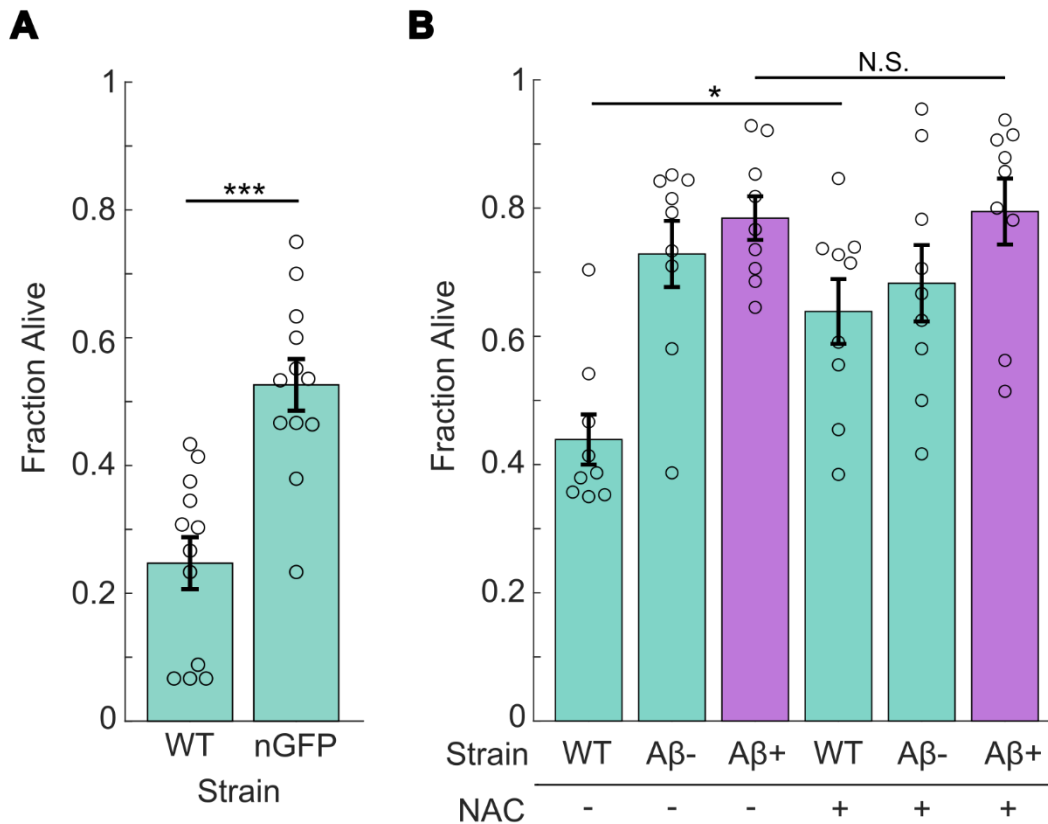


**Figure 3.3:** Heat stress resistance is partially replicated with other neuronally expressed proteins and is not eliminated with NAC treatment. A) Survival rate after 4 hr. 37 °C heat stress exposure and overnight 20 °C recovery in pan-neuronal GFP strain. (B) Survival rate after 4 hr. 37 °C heat stress exposure and overnight recovery in worms grown on control and 5 mM NAC plates for 24 hrs. before heat stress exposure. WT is wild-type N2 Bristol, nGFP is OH438, A $\beta$ + is JKM2, A $\beta$ - is JKM3. N=9 replicates per condition. Each dot represents a replicate of approx. 30 worms. Statistical analysis was performed using two-sample t-test and two-way ANOVA. \* is p-value < 0.05, \*\* is p-value < 0.01, \*\*\* is p-value < 0.005.

### 3.3.4 Antioxidant exposure does not suppress the protective effect of A $\beta$ .

Since A $\beta$  has been shown to induce oxidative stress in *C. elegans*<sup>32</sup>, we hypothesized that the protective effect induced by A $\beta$  could be the result of oxidative stress-driven hormesis<sup>33,34</sup>. To determine if A $\beta$ -induced oxidative stress drives increased stress resistance, we tested if the antioxidant NAC modulates the protective effect of A $\beta$ . We exposed worms to 5 mM NAC for 24

hrs., a dosage that has been shown to reduce oxidative stress in *C. elegans*<sup>35,36</sup>. After NAC exposure, animals were heat stressed at 37 °C for 4 hrs. and allowed to recover overnight. NAC had an insignificant effect on the A $\beta$ <sup>+</sup> and A $\beta$ <sup>-</sup> strains but increased WT resistance (Fig 3.3B). NAC has been previously shown to induce some heat stress resistance<sup>35,36</sup>, but it failed to significantly affect the A $\beta$ <sup>+</sup> strain. This suggests that A $\beta$ -induced heat stress resistance is independent of any NAC-induced effects. Additionally, reducing A $\beta$ -induced hormetic effects with NAC failed to produce a change, further indicating that A $\beta$  modulates stress resistance in an oxidative stress-independent manner.

### **3.3.5 A $\beta$ upregulates several stress response pathways.**

To elucidate how A $\beta$  induces stress resistance, we probed the gene expression of several stress resistance pathways using Nanostring nCounter analysis<sup>37</sup>. We targeted a predefined panel of targets that included several genes in the *daf-16*, *hsf-1*, *hif-1*, and *skn-1* pathways. RNA samples from 3 biological replicates of each of the WT, A $\beta$ <sup>+</sup> and A $\beta$ <sup>-</sup> strains were pooled for unstressed, heat stressed (2.5 hrs. at 37 °C), and hypoxic (<0.1% O<sub>2</sub> for 24 hrs.) conditions (Fig 3.4A-C). This analysis revealed several stress resistance genes that were upregulated in the A $\beta$ <sup>+</sup> strain in both unstressed and stressed conditions, including several heat-shock proteins (HSPs). HSPs are associated with protein misfolding and molecular chaperones involved in stress response, specifically heat stress, hypoxia, and oxidative stress<sup>18,38</sup>. During stress, they are typically upregulated in the neurons and intestine as a part of the stress response<sup>39</sup>. A $\beta$ <sup>+</sup> worms exhibited elevated levels of four HSPs under all conditions: *hsp-16.1*, *hsp-16.2*, *hsp-16.49*, and *hsp-70* (Fig 3.4A-C). This may indicate why A $\beta$  induces more stress resistance than wrmScarlet, as the A $\beta$ <sup>-</sup> strain only showed increased expression of these genes under hypoxia (Fig 3.4C). The HSPs are co-regulated by the *daf-16*, *hsf-1*, *hif-1*, and *skn-1* transcription factors<sup>18,40-42</sup>, making it

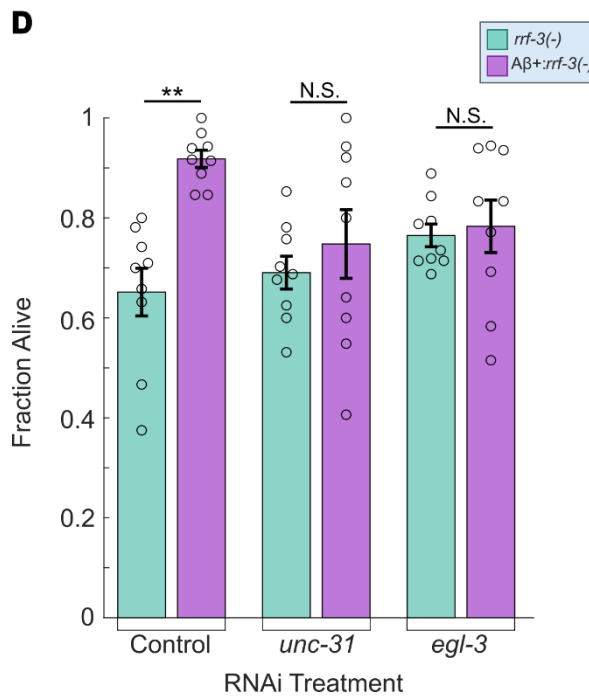
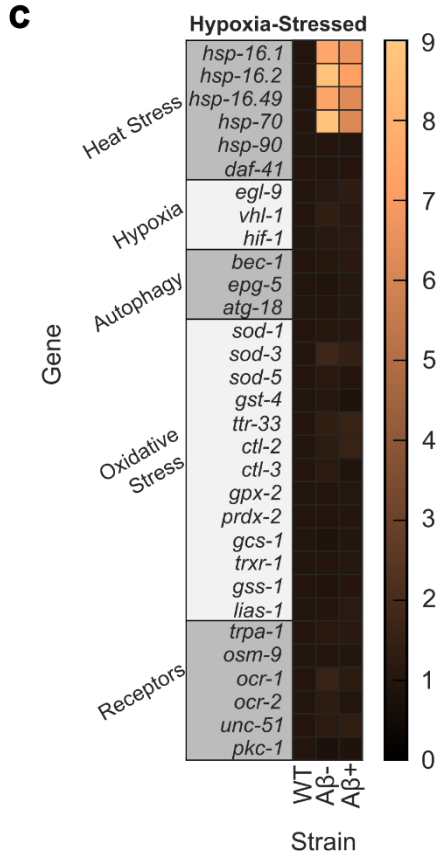
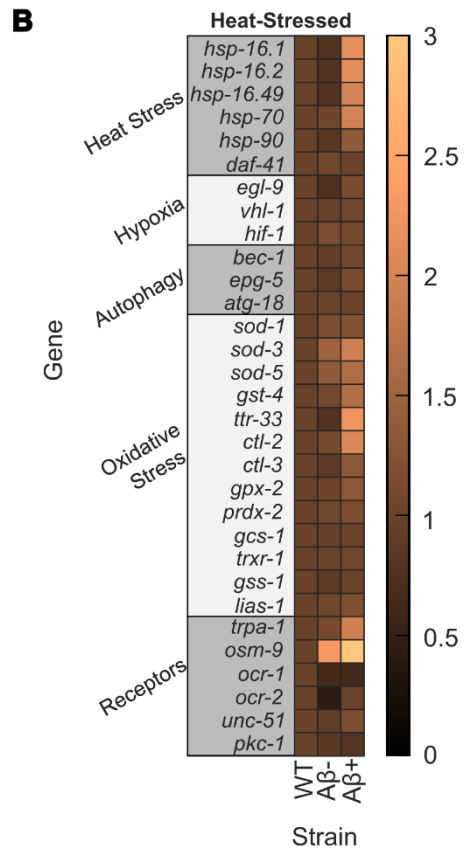
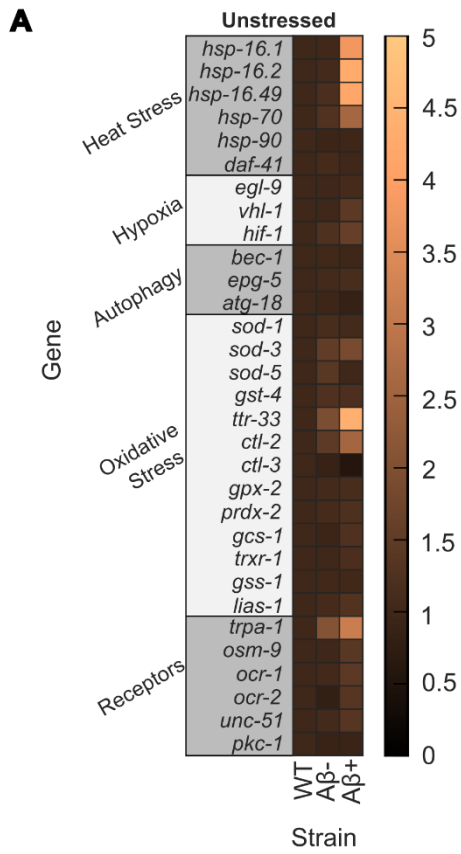
unclear which pathway or pathways A $\beta$  is inducing. Surprisingly, A $\beta$  expression doesn't upregulate any of the tested hypoxia or autophagy genes when compared to the controls, even under stressed conditions, suggesting the increased resistance is mediated mainly by the HSPs. Some of the main oxidative stress response genes, *sod-3* and *gst-4*<sup>43,44</sup>, are slightly upregulated despite the A $\beta$ <sup>+</sup> strain exhibiting lowered oxidative stress resistance, which is possibly due to A $\beta$ -induced oxidative stress. Interestingly, the *ttr-33* gene, another oxidative stress response gene responsible for paraquat and hydrogen peroxide resistance<sup>45</sup>, is highly upregulated in unstressed worms, but this doesn't translate to increased paraquat resistance when exposed (Fig 3.1B). Overall, this gene analysis suggests that A $\beta$  induces stress resistance through upregulation of HSPs.

### **3.3.6 A $\beta$ -induced stress resistance requires neuropeptide signaling.**

Stress resistance in *C. elegans* is a cell nonautonomous response mediated by communication between several tissues, most commonly the intestine and neurons<sup>39,46-48</sup>. Stress will upregulate transcription factors like *hif-1* in neurons which can activate serotonin signaling and other pathways in a cell nonautonomous manner<sup>18,39,46-48</sup>. Neuroendocrine communication to the intestine through neuropeptide signaling can drive stress resistance through the upregulation of transcription factors in the intestine like *daf-16*, *skn-1*, and *hsf-1*<sup>18,39,46-48</sup>. The intestine can also act as a sensor for stress, such as detecting dietary restriction through food intake and *daf-16* activation, oxidative stress through *skn-1* activation, and heat stress through *hsf-1* activation<sup>18,39,46-48</sup>. It can then communicate these stresses back to the neurons to trigger an organism-level stress response<sup>18,39,46-48</sup>. Therefore, we next focused on whether neuronal A $\beta$  could activate stress resistance pathways in the intestine through neuroendocrine communication. It has been previously shown that A $\beta$  can spread from neurons to other tissues in aged *C.*

*elegans*<sup>10</sup>. In our experiments, we evaluated young worms, before the age where A $\beta$  dispersal has been identified<sup>10</sup>, thus ensuring A $\beta$  is restricted to neurons. To understand how neuronal A $\beta$  influences organism-level stress resistance, we assessed whether disrupting neuropeptide signaling between the neurons and other tissues had an effect on stress resistance. To knockdown neuropeptide signaling, we used RNAi by feeding<sup>49</sup>, targeting two key neuropeptide signaling genes, *unc-31* and *egl-3*. *Unc-31* regulates neuropeptide release from dense core vesicles<sup>25</sup> and *egl-3* is necessary for neuropeptide maturation<sup>26</sup>; knocking out either would severely limit neuropeptide signaling. To ensure silencing was effective in neurons, we used an RNAi sensitive strain, NL2099 (*rrf-3(-)*)<sup>50</sup>, as our control. This strain was crossed with our A $\beta$ + strain to generate ASM35 (A $\beta$ +;*rrf-3(-)*). Upon knockdown of either gene (Fig 3.4D), A $\beta$ -induced stress resistance in A $\beta$ +;*rrf-3(-)* worms dropped to similar levels as *rrf-3(-)*. This result suggests that A $\beta$  in neurons upregulates stress resistance pathways in other tissues through neuropeptide signaling, thus driving increased organismal resistance to stress. It is unclear if A $\beta$  is directly initiating neuropeptide signaling, or if A $\beta$  is inducing another stress that may be responsible for the activation of the stress response at the organismal level.

**Figure 3.4:** Nanostring analysis indicates several resistance genes upregulated in both stressed and unstressed worms and RNAi suppression suggests resistance is communicated through neuropeptide signaling. (A-C) Nanostring analysis on unstressed (A), heat stressed (B), and hypoxic stressed (C) worms. Genes are grouped by type and box color indicates expression changes. 3 biological replicates were pooled per sample. (D) Survival rate after 4 hr. 37 °C heat stress exposure in RNAi suppressed worms. RNAi control was HT115 with empty vector. WT is wild-type N2 Bristol, A $\beta$ + is JKM2, A $\beta$ - is JKM3, *rrf-3(-)* is RNAi-sensitive strain NL2099, A $\beta$ +*rrf-3(-)* is ASM35, a cross between JKM2 and NL2099. N=9 replicates per condition. Each dot represents a replicate of approx. 30 worms. Statistical analysis was performed using two-sample t-test and two-way ANOVA. \* is p-value < 0.05, \*\* is p-value < 0.01, \*\*\* is p-value < 0.005.



### 3.3.7 Conclusions

In summary, this study found that A $\beta$  induces resistance to heat and hypoxic stress but not oxidative stress by activating key stress response genes. Several members of the HSP family of genes were induced in the A $\beta$ -expressing strain under both unstressed and stressed conditions. The location and levels of A $\beta$  have significant effects on the levels of stress resistance induced, with muscular A $\beta$  expression levels having no correlation with resistance. The stress resistance may be partially explained by neuronal expression of foreign protein, but A $\beta$  is able to provide higher stress resistance than either of the two other proteins tested. It is unclear if protein aggregation plays a role in this protective effect, as both A $\beta$  and wrmScarlet-tagged A $\beta$  aggregate<sup>10</sup>, but aggregation levels were not assessed in this work. Gene expression analysis indicates that A $\beta$  activates some combination of the *daf-16*, *hsf-1*, *hif-1*, and *skn-1* pathways to induce stress resistance, but further work is needed to determine if all four pathways participate in this effect. The HSP family of genes falls under numerous transcriptional regulators, and expanding the breadth of genes covered by this kind of screen may provide more insight into which pathways are activated. RNAi knockdown of *unc-31* and *egl-3* shows that to induce stress resistance, A $\beta$  activates neuropeptide signaling to communicate with other tissues. More work is needed to examine exactly how A $\beta$  activates neuropeptide signaling, whether that be directly or indirectly by inducing cellular stress. This study highlights the need to more fully characterize the effect of A $\beta$  on *C. elegans*, and to consider its complex organismal effects when using it as a model for AD. If the increased stress resistance is not consistent across species, there may be more limitations of *C. elegans* as a model for AD and more factors to consider before its use as such. Knowing these limitations and interactions will make interpretations of results more meaningful. The results of this work also imply that A $\beta$  may have beneficial effects for the host, outside of AD. The role of

A $\beta$  in healthy humans is still quite unclear, but several theories regarding its function include pathogen defense, injury recovery, and regulation synaptic function<sup>53</sup>. Inducing stress resistance pathways and acting as an early signal for stress may be another role it plays in human biology. It will be crucial to further characterize the role of A $\beta$  in *C. elegans* and other model organisms to better understand the mechanisms by which A $\beta$  induces physiological changes in AD and other human diseases.

### 3.4 Materials and methods

#### 3.4.1 Strains

Table 3.1. *C. elegans* strains used in this work

Strain	Genotype	Source
N2	Wild type	From CGC
JKM2	<i>Is</i> [ <i>rgef-1p</i> ::Signalpeptide-Abeta(1-42):: <i>hsp-3</i> (IRES):: <i>wrmScarlet</i> -Abeta(1-42):: <i>unc-54</i> (3'UTR) + <i>rps-0p</i> ::HygroR]	Kirstein Lab (Gallrein et al., 2021)
JKM3	<i>Is</i> [ <i>rgef-1p</i> :: <i>wrmScarlet</i> :: <i>unc-54</i> (3'UTR) + <i>rps-0p</i> ::HygroR]	Kirstein Lab (Gallrein et al., 2021)
CL2355	dvIs50 [pCL45 ( <i>snb-1</i> ::Abeta 1-42::3' UTR(long) + <i>mtl-2</i> ::GFP) I	From CGC
CL4176	dvIs27 [ <i>myo-3p</i> ::A-Beta (1-42):: <i>let-851</i> 3'UTR) + <i>rol-6</i> ( <i>su1006</i> )]	From CGC
	X	
OH438	otIs117 [ <i>unc-33p</i> ::GFP + <i>unc-4</i> (+)]	From CGC
NL2099	<i>rrf-3</i> ( <i>pk1426</i> ) II	From CGC
ASM35	JKM2xNL2099 Cross	This work

#### 3.4.2 *C. elegans* growth and maintenance

Nematodes were grown and maintained at 20 °C on nematode growth medium (NGM) seeded with *E. coli* OP50 as a food source, unless otherwise specified, according to standard protocols<sup>51</sup>. Age-synchronization for experiments was performed by washing plates with 1mL of a solution of M9 media supplemented with 0.01% v/v TX-100 (M9TX). Worms were allowed to settle, and supernatant was removed and replaced with 1mL of 1:2:1 mixture of bleach, 1M

NaOH, and water. Once eggs were released, they were washed 3 times with 1mL M9TX, and transferred to fresh plates.

### **3.4.3 *C. elegans* crossing**

The JKM2 strain naturally produces a higher proportion of males than N2, so no extra procedures were needed to obtain males for the cross. To cross, young-adult NL2099 hermaphrodites were isolated onto a plate with JKM2 males in a 1:10 ratio, hermaphrodites to males. After several days, offspring were isolated and checked from homozygous passing of transgenes. The JKM2 transgene was checked using fluorescence microscopy. Once the JKM2 transgene was confirmed for 100 % transmittance, individuals were picked to fresh plates and allowed to grow. When sufficient offspring were on each plate (minimum 100 worms) genomic DNA was collected using standard methods and PCR was performed using primers flanking the *rrf-3(pk1426)* deletion site obtained from the Wormbase online resource. DNA showing the deletion was then processed through Sanger sequencing to confirm the *rrf-3(pk1426)* mutation.

### **3.4.4 Oxidative stress assay**

Animals were age-synchronized by bleaching and cultured to the L4 stage at 20 °C. After another 24 hrs. of growth, approximately 30 worms were picked to a fresh plate containing 50mM paraquat (added during plate production after media was cooled to 50 °C) per cohort. These plates were transferred to a 20 °C incubator for 24 hrs. and then scored for survival by prodding with a platinum wire worm pick to check for movement. Animals that didn't respond were marked as dead.

### **3.4.5 Heat stress assay**

Animals were age-synchronized by bleaching and cultured to the L4 stage at 20 °C. After another 24 hrs. of growth, approximately 30 worms were picked to a fresh plate per cohort at room temperature (20 °C). These were transferred to an incubator set at 37 °C for the specified time (4 hrs. or 5.5 hrs.), before being returned to the 20 °C growth incubator for overnight recovery. For the 25 °C upshift experiments, these plates were instead first transferred to a 25 °C incubator for the specified time before the 37 °C stress. Animals were scored for survival by prodding with a platinum wire worm pick to check for movement. Animals that didn't respond were marked as dead.

### **3.4.6 Hypoxia assay**

Animals were age-synchronized by bleaching and cultured to the L4 stage at 20 °C. After another 24 hrs. of growth, approximately 30 worms were picked to a fresh plate per cohort. These plates were put in a GasPak chamber with 3 satchels to lower the oxygen concentration to below 0.1 %. After 48 hrs. the chamber was opened, and the worms were allowed to recover overnight before scoring. Animals were scored for survival by prodding with a platinum wire worm pick to check for movement. Animals that didn't respond were marked as dead.

### **3.4.7 RNA extraction and gene expression profiling**

Animals were age-synchronized by bleaching and cultured to the L4 stage at 20 °C. After another 24 hrs. of growth, worms were split into three treatment groups: unstressed, heat stressed, or hypoxia stressed. Unstressed worms were allowed to grow for another 24 hrs. before RNA was extracted. Heat stressed worms were stressed the next day at 37 °C for 2.5 hrs. Hypoxia stressed worms were stressed for 24 hrs. as described above. Following treatment, RNA was extracted according to the Direct-zol RNA Miniprep extraction kit (Cat# R2051). During the

Tri Reagent step, a motorized pestle was used for 1 min to help break the worm cuticle. RNA samples were then provided to the UNC Respiratory TRACTS Core, who performed the Nanostring nCounter analysis. For each combination of strain and condition, three biological replicates were pooled together.

### **3.4.8 RNAi plate preparation and suppression assay**

Bacteria and plates were prepared according to a modified protocol from Timmons et al.<sup>49</sup>. In summary, bacteria was cultured from the Ahringer RNAi Library<sup>52</sup> in fresh LB media supplemented with 50 µg/mL ampicillin and 12.5 µg/mL tetracycline. After overnight growth (16-18 hrs.), the culture was centrifuged and resuspended in fresh LB media supplemented with 50 µg/mL ampicillin and 1mM Isopropyl-β-d-thiogalactopyranoside (IPTG) to OD<sub>600</sub>=0.5. After another 4 hrs. of growth, bacteria was seeded onto NGM plates supplemented with 50 µg/mL ampicillin and 1mM IPTG. Animals were age-synchronized by bleaching and cultured to the L4 stage at 20 °C on plates containing the relevant RNAi *E. coli* strain (control, *unc-31*, *egl-3*). After another 24hrs of growth, approximately 30 worms were picked to a fresh plate per cohort containing their respective RNAi *E. coli* strain. The heat stress assay was then performed as described above.

### **3.4.9 Statistical analysis**

Statistical analysis (ANOVA and t-test) was performed using MATLAB. P-values were considered significant when:  $p < 0.05$  (\*),  $p < 0.01$  (\*\*), and  $p < 0.001$  (\*\*\*)).

### 3.5 References

1. Murke L. Neuroscience: alzheimer's disease. Nature. 2009;461:895-897.  
<https://doi.org/10.1038/461895a>
2. Alvarez J, Alvarez-Illera P, Santo-Domingo J, Fonteriz RI, Montero M. Modeling Alzheimer's Disease in *Caenorhabditis elegans*. Biomedicines. 2022; 10(2):288.  
<https://doi.org/10.3390/biomedicines10020288>
3. Blanchard J, Victor M, & Tsai L. Dissecting the complexities of Alzheimer disease with in vitro models of the human brain. Nat Rev Neurol 18, 25–39 (2022).  
<https://doi.org/10.1038/s41582-021-00578-6>
4. Yokoyama M, Kobayashi H, Tatsumi L, Tomita T. Mouse Models of Alzheimer's Disease. Frontiers of Molecular Neuroscience. 2022;15.  
<https://doi.org/10.3389/fnmol.2022.912995>
5. Deepak K, Choi S, Washicosky K, Eimer W, Tucker S, Ghofrani J, Lefkowitz A, McColl G, Goldstein L, Tanzi R, Moir R. Amyloid- $\beta$  peptide protects against microbial infection in mouse and worm models of Alzheimer's disease. Sci. Transl. Med. 2016; 8(340):340ra72. <https://doi.org/10.1126/scitranslmed.aaf1059>
6. Pastore A, Raimondi F, Rajendran L, Temussi P. Why does the A $\beta$  peptide of Alzheimer share structural similarity with antimicrobial peptides?. Commun Biol. 2020;3:135.  
<https://doi.org/10.1038/s42003-020-0865-9>
7. Busch L, Eggert S, Endres K, Bufe B. The Hidden Role of Non-Canonical Amyloid  $\beta$  Isoforms in Alzheimer's Disease. Cells. 2022; 11(21):3421.  
<https://doi.org/10.3390/cells11213421>

8. Gallego V, Bachmann L, Marks D, Brachthäuser M, Geidies A, Müller T. Role of Intracellular Amyloid  $\beta$  as Pathway Modulator, Biomarker, and Therapy Target. *International Journal of Molecular Sciences*. 2022; 23(9):4656.  
<https://doi.org/10.3390/ijms23094656>
9. Rosenblum W. Structure and location of amyloid beta peptide chains and arrays in Alzheimer's disease: new findings require reevaluation of the amyloid hypothesis and of tests of the hypothesis. *Neurobiology of Aging*. 2002;23(2):225-230.  
[https://doi.org/10.1016/S0197-4580\(01\)00283-4](https://doi.org/10.1016/S0197-4580(01)00283-4)
10. Gallrein C, Iburg M, Michelberger T, Kocak A, Puchkov D, Liu F, Mariscal S, Nayak T, Schierle G, Kirstein J. Novel amyloid-beta pathology *C. elegans* model reveals distinct neurons as seeds of pathogenicity. *Progress in Neurobiology*. 2021; 198.  
<https://doi.org/10.1016/j.pneurobio.2020.101907>
11. Link C, Taft A, Kapulkin V, Duke K, Kim S, Fei Q, Wood D, Sahagan B. Gene expression analysis in a transgenic *Caenorhabditis elegans* Alzheimer's disease model. *Neurobiology of Aging*. 2003;24(3)397-413. [https://doi.org/10.1016/S0197-4580\(02\)00224-5](https://doi.org/10.1016/S0197-4580(02)00224-5)
12. Wu Y, Wu Z, Butko P, Christen Y, Lambert M, Klein W, Link C, Luo Y. Amyloid-beta-induced pathological behaviors are suppressed by Ginkgo biloba extract EGb 761 and ginkgolides in transgenic *Caenorhabditis elegans*. *J Neurosci* 2006;26(50),13102–13.  
<https://doi.org/10.1523/JNEUROSCI.3448-06.2006>.
13. Corsi A, Wightman B, and Chalfie M. A Transparent window into biology: A primer on *Caenorhabditis elegans* (June 18, 2015), WormBook, ed. The *C. elegans* Research

Community, WormBook, <https://doi.org/10.1895/wormbook.1.177.1>,  
<http://www.wormbook.org>.

14. Teo E, Ravi S, Barardo D, Kim H, Fong S, Cazenave-Gassiot A, Tan T, Ching J, Kovalik J, Wenk M, Gunawan R, Moore P, Halliwell B, Tolwinski N, Gruber J. Metabolic stress is a primary pathogenic event in transgenic *Caenorhabditis elegans* expressing pan-neuronal human amyloid beta. *eLife*. 2019. <https://doi.org/10.7554/eLife.50069>
15. Bisht K, Sharma K, Tremblay M. Chronic stress as a risk factor for Alzheimer's Disease: Roles of microglia-mediated synaptic remodeling, inflammation, and oxidative stress. *Neurobiology of Stress*. 2018; 9:9-21. <https://doi.org/10.1016/j.ynstr.2018.05.003>.
16. Ionescu-Tucker A, Cotman C. Emerging roles of oxidative stress in brain aging and Alzheimer's disease. *Neurobiology of Aging*. 2021;107:86-95.  
<https://doi.org/10.1016/j.neurobiolaging.2021.07.014>
17. Tissenbaum H. Chapter One - DAF-16: FOXO in the Context of *C. elegans*. *Current Topics in Developmental Biology*, Academic Press. 2018;127:1-21.  
<https://doi.org/10.1016/bs.ctdb.2017.11.007>
18. Kyriakou E, Taouktsi E, Syntichaki P. The Thermal Stress Coping Network of the Nematode *Caenorhabditis elegans*. *International Journal of Molecular Sciences*. 2022; 23(23):14907. <https://doi.org/10.3390/ijms232314907>
19. Powell-Coffman J. Hypoxia signaling and resistance in *C. elegans*. *Trends in Endocrinology and Metabolism*. 2010;21(7):435-440.  
<https://doi.org/10.1016/j.tem.2010.02.006>

20. Blackwell K, Steinbaugh M, Hourihan J, Ewald C, Isik M. SKN-1/Nrf, stress responses, and aging in *Caenorhabditis elegans*. *Free Radical Biology and Medicine*. 2015; 88:290-301. <https://doi.org/10.1016/j.freeradbiomed.2015.06.008>.
21. Calderwood S, Murshid A. Molecular Chaperone Accumulation in Cancer and Decrease in Alzheimer's Disease: The Potential Roles of HSF1. *Frontiers in Neuroscience*. 2017; 11. <https://doi.org/10.3389/fnins.2017.00192>
22. Du S, Zheng H. Role of FoxO transcription factors in aging and age-related metabolic and neurodegenerative diseases. *Cell Biosci*. 2021; 11:188. <https://doi.org/10.1186/s13578-021-00700-7>
23. Hassan H, Chen R. Hypoxia in Alzheimer's disease: effects of hypoxia inducible factors. *Neural Regen Res*. 2021;16(2):310-311. <https://doi.org/10.4103/1673-5374.290898>
24. Yuan J, Zhang S, Zhang Y. Nrf1 is paved as a new strategic avenue to prevent and treat cancer, neurodegenerative and other diseases. *Toxicology and Applied Pharmacology*. 2018;360:273-283. <https://doi.org/10.1016/j.taap.2018.09.037>
25. Cornell R, Cao W, Liu J, Pocock R. Conditional Degradation of UNC-31/CAPS Enables Spatiotemporal Analysis of Neuropeptide Function. *J Neurosci*. 2022; 42(46):8599-8607. <https://doi.org/10.1523/JNEUROSCI.1368-22.2022>.
26. Salem J, Nkambeu B, Arvanitis D, Beaudry F. Deciphering the Role of EGL-3 for Neuropeptides Processing in *Caenorhabditis elegans* Using High-Resolution Quadrupole-Orbitrap Mass Spectrometry. *Neurochem Res*. 2018;43(11):2121-2131. <https://doi.org/10.1007/s11064-018-2636-2>

27. Gonzales-Moreno C, Fernandez-Hubeid LE, Holgado A, Virgolini MB. Low-dose N-acetyl cysteine prevents paraquat-induced mortality in *Caenorhabditis elegans*. *MicroPubl Biol.* 2023;10. <https://doi.org/10.17912/micropub.biology.000815>
28. Mendenhall A, Crane M, Leiser S, Sutphin G, Tedesco P, Kaerberlein M, Johson T, Brent R. Environmental Canalization of Life Span and Gene Expression in *Caenorhabditis elegans*. *The Journals of Gerontology.* 2017;72(8):1033-1037. <https://doi.org/10.1093/gerona/glx017>
29. Servello F, Apfeld J. The heat shock transcription factor HSF-1 protects *Caenorhabditis elegans* from peroxide stress. *Translational Medicine of Aging.* 2020;4:88-92. <https://doi.org/10.1016/j.tma.2020.07.002>
30. Kramer J, Johson J. Analysis of mutations in the *sqt-1* and *rol-6* collagen genes of *Caenorhabditis elegans*. *Genetics.* 1993;135(4):1035–1045. <https://doi.org/10.1093/genetics/135.4.1035>
31. Silveira T, Zamberlan D, Arantes L, Machado M, Silva T, Camara D, Santamaria A, Aschner M, Soares F. Quinolinic acid and glutamatergic neurodegeneration in *Caenorhabditis elegans*. *NeuroToxicology.* 2018;67:94-101. <https://doi.org/10.1016/j.neuro.2018.04.015>
32. Drake J, Link C, Butterfield A. Oxidative stress precedes fibrillar deposition of Alzheimer's disease amyloid  $\beta$ -peptide (1–42) in a transgenic *Caenorhabditis elegans* model. *Neurobiology of Aging.* 2003; 24(3):415-420. [https://doi.org/10.1016/S0197-4580\(02\)00225-7](https://doi.org/10.1016/S0197-4580(02)00225-7).

33. Cypser J, Johnson T. Multiple Stressors in *Caenorhabditis elegans* Induce Stress Hormesis and Extended Longevity. *The Journals of Gerontology*. 2002; 57(3)B109–B114. <https://doi.org/10.1093/Gerona/57.3.B109>
34. Ristow M, Zarse K. How increased oxidative stress promotes longevity and metabolic health: The concept of mitochondrial hormesis (mitohormesis). *Experimental Gerontology*. 2010;45(6):410-418. <https://doi.org/10.1016/j.exger.2010.03.014>
35. Oh S, Park J, Park S. Lifespan extension and increased resistance to environmental stressors by N-acetyl-L-cysteine in *Caenorhabditis elegans*. *Clinics (São Paulo)*. 2015;70:380–86. [https://doi.org/10.6061/clinics/2015\(05\)13](https://doi.org/10.6061/clinics/2015(05)13)
36. Gusarov I, Shamovsky I, Pani B, Gautier L, Eremina S, Zhukotskaya O, Mironov A, Makarov A, Nudler E. Dietary thiols accelerate aging of *C. elegans*. *Nat Commun*. 2021;12:4336. <https://doi.org/10.1038/s41467-021-24634-3>
37. Geiss G, Bumgarner R, Birditt B, Dahl T, Dowidar N, Dunaway DL, Fell H, Ferree S, George R, Grogan T, James J, Maysuria M, Mitton J, Oliveri P, Osborn J, Peng T, Ratcliffe A, Webster P, Davidson E, Hood L, Dimitrov K. Direct multiplexed measurement of gene expression with color-coded probe pairs. *Nat Biotechnol*. 2008;26:317–325. <https://doi.org/10.1038/nbt1385>.
38. Murshid A, Eguchi T, Calderwood S. Stress proteins in aging and life span. *International Journal of Hyperthermia*. 2013;29(5):442–447. <https://doi.org/10.3109/02656736.2013.798873>
39. Hodge F, Bajuszova V, van Oosten-Hawle P. The Intestine as a Lifespan- and Proteostasis-Promoting Signaling Tissue. *Front Aging*. 2022;3:897741. <https://doi.org/10.3389/fragi.2022.897741>

40. Park S, Tedesco P, Johnson, T. Oxidative stress and longevity in *Caenorhabditis elegans* as mediated by SKN-1. *Aging Cell*. 2009;8:258-269. <https://doi.org/10.1111/j.1474-9726.2009.00473.x>
41. Hesp K, Smant G, Kammenga J. *Caenorhabditis elegans* DAF-16/FOXO transcription factor and its mammalian homologs associate with age-related disease. *Experimental Gerontology*. 2015;72:1-7. <https://doi.org/10.1016/j.exger.2015.09.006>
42. Shamalnasab M, Dhaoui M, Thondamal M, Harvald E, Færgeman N, Aguilaniu H, Fabrizio P. HIF-1-dependent regulation of lifespan in *Caenorhabditis elegans* by the acyl-CoA-binding protein MAA-1. *Aging (Albany NY)*. 2017;9(7):1745-1769. <https://doi.org/10.18632/aging.101267>
43. Oliveira R, Porter Abate J, Dilks K, Landis J, Ashraf J, Murphy C, Blackwell K. Condition-adapted stress and longevity gene regulation by *Caenorhabditis elegans* SKN-1/Nrf. *Aging Cell*. 2009;8: 524–541. <https://doi.org/10.1111/j.1474-9726.2009.00501.x>
44. Wang J, Robida-Stubbs S, Tullet J, Rual J, Vidal M, Blackwell K. RNAi screening implicates a SKN-1-dependent transcriptional response in stress resistance and longevity deriving from translation inhibition. *PLoS Genet*. 2010;6: e1001048 <https://doi.org/10.1371/journal.pgen.1001048>
45. Offenburger S, Ho X, Tachie-Menson T, Coakley S, Hilliard M, Gartner A. 6-OHDA-induced dopaminergic neurodegeneration in *Caenorhabditis elegans* is promoted by the engulfment pathway and inhibited by the transthyretin-related protein TTR-33. *PLoS Genet*. 2018;14(1):e1007125. <https://doi.org/10.1371/journal.pgen.1007125>

46. Chen P, Zhang L, Chen D, Tian Y. Mitochondrial stress and aging: Lessons from *C. elegans*. *Seminars in Cell and Developmental Biology*. 2024; 154:69-76.  
<https://doi.org/10.1016/j.semcdb.2023.02.010>.
47. Dutta N, Garcia G, Higuchi-Sanabria R. Hijacking Cellular Stress Responses to Promote Lifespan. *Frontiers in Aging*. 2022; 3. <https://doi.org/10.3389/fragi.2022.860404>
48. Miller H, Dean E, Pletcher S, Leiser S. Cell non-autonomous regulation of health and longevity. *eLife*. 2020;9:e62659. <https://doi.org/10.7554/eLife.62659>
49. Timmons L, Court D, Fire A. Ingestion of bacterially expressed dsRNAs can produce specific and potent genetic interference in *Caenorhabditis elegans*. *Gene*. 2001;263(1-2)103-112. [https://doi.org/10.1016/S0378-1119\(00\)00579-5](https://doi.org/10.1016/S0378-1119(00)00579-5)
50. Simmer F, Tijsterman M, Parrish S, Koushika S, Nonet M, Fire A, Ahringer J, Plasterk R. Loss of the putative RNA-directed RNA polymerase RRF-3 makes *C. elegans* hypersensitive to RNAi. *Curr Biol*. 2002;12:1317–1319. [https://doi.org/10.1016/s0960-9822\(02\)01041-2](https://doi.org/10.1016/s0960-9822(02)01041-2)
51. Wood W. The nematode *Caenorhabditis elegans*. *Cold Spring Harb Monogr Arch*. 1988;17.
52. Kamath R, Ahringer J. Genome-wide RNAi screening in *Caenorhabditis elegans*. *Methods*. 2003;30(4):313-321. [https://doi.org/10.1016/S1046-2023\(03\)00050-1](https://doi.org/10.1016/S1046-2023(03)00050-1)
53. Brothers H, Gosztyla M, Robinson S. The Physiological Roles of Amyloid- $\beta$  Peptide Hint at New Ways to Treat Alzheimer's Disease. *Front Aging Neurosci*. 2018; 10:118.  
<https://doi.org/10.3389/fragi.2018.00118>.

## **CHAPTER 4: Mimicking traumatic brain injury in *C. elegans* using custom made devices**

### **4.1 Abstract**

Traumatic brain injury (TBI) is one of the best external predictors of developing Alzheimer's Disease (AD) later in life, but there has yet to be a consistent method for mimicking this in *C. elegans*. In this chapter, we describe the iterative design process for making a device capable of consistent, mechanical trauma of *C. elegans*. We initially began with a microfluidic device as it would allow for the most precise handling of *C. elegans* and allow for imaging immediately before and after trauma. Unfortunately, microfluidic devices were unable to produce sufficient force to induce injury due to pressure limitations; to address this, we developed an alternative 3D-printed guillotine design, named Nematine. The Nematine design uses gravity-controlled force by dropping a coverslip onto immobilized worms on an agarose pad from different heights. The starting height, and thus force, of the coverslip can be precisely controlled using different parameters such as device height and coverslip position. We show that this device can induce severe neuron damage, including complete severing of dendrites in the head. However, 3D printing resulted in rough surfaces that interfered with coverslip movement. Due to the rough surfaces and printer accessibility concerns, we redesigned using more readily available LEGO bricks. The LEGO design provides a high level of precision and smoothness, while maintaining customizability. The LEGO Nematine design can sufficiently injure neurons as well, producing common signs of neuron damage in a pair of head neurons in *C. elegans*.

### **4.2 Introduction**

The exact cause of AD is unknown but there are many predictors of developing the disease<sup>1-3</sup>. One of the best environmental predictors for developing AD and related dementias is TBI<sup>3-6</sup>. There are many theories on how a TBI may contribute to AD. After a TBI, amyloid  $\beta$

(A $\beta$ ) levels have been shown to increase and aggregate but drop back down during recovery<sup>7,8</sup>. It is possible that remnants of these A $\beta$  aggregates could act as seeds for future A $\beta$  aggregates during AD pathology<sup>3-6</sup>. TBI has been shown to disrupt the blood-brain barrier, which could allow for pathogens, immune cells, and other pollutants to penetrate into the brain, causing damage responsible for AD development. The microtubule-associated protein tau's (tau) structure and stability is affected by TBI as well, possibly leading to its aggregation as seen in AD<sup>3-6</sup>. The risks of AD from TBI have been well established in humans, from sources like sports injuries, car crashes, and other direct impact sources<sup>3-6</sup>.

Current models in *C. elegans* connecting TBI and AD have largely been limited to exposure A $\beta$  and tau extracted from mouse models of TBI<sup>9-11</sup>. While this method can induce AD-like effects in the animals, it doesn't directly damage neurons through impact, possibly missing characteristics of TBI that could further contribute to AD. To more accurately reflect how the two may interact, it is necessary to induce both in the organism, rather than relying on mice as the host and *C. elegans* as a biosensor<sup>9-11</sup>. Another more recent model was able to induce minor neuronal damage using surface wave acoustic irradiation<sup>12</sup>. With this model, Miansari et al. were able to induce immediate damage that caused short-term paralysis and learning issues using a microfluidic device. Animals showed impaired chemotaxis, reduced mobility, and reduced learning capacity after exposure<sup>12</sup>. Despite the similarities to human-TBI, these effects were still temporary when compared to the long-lasting effects seen in humans. This discrepancy was likely due to the difference in intensity between typical TBI exposures and the exposure used in their assay. Furthermore, their method is not directed at a specific part of the worm, as it is currently limited to whole-body trauma. Additionally, it is unclear if acoustic wave exposure is sufficient to induce neuronal morphological changes associated with neuron damage, such as

beading/blebbing, dendrite disorganization and loss, or complete neuron loss<sup>13</sup>. The lack of a design capable of mimicking targeted TBI in *C. elegans* highlights the need for a device that can consistently and accurately inflict trauma, producing an observable neuronal injury phenotype.

### **4.3 Results and discussion**

#### **4.3.1 Manual trauma results in inconsistent injury and difficult to control force**

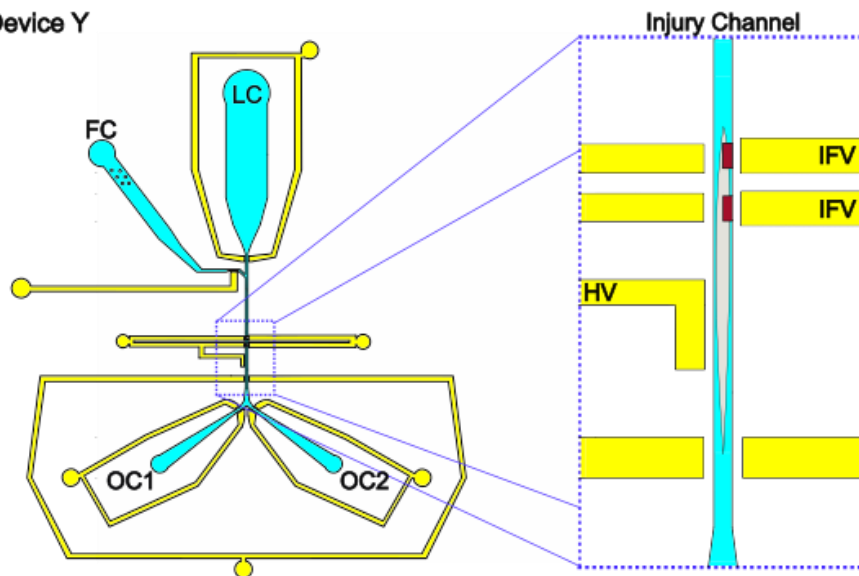
We first sought to confirm that sub-lethal mechanical trauma would be sufficient to induce neuronal injury. To accomplish this, mobile worms were injured with different regimes of manual trauma consisting of manual hits with a platinum wire worm pick. Worms were injured with 1, 5, or 10 hits and then imaged immediately after. While some injury was observed in the worms, force and location of trauma was difficult to manually control, producing inconsistent injury patterns. Worms could have been immobilized to improve consistency of trauma location, but force severity was still a concern. The manual trauma method was abandoned for this reason and for concerns of inconsistency between researchers during administration of the assay.

#### **4.3.2 Microfluidic trauma device fails to produce sufficient injury**

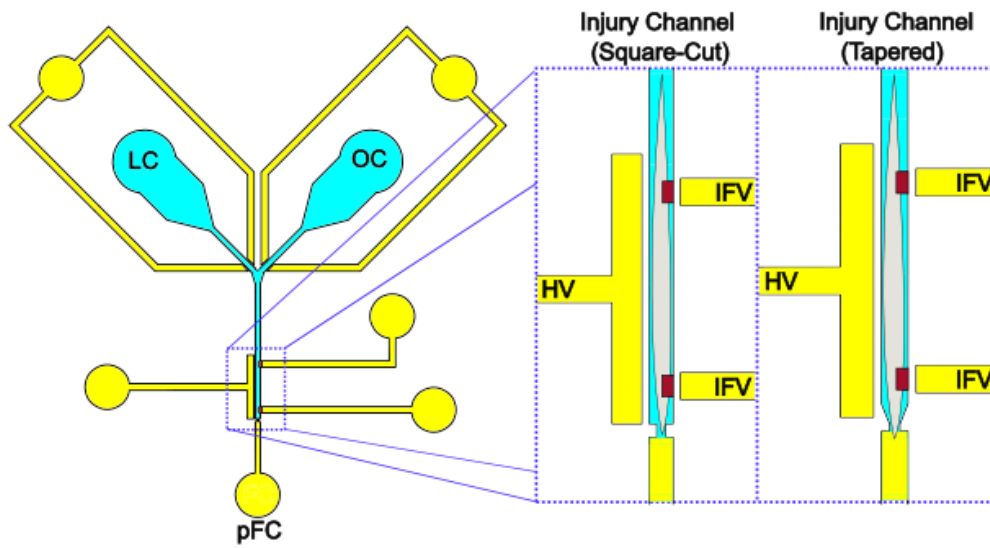
To address concerns with inconsistency, we next opted to use a custom designed PDMS microfluidic device (Fig. 4.1A). The initial device, device Y (DY), was previously designed by Rita Tejada (unpublished) and consists of a loading chamber (LC), injury channel (IC), flush channel (FC), and two outlet channels (OC1 and OC2) that could be selectively closed to sort the animals. Flow in each channel is regulated using pressure valves controlled by a Matlab software designed by Andrew Clark (unpublished). Additionally, within the IC, there are two injury feature valves (IFV) that are actuated to hit an animal once it is in position and a hold valve (HV) to hold animals in position. The IFVs have small protrusions into the IC to assist with their ability to inflict trauma. Animals entered the device through the LC and flow was maintained

**Figure 4.1:** Microfluidic device designs for mechanical injury to mimic TBI. Flow channels are cyan, valves are yellow, injury features are maroon, and example worms are gray. A) Device Y design and layout. Worms enter the device through the loading chamber (LC) and into the injury channel (IC). There they are held in place by the hold valve (HV) and the injury feature valves (IFV) are actuated to injure the worm. This design requires that worms enter the IC tail-first. After injury, the worm is flushed into either outlet channel (OC1 and OC2). The flush channel (FC) is used to move worms through the device. B) Device V design and layout. This device contains a single outlet channel (OC) and pseudo flush channel (pFC). The IFVs are split to allow separate control, eliminating the need for tail-first worms. The HV was lengthened to improve its ability to hold the worm in place. The IC is separated from the pFC by a channel restriction instead of a valve, and this restriction is either square-cut or tapered. C) Device V2 design and layout, similar to Device V with a few changes. Valves on the LC and OC were lengthened to improve flow control. The channel restriction in the IC was replaced with a series of smaller flush channels, to prevent worms from escaping into the pFC and reduce clogging during operation. Shown is the final 10  $\mu\text{m}$  design.

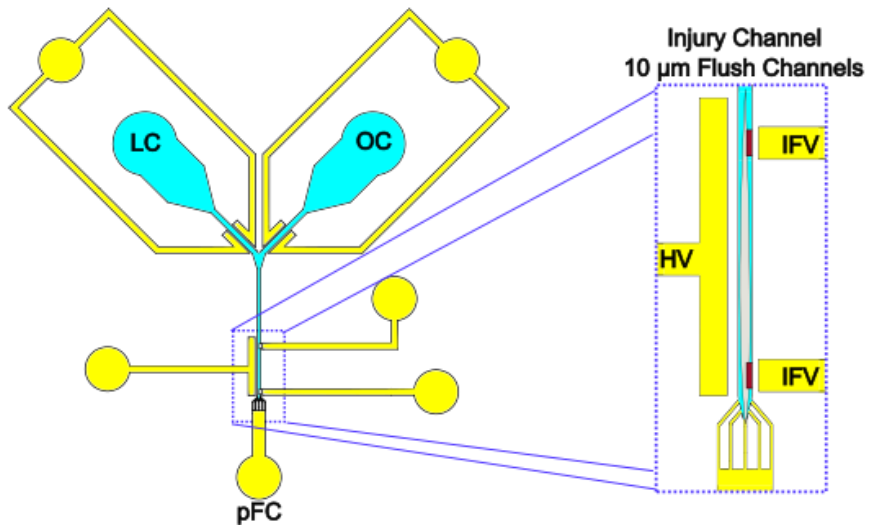
A) Device Y



B) Device V



C) Device V2



until a single animal was in the IC. If multiple animals entered the IC, the FC was opened to flush them back to the LC. Animals were required to enter tail-first, as the injury features were oriented that way. Once a single animal entered tail-first into the IC, the LC was sealed off, and the FC was used to put the animal in position for trauma. Animals were imaged, injured with the desired regime of 1, 5, or 20 hits, imaged again, and then the FC was used to send them to OC1 for collection. Once collected, animals could be monitored for recovery on a plate or in liquid. OC2 was used for clogs, animals which were too young or oriented incorrectly, and other undesirable materials. The trauma regime was controlled for number of hits, duration of hits, time in between hits, and pressure in the IFV. This device had a few key problems that we observed during operation. Firstly, the IC valve used to prevent animals from moving to OC1 and OC2 let animals through, regardless of what pressure was used to close it. Microfluidic valves close by deforming the PDMS and bulging the walls of the channel, but this does not create a perfect seal in the channel<sup>14</sup>. Similar issues also occurred with the LC, OC1, and OC2, valves. While an incomplete seal was expected, pressures necessary for maneuvering worms within the device were too high for the current valve design to contend with. Secondly, although there were two IFVs to allow for animals of different lengths to be injured, they could not be separately actuated in this design. Due to their connection, longer animals receive twice as many hits as shorter animals. Lastly, the IC was too wide, allowing the IFVs to push the animals out of the way rather than injuring them. While these problems could be resolved in this design by small changes in the device, such as increasing valve length and decreasing channel sizes, assembling and operating the device proved to be quite difficult, requiring a larger redesign.

The objective of our next design was not only to solve the problems mentioned above, but to also significantly simplify the design to improve device assembly and operation. To

achieve this, we designed device V (DV) (Fig. 4.1B). Whereas DY had two outlets and five flow valves, DV has a single outlet (OC) and two flow valves. Additionally, we lengthened the two valves by approximately 50% to improve their ability to block flow. Like DY, animals enter the device through the LC and flow into the IC. The IC width was decreased from 80  $\mu\text{m}$  to 50  $\mu\text{m}$ , which is the approximate width of the animals used in this work. We split the IFVs so that they could be actuated separately and spaced them such that we could injure animals whether they entered head- or tail-first. This change reduced the loss of ~50% of worms loaded into the device with DY down to < 5%. There are two versions of this change which vary the spacing of the IFVs, to allow for injuring of different sections of the animal. The HV was lengthened to improve its ability as well. Rather than an FC controlled by a valve, we constricted the IC after the IFVs to prevent animals from flowing through. This created a pseudo-FC (pFC), with which we could pull or push fluid through to position the animal in the IC. The pFC had two different constriction point designs, square-cut or tapered, to improve positioning of animals during trauma. After imaging and the trauma regime, animals would be flushed out of the device through the OC using flow from the pFC and collected for further observation. DV attempted to address challenges with DY, and succeeded in decreasing device complexity, improving IFV location and function, and almost eliminating animal loss due to positioning and orientation. Unfortunately, the constriction of the IC was not sufficient to prevent animals from escaping into the pFC at high flow rates. The constriction also increased clogging since it could not be actuated to allow detritus to flow through. Additionally, although the valves were lengthened, a 50% increase was not sufficient to prevent animal flow through. Although DV had several issues, there were significant improvements when compared to DY.

To address the issues with DV, it was minorly redesigned to generate device V2 (DV2) (Fig. 4.1C). DV2 had two major changes: significantly increased valve length and a complete redesign of the IC constriction; DV2 operated in much the same way as DV otherwise. The valve length was increased from 150% to ~450%, which eliminated problems with animal flow through. The constriction point was redesigned to have multiple smaller channels connecting to the IC. We generated multiple versions of this redesign, varying the small channel width from 8 to 12  $\mu\text{m}$ . The 12  $\mu\text{m}$  width was too large for high flow rates, but 10  $\mu\text{m}$  or less was sufficient for preventing animal flow through. We chose to continue with the 10  $\mu\text{m}$  design, as decreasing the channel width further provided no benefit and required higher pressures to achieve the same flow rates. Five channels were added to improve the design against clogging, as up to 3 channels can clog before the device sees significant drops in functionality. This resulted in the final device DV2-10 (Fig 4.1C).

To ascertain the device's ability to mimic TBI, we used the strain BY200, which expresses GFP in six dopaminergic head neurons<sup>15</sup>. Animals were injured in regimes of up to 20 hits, with 0.5 sec. duration and spacing between hits. All of the tested trauma regimes failed to produce injury levels detectable above baseline levels, both immediately after trauma and within 24 hrs. of recovery. This failure was likely due to the level of force that the IFVs can apply without bursting. Additionally, as the PDMS used is semi-flexible to allow for control of valves by pressure and the worms lack a hard exterior, we suspect that the worm was moved and deformed by the IFVs rather than taking the direct force of the hit. The pressure limitation and lack of direct hit highlighted a major issue with PDMS microfluidic devices for this application. Their flexibility severely hindered their ability to produce a solid hit for trauma to induce injury.

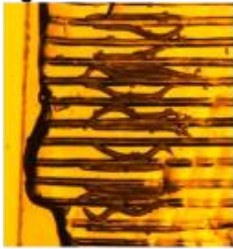
### **4.3.3 3D-Printed and LEGO injury devices induce severe neuronal damage in dopaminergic head neurons**

To eliminate the need for microfluidics since they were unable to produce the necessary blunt force for injury, we opted for a 3D-printed design using a filament printer. For the initial design, we aimed to meet three criteria: control, simplicity, and reproducibility. To meet these goals, we designed the wDrop (Fig. 4.2A). This device inflicts trauma by holding a coverslip in place to drop on immobilized worms on an agar pad below. The wDrop consists of a base brick and multiple stackable bricks, with each brick having slots in each corner to hold the brick above it in place. Immobilized worms are aligned on an agarose pad, imprinted with a music record or similar object which creates lanes, which is loaded into the injury slot on the bottom of the base brick. The worms are positioned such that they are straight, and their heads are injured near the anterior pharyngeal bulb. Depending on the severity of injury desired, trauma could be inflicted with either the base alone, or the base and additional stacked bricks to add height. A coverslip, chosen for its light weight and small thickness, is dropped through the drop slot on top of the device. This follows the channel to the bottom of the device where the coverslip strikes the worms loaded into the injury slot, resulting in a blunt force trauma. The wDrop design meets the first criteria, control, as the force of the impact onto the animal's head is directly controlled through gravity. Force is altered by changing the number of stackable bricks used, the weight of

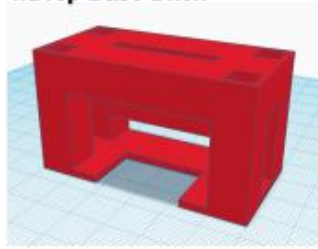
**Figure 4.2:** 3D printed and LEGO Nematine designs and injury. A) wDrop design overview. (Left) Agar pad that was imprinted onto a music record to generate lanes for aligning worms during injury. Each lane is wide enough for 1-2 worms to be aligned in. Worms were paralyzed with 2 mM tetramisole to assist in positioning. (Middle) wDrop base brick, with a slot on top for dropping the coverslip into for injury. Underneath is a slot to position the coverslip containing the agar pad and worms during injury. (Right) Stackable wDrop brick, used to increase height and thus severity of the injury. B) Guillotine-based 3D-printed Nematine design. The blade and tracks are indicated with arrows. C) Preliminary images collected from BY200 worms with the 3D-printed Nematine. Uninjured worms show little to no defects in the dendrites. Injured worms show significant blebbing (cyan arrows) or complete severing (yellow arrows) of the dendrites. Neuronal cell bodies are indicated with green stars. D) LEGO Nematine design. The blade and tracks are indicated with arrows. E) Preliminary image collected from BY200 worms with the LEGO Nematine. Injured worms show similar blebbing (cyan arrows) injury patterns as worms injured with the 3D-printed Nematine. Neuronal cell bodies are indicated with green stars.

A)

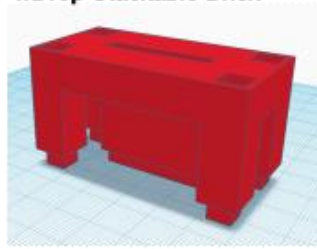
Agar Pad



wDrop Base Brick

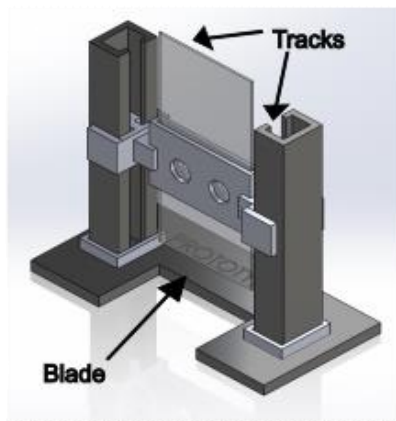


wDrop Stackable Brick

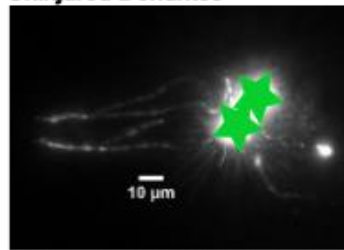


B)

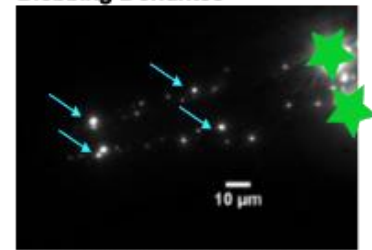
Nematine Device



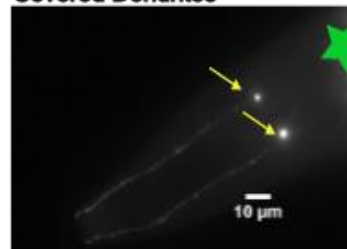
C) Uninjured Dendrites



Blebbing Dendrites

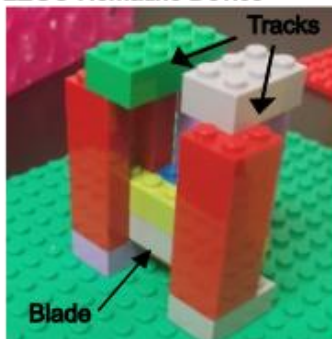


Severed Dendrites



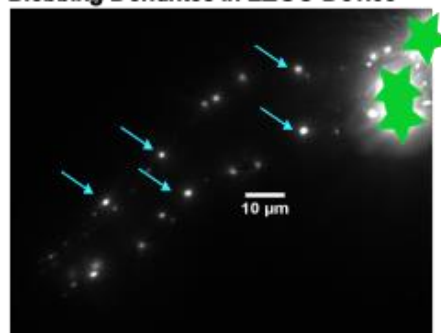
D)

LEGO Nematine Device



E)

Blebbing Dendrites in LEGO Device



the coverslip dropped, and the height of each brick. To accelerate testing of multiple drop heights we printed stackable bricks of multiple heights beforehand. The design also meets the second criteria, simplicity, as operating the device requires only lining up the worms on an agarose pad and dropping the injury coverslip. Additionally, the force of impact of the coverslip is easily calculated using the drop height and coverslip weight. Unfortunately, achieving reproducibility presented several problems. When the injury coverslip is dropped, it gets caught and slowed down by the channel designed to guide it down to the worms. The 3D printing method utilized in production of the device results in rough surfaces, providing many defects in the channel for the coverslip to catch on. The roughness of the material is a product of using a filament 3D printer, as this prints the device in layers, resulting in significant ridges on the surface. While resin 3D printing could prevent this, resin 3D printers are less accessible and have higher material and operating costs, which discouraged their use. The device surfaces could have been improved through sanding the channel to smooth the drop and using a lubricant, but the channel was too narrow for sanding and using a lubricant introduces a possible contaminant onto the worms when they're hit by the coverslip. Additionally, after the injury coverslip is dropped, the device didn't have a way to lift the coverslip up off the worms. This requires manually lifting the coverslip, which introduces further trauma than intended, often decapitating the worms in the process.

To address the problems with wDrop, we redesigned the entire device, instead modeling it after a guillotine. The new device, the Nematine, retains several of the properties of the wDrop, such as a slot for the worm coverslip and gravity-controlled force, but significantly alters how the injury coverslip is dropped (Fig 4.2B). The coverslip is instead glued into a 3D-printed holder, and this acts as the "blade" of the Nematine. The blade is guided by two tracks on each side, which ensure it falls in the place each time. These are also larger than the channel in the

wDrop, allowing for smoothing to improve drop accuracy. The blade is not contained within the device either, allowing for it to be easily lifted off the worms after trauma. To test the device's ability to mimic TBI, we used the BY200 strain mentioned above and ascertained neuronal damage after a single hit. Animals were loaded onto a coverslip and injured by a single hit at max device height, and then fluorescently imaged to examine neuronal injury. Animals injured with a single hit showed significant neuron damage, including beading/blebbing and complete severing of dendrites in the CEP head neurons (Fig. 4.2C). This indicates that the Nematine can adequately mimic several aspects of TBI and neuronal damage. However, despite the Nematine's success in this aspect, the design still had a significant problem with reproducibility. Although we were able to smooth the blade tracks with sandpaper, the surface was still not smooth enough to prevent the blade from catching or slowing as it falls. When the blade catches on the tracks, it hits the agarose pad and worms at an angle, producing an uneven hit pattern; this resulted in approximately 50% of blade drops being discarded, as it was unclear which worms were injured correctly and which weren't. The low success rate of Nematine trauma and limited access to resin printers indicated that 3D printing was not ideal to meet our goals of accessibility and reproducibility.

Luckily, there is another readily available material that has been previously used in DIY lab devices: LEGOs<sup>15,16</sup>. LEGO devices offer significant advantages over 3D printed devices: bricks are injection-molded, creating a smooth finish, inexpensive and widely available, and allow for easy device modification. Utilizing LEGO bricks, we retained the original Nematine design, making only minor changes to accommodate for the bricks size and shape (Fig 4.2D). The blade has two variations, one using a coverslip to hit the animals and another using a LEGO brick directly. The smoothness of the LEGO bricks eliminated problems with the blade catching

and slowing down. The drop height is easily modifiable by changing the number of bricks used. The blade is slightly heavier with the LEGO design, but this can be adjusted for by using shorter device heights and cutting off excess weight of the blade. Additionally, multiple blades allow for multiple hit “types” based on whether the hit was with a coverslip or LEGO brick. The LEGO Nematine produces similar injury patterns as the 3D-printed Nematine, indicating that despite the material change, the device retains similar functions (Fig 4.2E). Preliminary testing with this device showed increased beading in injured worms. This project and further testing are currently under development by Kin Gomez and Noah Torreyson.

## **4.4 Material and methods**

### **4.4.1 Strains, media, and culture**

*C. elegans* was maintained on standard Nematode Growth Medium (NGM) plates seeded with OP50 *E. coli* bacteria and kept at 20 °C unless otherwise stated<sup>17</sup>. Age-synchronization for experiments was performed by washing plates with a 1 mL of a solution of M9 media supplemented with 0.01% v/v TX-100 (M9TX). Worms were allowed to settle, and supernatant was removed and replaced with 1 mL of 1:2:1 mixture of bleach, 1M NaOH, and water. Once eggs were released, they were washed 3 times with 1 mL M9TX, and transferred to fresh plates. The BY200 strain was used for all experiments in this work<sup>18</sup>.

### **4.4.2 Microfluidic device design, assembly, and use**

The microfluidic devices used in this study were designed and fabricated through standard photo and soft-lithography techniques with the help of Andrew Clark<sup>19</sup>. The designs were created using AutoCAD to modify a previous design of another student in the lab, Rita Tejada Vaprio (Unpublished design). The device was operated using a pressure box and MATLAB code designed by Andrew Clark (Unpublished work). In short, age-synchronized worms were loaded into the injury chamber, imaged, hit with the desired injury regime, imaged again, and then flushed from the device into a collection chamber. Animals were immobilized in the injury channel using 5 mM tetramisole in M9 media and the hold valve. Image Z-stacks were collected using a 40x objective and GFP excitation/emission filter with a 0.5 μm step size. If further monitoring was required, worms were transferred to a fresh plate and stored at 20 °C.

### **4.4.3 3D-printed device design and use**

The 3D-printed devices were designed using the online Tinkercad software. Designs were collaboratively designed by James Lichty, Daisy Aguilar, Kin Gomez, and Noah Torreyson.

These were then printed by the NCSU library's 3D-printing services. To injure worms with a device, age-synchronized worms were loaded onto an agar pad imprinted from vinyl record. This gave the agar pad channels which were used to line up the worms. The worms were immobilized with a 10 mM tetramisole solution. The agar pad was lined up with the injury feature of the device and the feature was dropped to hit the worms for the desired injury regime. The worms were then imaged using fluorescent microscopy using the settings described above.

#### **4.4.4 LEGO device design and use**

The LEGO device was designed to mimic the 3D-printed design. Designs were collaboratively designed by James Lichty, Daisy Aguilar, Kin Gomez, and Noah Torreyson. Device designs were tested in the same way as the 3D-printed designs as described above.

## 4.5 References

1. John Hardy, Valentina Escott-Price, Genes, pathways and risk prediction in Alzheimer's disease, *Human Molecular Genetics*, Volume 28, Issue R2, 15 October 2019, Pages R235–R240, <https://doi.org/10.1093/hmg/ddz163>
2. Bendlin B, Carlsson C, Gleason C, Johnson S, Sodhi A, Gallagher C, Puglielli L, Engelman C, Ries M, Xu G, Wharton W, Asthana S. Midlife predictors of Alzheimer's disease. *Maturitas*. 2010;65(2):131-137. <https://doi.org/10.1016/j.maturitas.2009.12.014>
3. Ramos-Cejudo J, Wisniewski T, Marmar C, Zetterberg H, Blennow K, de Leon MJ, Fossati S. Traumatic Brain Injury and Alzheimer's Disease: The Cerebrovascular Link. *EBioMedicine*. 2018 Feb;28:21-30. doi: 10.1016/j.ebiom.2018.01.021. Epub 2018 Jan 31. PMID: 29396300; PMCID: PMC5835563.
4. Mielke MM, Ransom JE, Mandrekar J, Turcano P, Savica R, Brown AW. Traumatic Brain Injury and Risk of Alzheimer's Disease and Related Dementias in the Population. *J Alzheimers Dis*. 2022;88(3):1049-1059. doi: 10.3233/JAD-220159. PMID: 35723103; PMCID: PMC9378485.
5. Ramos-Cejudo J, Wisniewski T, Marmar C, Zetterberg H, Blennow K, Leon M, Fossati S. Traumatic Brain Injury and Alzheimer's Disease: The Cerebrovascular Link. *eBioMedicine*. 2018;28:21-30. <https://doi.org/10.1016/j.ebiom.2018.01.021>
6. Li L, Liang J, Fu H. An update on the association between traumatic brain injury and Alzheimer's disease: Focus on Tau pathology and synaptic dysfunction. *Neuroscience and Biobehavioral Reviews*. 2021;120:372-386. <https://doi.org/10.1016/j.neubiorev.2020.10.020>

7. [Johnson, V., Stewart, W. & Smith, D. Traumatic brain injury and amyloid- \$\beta\$  pathology: a link to Alzheimer's disease?. \*Nat Rev Neurosci\* \*\*11\*\*, 361–370 \(2010\).](#)  
<https://doi.org/10.1038/nrn2808>
8. [Edwards G, Moreno-Gonzalez I, Soto C. Amyloid-beta and tau pathology following repetitive mild traumatic brain injury. \*Biochemical and Biophysical Research Communications\*. 2017;483\(4\):1137-1142. <https://doi.org/10.1016/j.bbrc.2016.07.123>](#)
9. Zanier E, Barzago M, Vegliante G, Romeo M, Restelli E, Bertani I, Natale C, Colnaghi L, Colombo L, Russo L, Micotti E, Fioriti L, Chiesa R, Diomedede L. *C. elegans* detects toxicity of traumatic brain injury generated tau. *Neurobiology of Disease*. 2021;153:105330. <https://doi.org/10.1016/j.nbd.2021.105330>
10. Diomedede, L., Zanier, E.R., Moro, F. *et al.* A $\beta$ 1-6A<sub>2V</sub>(D) peptide, effective on A $\beta$  aggregation, inhibits tau misfolding and protects the brain after traumatic brain injury. *Mol Psychiatry* **28**, 2433–2444 (2023). <https://doi.org/10.1038/s41380-023-02101-3>
11. Yang Y, Wang M, Yang P, Wang Z, Huang L, Xu J, Wang W, Yu M, Bu L, Fei J, Huang F. The A $\beta$  Containing Brain Extracts Having Different Effects in Alzheimer's Disease Transgenic *Caenorhabditis elegans* and Mice. *Frontiers in Aging Neuroscience*. 2018;10. <https://doi.org/10.3389/fnagi.2018.00208>
12. Miansari, M., Mehta, M.D., Schilling, J.M. *et al.* Inducing Mild Traumatic Brain Injury in *C. elegans* via Cavitation-Free Surface Acoustic Wave-Driven Ultrasonic Irradiation. *Sci Rep* **9**, 12775 (2019). <https://doi.org/10.1038/s41598-019-47295-1>
13. Peng CY, Chen CH, Hsu JM, Pan CL. *C. elegans* model of neuronal aging. *Commun Integr Biol*. 2011 Nov 1;4(6):696-8. doi: 10.4161/cib.17138.

14. Unger, M. A., Chou, H.-P., Thorsen, T., Axel, S. & Quake, S. R. Monolithic microfabricated valves and pumps by multilayer soft lithography. *Science* **288**, 113–116 (2000). [DOI: 10.1126/science.288.5463.113](https://doi.org/10.1126/science.288.5463.113)
15. L. C. Gerber, A. Calasanz-Kaiser, L. Hyman, K. Voitiuk, U. Patil, I. H. Riedel-Kruse, *PLoS Biol.* 2017, **15**, 2001413.
16. Hajam M, Khan M. Microfluidics: a concise review of the history, principles, design, applications, and future outlook. *Biomaterials Science*. 2024;2. <https://doi.org/10.1039/D3BM01463K>
17. Wood W. The nematode *Caenorhabditis elegans*. Cold Spring Harb Monogr Arch. 1988;17.
18. Ray A., Martinez B., Berkowitz L., Caldwell G., Caldwell K. Mitochondrial dysfunction, oxidative stress, and neurodegeneration elicited by a bacterial metabolite in a *C. elegans* Parkinson's model. *Cell Death and Disease*. 2014;5:e984. <https://doi.org/10.1038/cddis.2013.513>
19. Clark A., San Miguel A. A bioinspired, passive microfluidic lobe filtration system. *Lab on a Chip*. 2021;19. <https://doi.org/10.1039/D1LC00449B>

## CHAPTER 5: Gutbow: Labeling *C. elegans* for pooled screens

### 5.1 Abstract

A major advantage of using *C. elegans* as a model for Alzheimer's and other diseases is the ease with which large populations can be generated to facilitate drug screens. These screens require a large number of separate populations so that a wide array of drugs and genes can be tested at once. However, a difficulty with these screens is the high material and time costs, due to managing so many populations during drug exposure, effectiveness assaying, and data collection. *C. elegans* are visually indistinguishable from each other, requiring that each treatment group of animals be kept separate to track the effects of a treatment. Drug effectiveness assays involving chemical exposure, animal fitness, or similar complex experiments would need to be replicated for each treatment group, multiplying the resources and time necessary. Although possible, throughput on assaying each group individually would be severely limited by the length of the assay and difficulty of data collection. Labeling animals is a possible method to address this problem, as labeled groups can be pooled together for a single assay but has several caveats that prevent its widespread use. While there are phenotypical markers, such as roller and dumpy phenotypes, that allow for visually identifying different worms, these markers are not always visually distinct, and can affect the animal's response to a drug or assay. Other markers, such as fluorescent markers, run into similar issues, as well as interfering with any fluorescent output an experiment examines. Throughput of drug screens is often improved with microfluidic devices, as these can automate handling of animals during assaying and data collection. The devices fail to address the core problem though, as animals still need to be kept physically separate during assaying and data collection. The scope of these screens, despite microfluidic devices, are limited by a combination of the material costs, time costs, and variety of markers available. In this

chapter, we describe a method for labeling worms with an inducible fluorescent marker from an *E. coli* food source library, Gutbow. This library does not directly modify the worm's genetics, instead relying on colonization of the worm gut with a fluorescent bacterial strain. Worms are fed a unique fluorescent *E. coli* strain from the library, colonizing their gut with a bacterial label associated with a drug treatment. These animals are then pooled together for a single effectiveness assay, such as environmental stress, chemical exposure, or fitness assay. During data collection, the fluorescent protein in the *E. coli* is induced to reactivate the label, allowing for the connection of results to initial drug treatment. The label is inducible to prevent interference with fluorescent signals during data collection and allow for blinding during the assay. We show that fluorescent bacteria can be visually detected in worms for up to 3 days after the initial feeding, allowing this method to be applied to a wide range of assay types. We designed the *E. coli* library using a randomized construct containing a combination of fluorescent markers, with a theoretical maximum of 1024 variations. The library significantly improves the number of labels available for use in *C. elegans* and can be implemented alongside most microfluidic devices used in drug screens. The combination of our technique and current microfluidic designs would both improve throughput through automation and reduce the associated costs by requiring only a single effectiveness assay. Additionally, as Gutbow does not require genetically modifying the worms, other researchers can easily adapt it for use in already established drug screening pipelines by simply altering the food source during drug exposure.

## **5.2 Introduction**

Large scale drug screening assays utilizing *C. elegans* suffer from a major limitation in that they require sacrificing resolution to limit material and time costs of managing large numbers of populations<sup>1-3</sup>. In a typical drug screening assay, a large starting population of *C.*

*elegans* is split into treatment groups. These treatment groups are then each exposed to a different drug of interest from a library. A goal with drug screens is typically to cover as many drugs at once as possible, to limit the number of rounds necessary to screen the entire library. This goal poses a problem though, as each of these different treatment groups need to undergo the same assay, to ascertain each drug's effectiveness. To prevent multiple rounds of screening, many replicates of the same assay need to be run simultaneously, requiring a high amount of labor to manage each of the assays. Each assay needs to be kept separate as well, as the worms, and thus treatment groups, are indistinguishable from each other, multiplying the material costs by the number of drugs being tested<sup>4</sup>. The labor required at one time could be reduced by running multiple rounds of assays, but depending on the treatment method and testing assay, this could significantly increase the time required. That solution would also not reduce the total amount of labor required, just spread it out over time. To address problems with the size and scope of drug screens, a solution would need to reduce the costs of handling many groups of animals, reduce the number of assays necessary for the screen, or increase the throughput of assaying and data collection.

There are multiple avenues to address concerns over a drug screen's size and scope. One such method is to reduce labor costs by automating parts of the process; microfluidic devices are a common way to do this<sup>5-9</sup>. These devices designed for use in drug screens typically work by separately exposing animals to drugs and then automating the assay and data collection steps inside the device<sup>5-9</sup>. Several of these devices boast a throughput orders of magnitude higher than what one could achieve manually, but still exhibit many limitations that prevent their widespread use<sup>5,7,8</sup>. One such limitation is the lack of accessibility to materials and personnel required for these microfluidic devices. Mondal et al. developed a microfluidic chip device capable of

automating fluorescence imaging of a protein aggregation model; the device allowed imaging of almost 14,000 animals per hour, a rate not achievable through manual imaging<sup>5</sup>. However, that rate requires accurately printing, assembling, and running microfluidic chips containing 96 separate devices, each containing multiple imaging channels, and specialized software to automatically collect and analyze images<sup>5</sup>. Drug screening devices such as this can be quite complex both in operation and assembly, and labs not experienced in microfluidics will not be able to utilize them effectively. Additionally, designs like the Mondal et al. device are typically specialized for one purpose, in this case, fluorescent imaging of poly-glutamine<sup>5</sup>. While not impossible, altering a device such as this requires a high level of understanding in both microfluidics and image analysis; specialization can increase the throughput of a device but restrict its adaptation for other purposes. Decreasing the complexity of a device can combat these restrictions to improve both adaptability and ease of use, but will limit throughput, as in the Chung et al. and Caceres et al. designs<sup>6,9</sup>. Both of these devices contain a single imaging channel, dramatically decreasing complexity, but increasing data collection time and requiring a separate device for each treatment group<sup>6,9</sup>. Regardless of device used, none of the above designs reduce assay costs, as each treatment group undergoes the effectiveness assay individually. Also, by keeping groups physically separate, the above designs also introduce variability into the experiments, as each treatment group may experience different conditions within the devices. While microfluidics work to improve many experiments, there remains a need for a microfluidic-independent way of improving drug screens.

Another possible way to address problems with drug screens is to visually label drug treatment groups and then combine them into one group during the assay and data collection portions. These labels could take the form of a behavioral or physical phenotype, such roller and

dumpy worms, or as fluorescent marker inside the worm, generated through a microinjected marker<sup>10,11</sup>. This method would reduce the material and labor costs of these steps by not requiring that each treatment group be individually assayed, only slightly increasing the duration of data collection to read each label. Additionally, visual labeling isn't mutually exclusive with microfluidic devices, allowing for utilization of both simultaneously; an experimental setup could use this method to label each treatment group and then pool all groups in a single device. A combined method would reduce the material costs of running the assay with labeling, while simultaneously reducing labor and time costs of collecting data with the microfluidic device. Labeling isn't used in drug screens though, as the scale of the screens is typically many orders of magnitude larger than the number of available markers. An attempt to increase the number of available markers, NeuroPAL, utilized a few fluorescent markers to label each neuron in *C. elegans*<sup>12</sup>. NeuroPAL relied on the ratios and location of each fluorescent protein to identify each neuron, dramatically increasing the number of "labels", without needing more fluorescent proteins. While labeling worms in a drug screen couldn't rely on label position, a similar method could be developed using fluorescent protein ratios. Inserting the marker would need to be done with care, as it may interfere with the drug treatment or assay, such as in the microfluidic devices described above<sup>5-9</sup>. Those devices rely on a fluorescent signal as an output, and introducing fluorescent markers may cause spectral overlap, convoluting the data unnecessarily. In non-fluorescence-based assays, a fluorescent marker could influence the animal's response such as seen in Chapter 3, changing the results of a stress assay. As these markers are typically always visible, blinding an assay can also prove difficult, as the label would need to be actively avoided. Lastly, managing the populations required to maintain the number of fluorescent markers necessary for a drug screen would require significantly more effort than current methods;

differentially marked strains would need to be stored, grown, and prepared separately before each drug exposure rather than a single population as is used currently. For these reasons, utilizing a microinjected fluorescent marker isn't feasible for drug screening; a microfluidic-independent, label-based method for improving drug screens needs to overcome the current issues with labeling worms to be viable.

## **5.3 Results and discussion**

### **5.3.1 Gutbow overview**

A microfluidic-independent method for visually labeling would need to overcome the following problems before it could be implemented in drug screens:

1. Labels should have a wide variety, to have a similar magnitude of options as drugs in a drug screen.
2. Labels need to have minimal effect on worm health, behavior, etc., to prevent interference with assay outputs.
3. Labels need to be designed such that they produce little interference in assay output and data collection and allow for blinding of experiments.

To address the above problems, we designed an *E. coli*-based system for fluorescently labeling *C. elegans*, Gutbow (Fig. 5.1). Gutbow utilizes an *E. coli* library containing 1024 variations of the same construct expressing fluorescent proteins. The system is designed such that worms are fed an *E. coli* strain from the library before and during drug exposure. This strain colonizes their gut, "labeling" them. During or after data collection, the label is activated with isopropyl  $\beta$ -D-1-thiogalactopyranoside (IPTG) to produce a fluorescent signal, identifying which drug treatment that worm received. This allows for the results for each worm to be connected directly to its drug treatment, without needing to keep each treatment group separate during the assay.

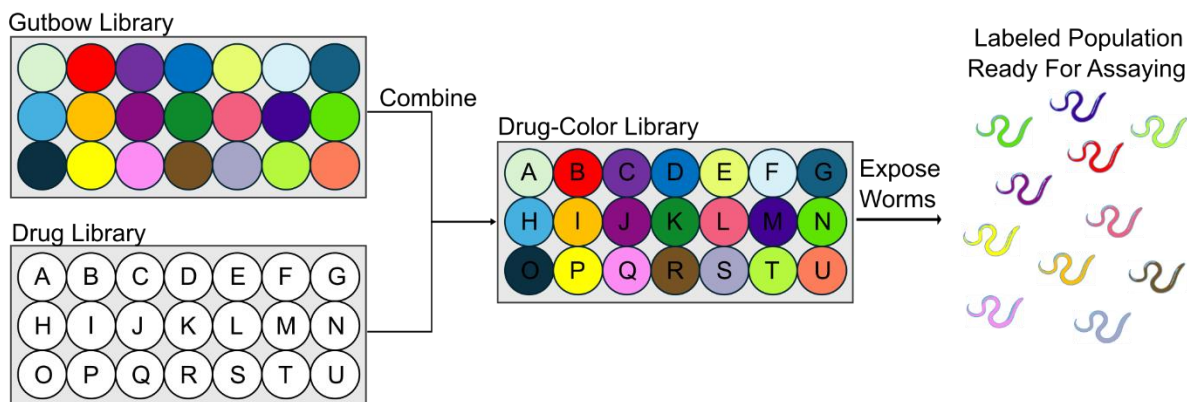


**Figure 5.1:** Proposed Gutbow method for labeling worms during a drug screen. The Gutbow library is combined with a drug library to associate each drug with a specific Gutbow label. This drug-color library is then exposed to worms, allowing for the drug to take effect and for the Gutbow label to colonize the worm gut. These worms can then be combined into a single population for assaying. During or after data collection, the Gutbow label can be reread for each worm to connect the worm’s results with the drug treatment it received.

### 5.3.2 Gutbow Design and Considerations

During the design Gutbow, we first sought to eliminate the issues with traditional fluorescent labeling methods, as this class of labels are simple to identify utilizing fluorescent imaging. To expand the repertoire of fluorescent labels available, we adopted a NeuroPAL-like method<sup>12</sup>, expressing multiple proteins to generate a combinatorial label, but not within *C. elegans*. Expressing the number of labels necessary for a drug screen would require managing those strains before, during, and after the screen, needing more effort than current methods. Additionally, as seen in Chapter 3, fluorescent labels can influence stress response when expressed in neurons. Rather than risk Gutbow creating a similar effect in a worm tissue and requiring management of that many strains, we eliminated these two concerns by expressing the fluorescent labels in their *E. coli* food source. *E. coli* is well established as a food source for *C. elegans*, and other methods, such as RNAi suppression by feeding dsRNA-expressing bacteria, make use of this fact<sup>13-15</sup>. To ascertain *E. coli*’s ability to colonize the worm gut, wild-type N2 *C. elegans* were fed two different fluorescent *E. coli* strains in a preliminary experiment: an RFP

strain and GFP strain. The bacteria's ability to colonize the worm gut was necessary, as during a drug screen using Gutbow, animals would be pooled for the effectiveness assay after drug exposure and labeling requiring a separate non-fluorescent food source, such as *E. coli* OP50<sup>13</sup>; using the same Gutbow food source would contaminate each treatment group with labels from other groups. Many assays require less than 48 hrs. to run, such as examining neuronal morphology, stress survival, or chemical exposure<sup>16-18</sup>; the target colonization duration was set at 48 hrs. Worms were fed one of the strains for 24 hrs. starting from larval stage 4. After those initial 24 hrs. worms were washed several times and then transferred to non-fluorescent OP50 *E. coli*. Optimally, the fluorescent bacteria would be detected within the worm gut using fluorescent imaging, as this would allow for detection during data collection. As it was unclear if this would be sufficient, an alternative method of transferring a worm to LB media to culture its feces was also employed. Both methods would rely on visual detection of any signal with fluorescence microscopy; if fluorescent signal could not be visually observed to 48 hrs. fluorescent imaging would be employed to increase the sensitivity of detection. Every 24 hrs. after transfer to OP50, worms were examined for the presence of fluorescent bacteria in their gut and a single worm was transferred to LB media to grow bacteria from its gut overnight. The overnight growth was checked for fluorescence the following day. We observed fluorescent signal from both food sources detectable in the worm gut every day consistently up to 3 days after transfer to OP50. Fluorescent signal was observed in the overnight growth of worms taken each day for up to 5 days after transfer to OP50. The preliminary experiment was not continued past 5 days. This indicated that *E. coli* was able to colonize the worm gut and remain colonized for up to 3 days after transfer to a new food source. This period is long enough for many experimental assays<sup>16-18</sup>, which typically last less than 48 hrs. The *E. coli* strain BL21 (DE3) was used as the base strain

for the library due to its improved protein production capabilities<sup>19</sup>. Additionally, this strain is a derivative of the strain used in the Ahringer RNAi Library<sup>15</sup>, which acts as a food source in RNAi genetic screens. As the food source used to feed *C. elegans* can have significant impacts on the animal's health<sup>20</sup>, utilizing a closely-related strain to well-established method, such as RNAi suppression by feeding dsRNA-expressing bacteria<sup>13-15</sup>, eliminates concerns regarding these health effects.

Once the base strain was chosen, we next focused on the construct design. Gutbow requires a variety of fluorescent labels similar in magnitude of size to some drug libraries to be effective<sup>21-22</sup>. As available fluorescent wavelengths are limited due to spectral overlap and the number of fluorescent proteins is not infinite, we utilized a modified method similar to NeuroPAL<sup>12</sup>; specifically, using fluorescent ratios of different proteins to generate unique labels. By measuring the ratios of different proteins with fluorescence microscopy or similar method, if those protein levels can be carefully controlled, unique “colors” are created through association with a specific ratio. Once *E. coli* expressing these colors colonizes a worm's gut, that worm can be identified by measuring the ratios of the fluorescent proteins. To produce the ratios, we designed a library of constructs containing 5 fluorescent proteins under a single promoter creating a polycistronic insert. The fluorescent proteins in each construct are randomized from a selection of GFP, RFP, eBFP, and YFP<sup>23</sup>, such that a construct can have multiple copies of a single protein, but no more than 5 total. We theorized that the levels of each protein in a strain are dictated by the number of copies in the construct and distance from the first translational initiation site<sup>24</sup>. An additional level of control is added by using the T5 promoter<sup>25</sup>, an IPTG-inducible promoter, so protein levels can be further modulated by altering IPTG concentration.

This promoter has an added benefit of allowing labels to be turned “off” during data collection to prevent interference with assay outputs and allow for proper blinding of experiments.

Manually generating that many unique constructs using traditional cloning methods requires a large amount of labor. To simplify the process, we used Goldengate assembly. Goldengate assembly generates a construct by cleaving restriction sites, typically Bsa1, on each DNA piece to produce sticky ends. Each sticky end will have a corresponding sticky end on another piece of DNA. During the assembly, corresponding sticky ends match and are annealed to produce the entire construct. We designed our construct such that it consisted of a backbone and 5 inserts, each with their own corresponding pair of sticky ends. Although including more inserts meant more variants in the final library, the construct was limited to 5 inserts, as according to the NEBridge Golden Gate Assembly kit (NEB, E1601S), that number was a good balance between efficiency and length. Based on that number of inserts, we chose the 4 fluorescent proteins, GFP, RFP, eBFP, and YFP<sup>23</sup>, as inserting those into the construct randomly would give up to 1024 ( $4^5$ ) different combinations, assuming each position and copy number combination can produce a unique signal. The fluorescent proteins were chosen as they are common colors used in *C. elegans* research, such that a high proportion of labs would have access to imaging equipment capable of measuring them. Although there is some overlap in their spectra, by measuring the ratios of signal for each protein, we theorized that each construct in the library would produce a unique identifier, similar to that of NeuroPAL<sup>12</sup>. Identification of a label would require four measurements, one for each of the available proteins (Fig 5.2). While some variants will contain the same combination of colors, we also theorize that each position in the construct will result in different expression levels due to the regulation of polycistronic mRNA during translation<sup>24</sup>. This difference in expression level would fluctuate the fluorescent signal of

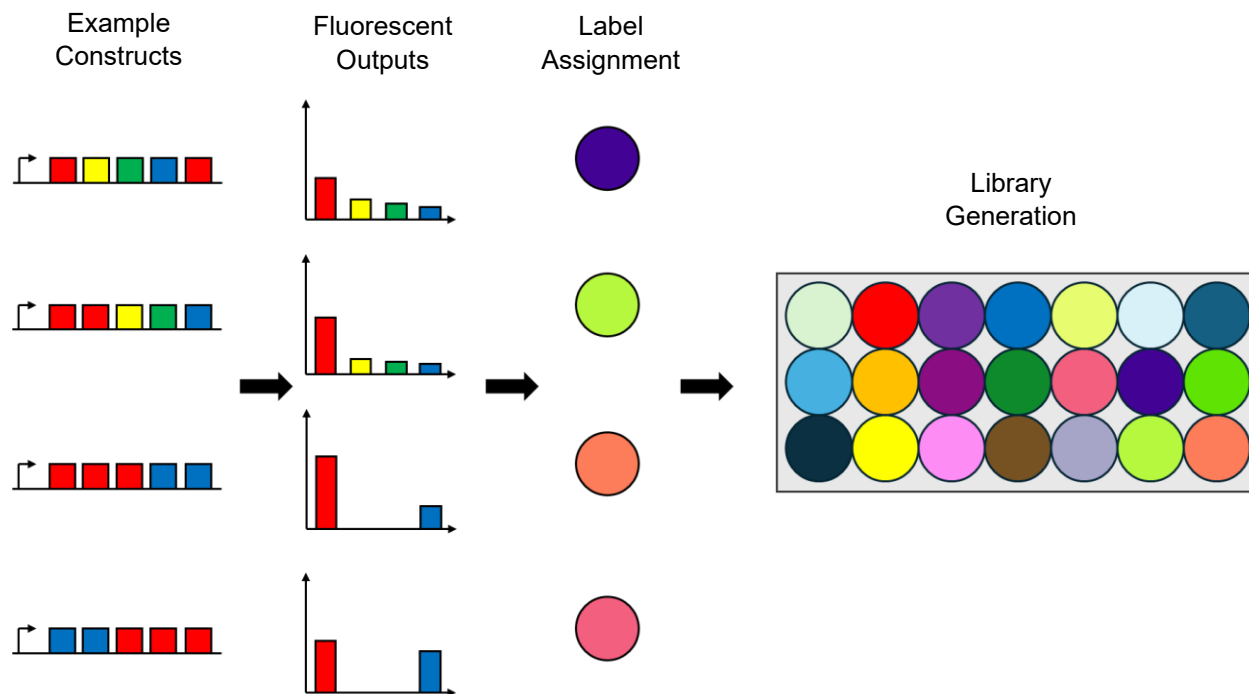


**Figure 5.2:** Proposed label identification method for Gutbow. Fluorescent readings are collected from each construct in the library for RFP, YFP, GFP, and eBFP. The ratios of each are associated with a randomly assigned label, visualized here using randomized colors. The library is identified by these labels. After assaying and data collection, fluorescent readings are collected for each animal and characterized in a similar manner to identify the label.

each protein based on their position, resulting in similar protein combinations producing different outputs. To prepare the 4 proteins for Goldengate assembly, we first designed the sticky ends that corresponded to each of the 5 positions, P1, P2, P3, P4, and P5. Sticky ends were designed to contain the Bsa1 restriction site, the sticky end sequence, and 3-5 buffer bases to protect the rest of the sequence. By combining those sticky ends with the 4 sets of primers we designed to amplify each fluorescent protein from its original plasmid, we produced 20 sets of primers (Table 5.1). The primers were also designed to add ribosome binding sites (RBS) in front of each location, to allow for each position to be translated individually by ribosomes. The RBSs were determined using the online RBS calculator from the Salis Lab<sup>26-31</sup>. Each protein had 5 sets of primers, 1 set per possible position on the construct. Additionally, one more set was designed for the backbone plasmid, pD441\_WT\_hi<sup>32</sup>, such that it could anneal to P1 and P5 properly

(Table 5.1). This backbone was chosen as it contained the IPTG-inducible T5 promoter and a kanamycin selection marker. The other plasmids used in this work contain an ampicillin selection marker, reducing the risk of contamination from those plasmids. The T5 promoter allows for the fluorescent protein expression to be controlled by the dosing of IPTG, which would limit the fluorescence levels during experiments and data collection. Additionally, since the labels can be turned “off”, experiments could be appropriately blinded. Once each fluorescent protein and the backbone were amplified, they were combined into a single reaction and conditions were optimized for 20 inserts. Although there were only 5 positions in the construct, the reaction contained 4 products for each position, which resulted in 20 total inserts. Designing the reaction this way allowed us to run a single reaction instead of 1024 reactions. Initial characterizations of the construct using whole-plasmid sequencing revealed possible issues with the primer design, as tested constructs only contained 2-3 of the inserts. We suspect that the sticky end sequences for different positions are too similar, as they only consist of 4 bases and similar bases could mis-anneal during the assembly process. This issue can be fixed by altering the primer sequences to reduce the similarities. Further characterization of the constructs and completion of this project are being transferred to another lab member.

As it has been designed, Gutbow addresses the 3 problems we sought to fix. Gutbow produced a very high limit on label variety at 1024 possible combinations. This number can be further increased by adapting Gutbow to include more inserts or more options for fluorescent markers. The system is very amenable to these adaptations as Goldengate assembly can handle a large number of inserts with relatively high efficiency. Gutbow will also have minimal effect on the worm as it is entirely contained within the bacterial food source. If BL21(DE3) is not an optimal food source for an experiment, this method can be repeated using a different host strain,

only needing to repeat the single assembly reaction and transformation. Lastly, as the labels are inducible with IPTG, they can be turned “off” during data collection to prevent interference with assay outputs and allow for proper blinding of experiments. These factors make Gutbow an excellent option for reducing material and labor costs when running drug screens, by allowing multiple drug treatment groups to run together in a single assay. This would also reduce variability in those assays as drug treatment group could be run under the same exact conditions.

Table 5.1. DNA primers used in this work.

Target	Position	Forward Primer	Reverse Primer
GFP	1	ggctacggctctcTGGCatgcgtaaaggaga agaactttcac	ggctacggctctcTTGTtatttgtagttcatccat gccatg
GFP	2	ggctacggctctcACAAGAAATACAA GAATACAATAAGGAGatgcgtaaa ggagaagaac	ggctacggctctcTCTCtatttgtagttcatccat gccatg
GFP	3	ggctacggctctcGAGAGAAATACAA GAATACAATAAGGAGatgcgtaaa ggagaagaac	ggctacggctctcTTTGtatttgtagttcatccat gccatg
GFP	4	ggctacggctctcCAAAGAAATACAA GAATACAATAAGGAGatgcgtaaa ggagaagaac	ggctacggctctcAGTTtatttgtagttcatccat gccatg
GFP	5	ggctacggctctcAACTGAAATACAA GAATACAATAAGGAGatgcgtaaa ggagaagaac	ggctacggctctcATAGtatttgtagttcatccat gccatg
RFP	1	ggctacggctctcTGGCatggcttctccgag gatg	ggctacggctctcTTGTttaagcaccggaggatg ac

Table 5.1 (continued).

RFP	2	ggctacggtctcACAAGAAATACAA GAATACAATAAGGAGatggcttct ccgaggatg	ggctacggtctcTCTCttaagcaccggtggagt ac
RFP	3	ggctacggtctcGAGAGAAATACAA GAATACAATAAGGAGatggcttct ccgaggatg	ggctacggtctcTTTGttaagcaccggtggagt ac
RFP	4	ggctacggtctcCAAAGAAATACAA GAATACAATAAGGAGatggcttct ccgaggatg	ggctacggtctcAGTTtaagcaccggtggagt gac
RFP	5	ggctacggtctcAACTGAAATACAA GAATACAATAAGGAGatggcttct ccgaggatg	ggctacggtctcATAGttaagcaccggtggagt ac
YFP	1	ggctacggtctcTGGCatggtgagcaagg cgag	ggctacggtctcTTGTtactgtacagctcgcc atgc
YFP	2	ggctacggtctcACAAGAAATACAA GAATACAATAAGGAGatggtgagc aagggcgag	ggctacggtctcTCTCtactgtacagctcgcc atgc
YFP	3	ggctacggtctcGAGAGAAATACAA GAATACAATAAGGAGatggtgagc aagggcgag	ggctacggtctcTTTGtactgtacagctcgcc atgc
YFP	4	ggctacggtctcCAAAGAAATACAA GAATACAATAAGGAGatggtgagc aagggcgag	ggctacggtctcAGTTtactgtacagctcgcc atgc

Table 5.1 (continued).

YFP	5	ggctacggctcAACTGAAATACAA GAATACAATAAGGAGatggtgagc aagggcgag	ggctacggctcATAGttactgtacagctcgcc atgc
eBFP	1	ggctacggctcTGGCatggtgagcaaggg cgag	ggctacggctcTTGTtactgtacagctcgcc atgc
eBFP	2	ggctacggctcACAAGAAATACAA GAATACAATAAGGAGatggtgagc aagggcgag	ggctacggctcTCTCtactgtacagctcgcc atgc
eBFP	3	ggctacggctcGAGAGAAATACAA GAATACAATAAGGAGatggtgagc aagggcgag	ggctacggctcTTTGtactgtacagctcgcc atgc
eBFP	4	ggctacggctcCAAAGAAATACAA GAATACAATAAGGAGatggtgagc aagggcgag	ggctacggctcAGTTtactgtacagctcgcc atgc
eBFP	5	ggctacggctcAACTGAAATACAA GAATACAATAAGGAGatggtgagc aagggcgag	ggctacggctcATAGttactgtacagctcgcc atgc
Backbone	N/A	ggctacggctcCTATGAATTCTGAT CACACTGGCTACC	ggctacggctcGCCAGGTTTACCTCC TTAAAAGTTAAACAAAATTATTT C

## 5.4 Materials and methods

### 5.4.1 Strains, media, and culture

*C. elegans* was maintained on standard Nematode Growth Medium (NGM) plates seeded with OP50 *E. coli* bacteria and kept at 20 °C unless otherwise stated<sup>33</sup>. Age-synchronization for experiments was performed by washing plates with a 1 mL of a solution of M9 media supplemented with 0.01% v/v TX-100 (M9TX). Worms were allowed to settle, and supernatant was removed and replaced with 1 mL of 1:2:1 mixture of bleach, 1M NaOH, and water. Once eggs were released, they were washed 3 times with 1 mL M9TX, and transferred to fresh plates. Wild-type Bristol N2s were used for all experiments described in this work.

### 5.4.2 Library construct design and assembly

The library construct was assembled using the NEBridge Golden Gate Assembly kit (NEB E1601S). Fluorescent proteins were amplified from eBFP2, E0030, E0040m, and E1010m<sup>23</sup> (Addgene) using primers designed to add on unique *bsaI* sites corresponding with each position in the construct. eBFP2, E0030, E0040m, and E1010m were gifts from Douglas Densmore (Addgene plasmid #66034, 66031, 66032, and 66033). The backbone was amplified from pD441\_WT\_hi<sup>32</sup> (Addgene) with primers designed to add on *bsaI* sites corresponding to the beginning and end positions. pD441\_WT\_hi was a gift from Mark Pallen (Addgene plasmid # 128857; <http://n2t.net/addgene:128857>; RRID: Addgene\_128857). This produced 21 unique products: 1 backbone and 5 of each of the fluorescent proteins (1 version per position in the construct). These were mixed in different ratios and assembly was performed as described in the kit. Construct sequences were confirmed using whole plasmid sequencing.

### **5.4.3 Fluorescent *E. coli* longevity in the worm gut**

To test the longevity of *E. coli* in the gut, we age-synchronized worms to the L4 stage at 20 °C. Worms were then transferred to plates containing either red or green fluorescent *E. coli*, provided by the Crook Lab. After 24 hrs. of growth, worms were transferred again to plates containing non-fluorescent *E. coli* and checked once per day for fluorescence in their gut using fluorescence microscopy. Single worms were also picked to tubes of LB media to allow for growth of bacteria from their feces and these were checked the next day for fluorescence.

## 5.5 References

1. Teo E, Lim S, Fong S, Larbi A, Wright G, Tolwinski N, Gruber J. A high throughput drug screening paradigm using transgenic *Caenorhabditis elegans* model of Alzheimer's disease. *Translational Medicine of Aging*. 2020;4:11-21.  
<https://doi.org/10.1016/j.tma.2019.12.002>
2. Partridge F, Brown A, Buckingham S, Willis N, Wynne G, Forman R, Else K, Morrison A, Matthews J, Russell A, Lomas D, Sattelle D. An automated high-throughput system for phenotypic screening of chemical libraries on *C. elegans* and parasitic nematodes. *International Journal for Parasitology: Drugs and Drug Resistance*. 2018;8(1):8-21.  
<https://doi.org/10.1016/j.ijpddr.2017.11.004>
3. Ma L, Zhao Y, Chen Y, Cheng B, Peng A, Huang K. *Caenorhabditis elegans* as a model system for target identification and drug screening against neurodegenerative diseases. *European Journal of Pharmacology*. 2018;819:169-180.  
<https://doi.org/10.1016/j.ejphar.2017.11.051>
4. Hodgkin J. Introduction to genetics and genomics (September 6, 2005), *WormBook*, ed. The *C. elegans* Research Community, WormBook, doi/10.1895/wormbook.1.17.1, <http://www.wormbook.org>
5. Mondal, S., Hegarty, E., Martin, C. *et al.* Large-scale microfluidics providing high-resolution and high-throughput screening of *Caenorhabditis elegans* poly-glutamine aggregation model. *Nat Commun* 7, 13023 (2016). <https://doi.org/10.1038/ncomms13023>
6. Chung, K., Crane, M. M. & Lu, H. Automated on-chip rapid microscopy, phenotyping and sorting of *C. elegans*. *Nat. Methods* 5, 637–643 (2008).  
<https://doi.org/10.1038/nmeth.1227>

7. Hulme, S. E., Shevkoplyas, S. S., Apfeld, J., Fontana, W. & Whitesides, G. M. A microfabricated array of clamps for immobilizing and imaging *C. elegans*. *Lab. Chip* 7, 1515–1523 (2007). <https://doi.org/10.1039/B707861G>
8. Lee, H, Kim S, Coakley S, Mugno P, Hammarlund M, Hilliard M, Lu H. A multi-channel device for high-density target-selective stimulation and long-term monitoring of cells and subcellular features in *C. elegans*. *Lab on a Chip*. 2014;23. <https://doi.org/10.1039/C4LC00789A>
9. Caceres Ide, C., Valmas, N., Hilliard, M. A. & Lu, H. Laterally orienting *C. elegans* using geometry at microscale for high-throughput visual screens in neurodegeneration and neuronal development studies. *PLoS ONE* 7, e35037 (2012). <https://doi.org/10.1371/journal.pone.0035037>
10. Evans, T. C., ed. Transformation and microinjection (April 6, 2006), *WormBook*, ed. The *C. elegans* Research Community, WormBook, doi/10.1895/wormbook.1.108.1, <http://www.wormbook.org>.
11. Jin H, Emmons SW, Kim B. Expressional artifact caused by a co-injection marker rol-6 in *C. elegans*. *PLoS One*. 2019 Dec 4;14(12):e0224533. doi:10.1371/journal.pone.0224533. PMID: 31800569; PMCID: PMC6892501.
12. Yemini E., Lin A., Nejatbakhsh A., Varol E., Sun R., Mena G., Samuel A., Paninski L., Venkatachalam V., Hobert O. NeuroPAL: A multicolor atlas for whole-brain neuronal identification in *C. elegans*. *Cell*. 2020;184:272-288. <https://doi.org/10.1016/j.cell.2020.12.012>

13. Corsi A.K., Wightman B., and Chalfie M. A Transparent window into biology: A primer on *Caenorhabditis elegans* (June 18, 2015), *WormBook*, ed. The *C. elegans* Research Community, WormBook, doi/10.1895/wormbook.1.177.1, <http://www.wormbook.org>
14. Ahringer, J., ed. Reverse genetics (April 6, 2006), *WormBook*, ed. The *C. elegans* Research Community, WormBook, doi/10.1895/wormbook.1.47.1, <http://www.wormbook.org>
15. Kamath R, Ahringer J. Genome-wide RNAi screening in *Caenorhabditis elegans*. *Methods*. 2003;30(4):313-321. [https://doi.org/10.1016/S1046-2023\(03\)00050-1](https://doi.org/10.1016/S1046-2023(03)00050-1)
16. Wittenburg, N., Eimer, S., Lakowski, B. *et al.* Presenilin is required for proper morphology and function of neurons in *C. elegans*. *Nature* 406, 306–309 (2000). <https://doi.org/10.1038/35018575>
17. Park H., Jung Y., Lee S. Survival assays using *Caenorhabditis elegans*. *Molecules and Cells*. 2017;40(2):90-99. <https://doi.org/10.14348/molcells.2017.0017>
18. Roh J., Park Y., Park K., Choi J. Ecotoxicological investigation of CeO<sub>2</sub> and TiO<sub>2</sub> nanoparticles on the soil nematode *Caenorhabditis elegans* using gene expression, growth, fertility, and survival as endpoints. *Environmental Toxicology and Pharmacology*. 2010;29(2):167-172. <https://doi.org/10.1016/j.etap.2009.12.003>
19. Jeong H, Kim HJ, Lee SJ. 2015. Complete genome sequence of *Escherichia coli* strain BL21. *Genome Announc* 3(2):e00134-15. doi:10.1128/genomeA.00134-15.
20. Beydoun, S., Choi, H.S., Dela-Cruz, G. *et al.* An alternative food source for metabolism and longevity studies in *Caenorhabditis elegans*. *Commun Biol* 4, 258 (2021). <https://doi.org/10.1038/s42003-021-01764-4>

21. Corsello, S., Bittker, J., Liu, Z. *et al.* The Drug Repurposing Hub: a next-generation drug library and information resource. *Nat Med* **23**, 405–408 (2017).  
<https://doi.org/10.1038/nm.4306>
22. Feng B., Simeonov A., Jadhav A., Babaoglu K., Inglese J., Shoichet B., Austin C. A High-Throughput Screen for Aggregation-Based Inhibition in a Large Compound Library. *Journal of Medicinal Chemistry* 2007 50 (10), 2385-2390 DOI: 10.1021/jm061317y
23. Iverson SV, Haddock TL, Beal J, Densmore DM. CIDAR MoClo: Improved MoClo Assembly Standard and New E. coli Part Library Enable Rapid Combinatorial Design for Synthetic and Traditional Biology. *ACS Synth Biol.* 2016 Jan 15;5(1):99-103. doi: 10.1021/acssynbio.5b00124. Epub 2015 Nov 4. 10.1021/acssynbio.5b00124 [PubMed 26479688](#)
24. Metelev, M., Lundin, E., Volkov, I.L. *et al.* Direct measurements of mRNA translation kinetics in living cells. *Nat Commun* 13, 1852 (2022). <https://doi.org/10.1038/s41467-022-29515-x>
25. T5 promoter
26. Reis A, Salis H. An automated model test system for systematic development and improvement of gene expression models. *ACS Synthetic Biology.* 2020;9(11):3145-3156.
27. Cetnar D, Salis H. Systematic quantification of sequence and structural determinants controlling mRNA stability in bacterial operons. *ACS Synthetic Biology.* 2021;10(2):318-332.
28. Espah Borujeni A, Cetnar D, Farasat I, Smith A, Lundgren N, Salis H. Precise quantification of translation inhibition by mRNA structures that overlap with the

- ribosomal footprint of N-terminal coding sequences. *Nucleic acids research*. 2017;45(9):5437-5448.
29. Espah Borujeni A, Salis H. Translation initiation is controlled by RNA folding kinetics via a ribosome drafting mechanism. *Journal of the American Chemical Society*. 2016;138(22):7016-7023.
30. Espah Borujeni A, Channarasappa A, Salis H. Translation rate is controlled by coupled trade-offs between site accessibility, selective RNA unfolding and sliding at upstream standby sites. *Nucleic acids research*. 2013;42(4):2646-2659.
31. Salis H, Mirsky E, Voigt C. Automated design of synthetic ribosome binding sites to control protein expression. *Nature biotechnology*. 2009;27(10):946.
32. Restoration of wild-type motility to flagellin-knockout *Escherichia coli* by varying promoter, copy number and induction strength in plasmid-based expression of flagellin. Thomson NM, Pallen MJ. *Curr Res Biotechnol*. 2020 Nov;2:45-52. doi: 10.1016/j.crbiot.2020.03.001. 10.1016/j.crbiot.2020.03.001 [PubMed 33381753](https://pubmed.ncbi.nlm.nih.gov/33381753/)
33. Wood W. The nematode *Caenorhabditis elegans*. Cold Spring Harb Monogr Arch. 1988;17.

## CHAPTER 6: Conclusions

### 6.1 Summary and overview of projects

Alzheimer's disease (AD) represents a growing problem for the world due to its high rates in the elderly and the world's aging population<sup>1-3</sup>. The need to address its burden on both the medical and financial situation of the world continues to become more and more apparent. Much information of the information about AD is still lacking, there is currently no cure, and research in humans is limited by the dangers posed with invasive procedures required to study it. This highlights the need for appropriate models for AD, of which *C. elegans* stands as a prime candidate. *C. elegans* shares many neuron subtypes with humans, including using many of the same neurotransmitters, and its genome is approximately 60-70% homologous to the human genome<sup>4</sup>. Additionally, *C. elegans* has many tools specially designed for it, including microfluidic devices, image analysis software, and large genetic libraries for gene suppression and knockout<sup>5-10</sup>. Despite this, there still several improvements that can be made to increase its functionality as a model for AD. Firstly, *C. elegans* AD models only encapsulate intracellular amyloid  $\beta$  ( $A\beta$ ) effects and fail to account for extracellular  $A\beta$ <sup>11-13</sup>. Secondly, while  $A\beta$  expression in *C. elegans* has been connected with increased pathogen resistance, very little is known about how other environmental stressors may interact with  $A\beta$ <sup>14</sup>. Thirdly, there isn't a method for severe mechanical injury in *C. elegans*, despite traumatic brain injury's (TBI) strong association with the development of AD and other dementias<sup>15,16</sup>. Lastly, large-scale drug screens in *C. elegans* have high costs associated with them due to the inability to distinguish or label different groups of animals within mixed populations. Thus, in this dissertation, we developed techniques and tools to attempt to address four issues. We designed an expression system utilizing the C99 fragment of the human amyloid precursor protein (APP) to express  $A\beta$

extracellularly. We examined the relationship between A $\beta$  expression and resistance to external stressor, determining that A $\beta$  produces a hormesis-like effect in *C. elegans*. We developed a tool capable of inducing neuronal damage, characterized by dendritic blebbing and breakage, through blunt force trauma to the worm head. Lastly, we developed Gutbow, a gut colonization-based method of labeling groups of animals using an *E. coli* food source to improve throughput and reduce material costs in AD drug screens. The tools and techniques developed in this dissertation will significantly improve *C. elegans*' usefulness as a model for AD by increasing the scope and type of AD experiments that can be run using this model organism.

### **6.1.1 Extracellular A $\beta$ expression in *C. elegans***

A $\beta$  in AD is typically associated with large extracellular aggregates seen in advanced cases of AD<sup>1-3</sup>. Despite this, both intracellular and extracellular A $\beta$  have been associated with detrimental health effects in AD. Intracellular A $\beta$  has been associated with mitochondrial dysfunction, synaptic dysfunction, disruption of telomeres, and loss of calcium homeostasis<sup>17-20</sup>; conversely, extracellular A $\beta$  is connected to membrane depolarization and pore formation, and immune activation, in addition to loss of calcium homeostasis<sup>20-22</sup>. A $\beta$  is produced in the brain through the sequential cleavage of APP<sup>23-25</sup>. APP is included into the cell membrane during processing where it is cleaved by human  $\beta$ -secretase to produce the membrane-bound C99 fragment containing A $\beta$  and  $\gamma$ -secretase to release A $\beta$  from C99 extracellularly<sup>23-25</sup>. Intracellular A $\beta$  is hypothesized to come from two possible routes: cleavage of APP not at the membrane and reuptake of A $\beta$  after cleavage from C99. Regardless of its source, both intracellular and extracellular A $\beta$  have a significant impact on the progression of AD.

Current A $\beta$  models of AD in *C. elegans* lack the ability to produce extracellular A $\beta$ <sup>11-13</sup>. While A $\beta$  has been shown to leak from neurons into surrounding tissues later in life, this is not

reflective of AD in humans where both intracellular and extracellular A $\beta$  are present throughout most stages of the disease<sup>17-22</sup>. Previous attempts at extracellular are theorized to have failed due to redirection of A $\beta$  during post-translational processing (Personal Communication, Chris Link, June 2020)<sup>12</sup>. To address this problem, we developed a novel system for extracellular expression of A $\beta$  which utilizes several key changes to improve expression. Firstly, while previous attempts utilized an artificial signal peptide to direct A $\beta$  to the extracellular space, this system replaced that with an endogenous *C. elegans* signal peptide. This signal peptide is 1 of 15 from a library *C. elegans* signal peptides taken from neuronal proteins directed either to neuron membrane or extracellular space. The library was generated using the online GExplore database<sup>26</sup> to extract the signal peptide sequences from candidate neuronal proteins. Candidate signal peptide sequences were tested using SignalP 5.0<sup>27</sup>, an online software that predicts signal peptide cleavage in eukaryotic organisms. Signal peptides were screened for their size and number of cleavage sites, optimizing for a size of 100 bp or less and a single cleavage site. These endogenous signal peptides were theorized to better direct to the cell membrane than an artificial signal peptide as they were taken directly from *C. elegans* proteins. The second major change was in the expressed protein. Rather than expressing human A $\beta$ , the C99 fragment of APP was used. This fragment contains A $\beta$ , and while worms lack a  $\beta$ -secretase, they have sufficient  $\gamma$ -secretase activity for cleavage<sup>28-31</sup>. We theorized that as C99 contains the transmembrane domain of APP, it could be integrated into the cell membrane during processing and be cleaved by worm  $\gamma$ -secretase to release A $\beta$  extracellularly, such as in human processing of APP. These two changes to standard A $\beta$  were thought to be sufficient for achieving extracellular A $\beta$  expression.

Once a plasmid construct containing these two changes was generated and integrated into an extrachromosomal array in *C. elegans*, we sought to confirm the presence of extracellular A $\beta$ .

C99 DNA was confirmed using PCR and gel electrophoresis; C99 RNA was confirmed using RT-qPCR, screening for C99 RNA. These two assays successfully confirmed the presence of C99 DNA and RNA within the strain. To verify translation of C99 and cleavage to release A $\beta$ , we stained the strain with the A $\beta$  specific fluorescent dye, 1,4-bis(3-carboxy-4-hydroxyphenylethenyl)-benzene (X-34). X-34 selectively binds A $\beta$  fibrils and aggregates, which were expected if C99 was successfully cleaved<sup>32,33</sup>. Initial assays showed significant deposition and aggregation of A $\beta$  in the head, but after imaging of an unstained control, it was realized that the fluorescent pharyngeal coinjection marker was interfering with detection. Antibody staining targeting both C99 and A $\beta$  with an alternative fluorescent signal showed no distinguishable signal for the strain and another control intracellular A $\beta$  strain. This is despite using a two-step antibody staining procedure to amplify the signal. A literature search for methods to improve antibody staining in *C. elegans* neurons showed little success in staining neuronal A $\beta$  strains<sup>11-13</sup>. While Elisa and Western blot assays on those same strains showed signal, in many cases the signal was faint until late in life, indicating that A $\beta$  likely accumulates slowly in neurons for an unknown reason<sup>11-13</sup>. We theorized 1 of 3 issues was occurring with our strain: antibody staining was not working, A $\beta$  levels in neurons is lower than the detection threshold for most dyes and antibody staining, or A $\beta$  is not produced due to an error in the method. Regardless of which problem is occurring, without significant improvements to A $\beta$  detection methods in *C. elegans*, effectiveness of the method cannot be estimated. While an Elisa or Western blot assay could detect the presence of C99 or A $\beta$ , without a method for visualizing the location of A $\beta$ , project success could not be determined.

### 6.1.2 Interactions between A $\beta$ and external stressors

A significant amount of research has been invested in studying AD and its risk factors. Despite this, there is no clear cause of AD in most cases. Several environmental stressors including chemical and pathogen exposure have been associated with an increased risk of AD after exposure<sup>1-3</sup>. To relate this fact to AD, the AD peptide A $\beta$  has been theorized to interact with some of these stressors by acting as an antimicrobial peptide due to its size and structure<sup>14,34</sup>. In a *C. elegans* model of AD expressing A $\beta$  pan-neuronally, A $\beta$  was shown to have a protective effect against a pathogen external stressor, further supporting this theory<sup>14</sup>. Despite AD's association with other external stressors, there is little research to examine how A $\beta$  may interact with other external stressors. This highlights a promising avenue of research to explore further using *C. elegans*.

To investigate the interactions between A $\beta$  and various external stressors in *C. elegans*, we expose a *C. elegans* AD model expressing A $\beta$  pan-neuronally to those external stressors. We theorized that if A $\beta$  only had antimicrobial activity, exposure to non-pathogenic external stressors would reduce worm survival more when compared to non-AD controls. Worms were exposed to a 37 °C heat stress, a hypoxic stress of O<sub>2</sub> < 0.1%, and a 5 mM paraquat-induced oxidative stress. As expected, when exposed to paraquat-induced oxidative stress, AD worms exhibited significantly lower survival rates than non-AD controls. Interestingly though, AD worms showed higher stress resistance than non-AD worms when exposed to heat and hypoxia stresses, indicating a possible hormesis-like effect towards these stressors. To further expand on this hormesis-like effect, we next examined if A $\beta$  dosage or location affected stress resistance. Using strains which express A $\beta$  either pan-neuronally or pan-muscularly upon upshift from 20 °C to 25 °C, resistance was observed to increase only in the neuronal strain upon upshift to 25

°C. Additionally, time spent at 25 °C after the upshift correlated with resistance levels. This indicates that specifically neuronal A $\beta$  matters for the hormesis-like effects. The muscular strain exhibited increased stress resistance regardless of time spent at 25 °C, indicating that some other factor in the strain increased stress resistance and not A $\beta$  levels. To investigate the stress resistance's specificity to A $\beta$ , another strain expressing GFP in all neurons was heat stressed. While this strain showed increased stress resistance levels, the level was lower than A $\beta$ -induced levels, like the wrmScarlet controls used in previous experiments, indicating A $\beta$  produced a unique effect when compared to other proteins. A $\beta$  has been previously shown to induce oxidative stress, which could lead to a hormetic effect<sup>35</sup>. To determine the effect of this on stress resistance, AD worms were exposed to an antioxidant, n-acetyl cysteine (NAC), before heat stress to alleviate A $\beta$ -induced oxidative stress. NAC exposure had no effect on the resistance of the AD worms, suggesting that A $\beta$ -induced stress resistance is independent of any oxidative stress hormetic effects.

Using Nanostring analysis to elucidate which genetic pathways A $\beta$  is influencing, we identified the *hsp* family of genes as they are upregulated in AD worms in unstressed, heat stressed, and hypoxia stressed conditions. This family of genes is under the control of the *daf-16*, *hif-1*, *hsf-1*, and *skn-1* transcription factors, which all contribute to major stress response pathways<sup>36-39</sup>. The *daf-16* and *skn-1* pathways are typically associated with oxidative stress, *hif-1* is associated with hypoxia stress, and *hsf-1* is associated with heat stress<sup>36-39</sup>. Interestingly, the human homologs to these four pathways have all been implicated in AD, indicating a possible connection between their activation in these *C. elegans* strains and AD<sup>40-43</sup>. Many of the pathways controlled by these transcription factors require communication between tissues such as the neurons to the intestine<sup>36-39</sup>. By perturbing neuropeptide signaling by knocking down *unc-*

31 and *egl-3*, the stress resistance levels in AD worms dropped to wild-type levels. This suggests that neuropeptide signaling, and thus cell non-autonomous signaling, is necessary for the effects induced by A $\beta$ . It is unclear whether A $\beta$  is directly inducing neuropeptide signaling or inducing another stress that may be responsible for activation of the stress response at the organismal level.

### 6.1.3 Devices for mimicking TBI

Of external indicators, traumatic brain injury (TBI) is the best predictor for developing AD later in life<sup>15,16</sup>. It is unclear exactly how TBI increases chances of AD, but TBIs have been shown to generate a temporary increase in A $\beta$  levels acutely after and disrupt the blood-brain barrier, possibly allowing contaminants and pathogens into the brain<sup>15,16,44-47</sup>. The risks of AD from TBI are well established in humans, from sources like sports injuries, car crashes, and other direct impact sources<sup>15,16,44-47</sup>. Current models in *C. elegans* connecting TBI and AD have largely been limited to exposure to A $\beta$  from TBI mice<sup>48-50</sup>. Additionally, while there is a microfluidic device that attempts to mimic TBI using acoustic waves, it induces minor damage on an organismal level that only produces temporary behavioral effects<sup>51</sup>. Thus, there is a need for a tool capable of mimicking targeted blunt force trauma TBI, that also examines for characteristic neuronal damage attributes such as neuronal blebbing and dendritic breakage.

To address this need for a device capable of delivering a blunt force trauma, we initially developed a microfluidic injury device, repurposed from a design for another project. The device consists of a loading chamber, injury channel, flush channel, and two outlet channels. Animals are loaded into the injury channel through the loading chamber and immobilized into position utilizing a hold valve. If animals enter in the correct orientation, tail first, an injury valve that protrudes into the injury channel is actuated to simulate injury. Animals are then sorted into one

of two outlet channels depending on the success of the injury. This initial device had several issues that need to be addressed by a redesign; namely issues with the injury valve and flow valves separating each chamber and channel. Upon redesign, the new device was simplified to have a single outlet, fewer flow valves, and two separate injury valves. These new injury valves could be separately actuated to allow injury of worms in either orientation, head or tail first. After another minor redesign to reduce clogging and improve flow, animals expressing GFP in six head neurons were injured in the device using a regime of 20 hits per worm. After imaging both immediately after injury and 24 hrs. after injury, it was determined that microfluidic devices were unable to properly injure the animals. PDMS and worms are both too flexible to inflict injury, as the injury valves simply move the worms out of the path of injury when expanding. While increasing the pressure of a valve could possibly improve this, the maximum pressure before the injury valve bursts was not sufficient for injury.

By switching to a 3D printed design, we sought to solve issues observed with the microfluidic designs. The initial 3D printed design used drop based design; a coverslip is dropped into a slot at the top of the device and falls down an injury channel to hit the worms lined up below. The immobilized worms were oriented using an agar imprinted onto a music record. This created lanes for the worms, which could be lined up as desired. The force of the impact was determined using the coverslip drop height; this was controlled by increasing the height of the device with stackable bricks on top of a base brick for holding the agar pad in the correct position. These bricks were printed using a filament 3D printer, which produces ridges as it prints layer by layer. While these ridges can normally be removed by sanding, the small size of the injury channel prevented this. Due to this, the coverslip was frequently slowed and stopped during its fall, preventing a successful hit. Rather than swap to a resin printer which wouldn't

produce those ridges, a new design based on a guillotine, the Nematine, was generated. The Nematine instead used two rails on either side of a coverslip holder “blade”. The blade falls along the rails to accurately hit the worms below. Similarly to the drop device, the Nematine controls force by altering the height from which the blade is dropped. This device was used to injure the strain used in the microfluidic device and a significant improvement in injury was observed. After a single hit from the Nematine, worms exhibited significant neuronal damage in the form of blebbing and partial or complete dendritic severing. Despite its success in injuring worms, the Nematine exhibited a similar problem to the drop device; the rails that guide the blade could not be sufficiently sanded to prevent slowing and stoppage of the blade during some injury attempts. As resin printers are significantly less accessible to labs when compared to filament printers, we opted for an alternative that was widely available: LEGO bricks. We generated a LEGO brick device following the same design principles as the original Nematine. This new LEGO design was able produce similar results to the Nematine, but without the roughness issue and more modularity, as a new design didn’t need to be printed with every change. This device is the first of its kind for successfully mimicking this kind of injury in *C. elegans*.

#### **6.1.4 Gutbow labeling for drug screens**

AD remains without a cure despite the vast number of drugs in research and clinical trials with that goal<sup>52</sup>. AD drugs have an extremely high failure rate so ensuring costs are minimized during testing is an integral part of assay design<sup>52</sup>. The model organism *C. elegans* is an attractive option for achieving this, as large populations are relatively easy to generate when compared to other model organisms. This facilitates drug screens covering a wide range of targets, as the number of animals isn’t limited. *C. elegans* drug screens do have a limit though; as

animals are indistinguishable from each other, different treatment groups need to be kept physically separate in order to keep track of the drug administered. This dramatically increases costs associated with running an assay to determine drug effectiveness, as each treatment group needs to be assayed individually. This also decreases throughput as more assays need to be performed and increases variability since each treatment group could be exposed to different conditions. There are several microfluidic devices designed to assist with this, but they fail to address the main issue<sup>6-10</sup>. While several of them boast dramatically increased throughput by automating the process, sometimes several orders of magnitude greater than manually assaying, treatment groups are kept separate during the entire process<sup>6-10</sup>. Any assays still need to be repeated for each treatment group, those assays are just completed faster. While these devices are a great addition to the tool kit for *C. elegans* drug screens, a non-microfluidic solution is needed to address this issue.

To track different treatment groups within a drug screen, we developed a *C. elegans* labeling system, Gutbow. This system utilizes a fluorescently labeled *E. coli* library as a food source for the animals. Each treatment group is fed a different label from the library either before or during drug exposure, which colonizes their gut. During assaying and data collection, animals from different treatment groups are pooled into one large assay group, fed on a standard OP50 *E. coli* food source. During or after data collection, the fluorescent label is induced through the addition of isopropyl- $\beta$ -d-thiogalactopyranoside (IPTG) and read using fluorescent instruments. As determined from preliminary testing with two fluorescent strains of *E. coli*, the animals' guts remained colonized for 3-5 days after switching to a non-fluorescent food source, which is longer than most assays. This system allows pooling of the treatment groups during assays, significantly reducing costs associated with the assays, as fewer overall assays need to be run.

Additionally, variability in assays is reduced as all treatment groups are exposed to the same conditions.

The Gutbow library was generated utilizing Goldengate assembly and a predefined backbone construct with 5 slots for inserts under the same promoter. Distance to the promoter determines the production rate; proteins closer to the promoter have higher production rates. Four proteins, GFP, RFP, eBFP, and YFP, were used to fill these slots, generating 1024 variants of the plasmid ( $4^5$ ). Those proteins were chosen for their limited overlap in spectra and accessibility for measurements. This method produces a library with a similar scale of variants as many drug screen libraries. As the promoter used is inducible, fluorescent interference during data collection should be minimal. This has the added benefit of allowing for easier blinding during experiments, as the signal is only present when desired. Initial tests with the library revealed an issue with primer design that can be easily corrected by changing the BsaI sites used in the Goldengate assembly. Gutbow is an excellent candidate for improving drug screening with *C. elegans*, as it will reduce material, time, and labor costs associated with high volume screens. Additionally, Gutbow is not mutually exclusive with previously described microfluidic devices, allowing for their use in conjunction with Gutbow.

## **6.2 Applications beyond the scope of this dissertation**

### **6.2.1 Extracellular A $\beta$ expression in *C. elegans***

We developed a method for expressing A $\beta$  extracellularly, using novel ideas for changing expression patterns of A $\beta$  in *C. elegans*. Although the method was unable to be confirmed successful, this highlighted several problems with *C. elegans* AD research; namely issues regarding visualization neuronally expressed A $\beta$ . Without effective methods to visualize A $\beta$  within the neurons, it is unclear how intracellular A $\beta$  is distributed within the organism. Recent

work on a new model utilizing expression of A $\beta$  and tagged-A $\beta$  has illustrated this clearly, as in that model it was discovered that A $\beta$  disrupts the cell membrane and migrates to other tissues later in life<sup>13</sup>. Additionally, our work highlights an area of *C. elegans* AD research that is still lacking, extracellular A $\beta$ . As described in Chapter 2, both intracellular and extracellular A $\beta$  has effects on AD. Capturing both of those aspects in AD research is necessary to generate a clearer picture of the disease. This has important implications not only for research looking at A $\beta$  specifically, but also any AD drug screens utilizing *C. elegans*. If a drug is designed to target A $\beta$ , it may have drastically different effects depending the location of A $\beta$ . By more accurately reflecting the disease in drug screens, ineffective drugs are more likely to be eliminated, saving both time and resources for other drugs.

### **6.2.2 Interactions between A $\beta$ and external stressors**

Here we described a novel interaction between A $\beta$  and environmental stressors. Other than an interaction between A $\beta$  and a pathogen stressor, these types of interactions have not been previously characterized. This has important implications for *C. elegans* as a model for AD. Understanding how A $\beta$  influences the host animal is important for interpretation of results in that model organism. That these interactions had not been previously reported indicates there is much work still to be done characterizing *C. elegans* AD models. Additionally, despite the identified genes being associated with AD in humans, it is unclear how the effects seen in our work can be translated to humans. Although A $\beta$  may interact with the same genetic pathways in humans, the end results of the pathways can be very different. The role of A $\beta$  in healthy humans isn't quite clear, but this indicates that A $\beta$  may have a larger role than just as an antimicrobial peptide, possibly acting as a signaling molecule, regulating synaptic function, or influencing injury recovery. Inducing stress resistance pathways and acting as an early signal for stress may be

another role it plays in human biology, which could be why it accumulates in AD. It will be crucial to further characterize *C. elegans* and other model organisms like this so that we can better understand the results when using them to study AD and other human diseases.

### **6.2.3 Devices for mimicking TBI**

In this work, we present a device for mechanical injury of *C. elegans* using the 3D printed and LEGO Nematine. This device was designed such that it is easily accessible to a wide range of researchers. Although the device was designed to study how TBI may impact AD, TBI is also a predictor of various other forms of dementia as well<sup>15,16</sup>. The Nematine could be easily adapted for use in those dementias, requiring only a different *C. elegans* strain. Additionally, through scale-up that device could be adapted to other organisms as well such as flies or zebrafish. The Nematine device presents a new avenue of exploration for dementia researchers, due to its ease of adaption and accessibility.

### **6.2.4 Gutbow labeling for drug screens**

We developed a novel method for labeling *C. elegans*, Gutbow, which labels animals by colonizing their gut with a fluorescent tag. While our focus was on its applications in AD drug screens, it can be easily adapted for a wide range of purposes. Although AD drugs are important as AD doesn't currently have cure, Gutbow can be used with other *C. elegans* drug screens as well. Most drug screens are performed in a similar manner, so the Gutbow library can be fed along any set of treatments. Additionally, Gutbow can be adapted beyond drug screens; RNAi genetic screens can be performed in a similar manner, with the Gutbow library fed alongside the RNAi treatment before screening. The entire library need not be used either. A researcher could feed a few of the labels to several strains and then combine them together for any assay, effectively blinding the assay until induction of the label. This would also reduce the materials

costs for that assay, as worms wouldn't need to be kept separate. A method for non-permanently, inducibly labeling different strains or conditions within an experiment is a great tool for *C. elegans* researchers.

### 6.3 References

- 1) Alzheimer's Association (2020). *2020 Alzheimer's Disease Facts and Figures. On the Front Lines: Primary Care Physicians and Alzheimer's Care in America.*
- 2) *Alzheimer's Disease Fact Sheet | National Institute on Aging.* (n.d.). Retrieved November 23, 2020, from <https://www.nia.nih.gov/health/alzheimers-disease-fact-sheet>
- 3) *What is Alzheimer's Disease? | CDC.* (n.d.). Retrieved November 23, 2020, from <https://www.cdc.gov/aging/aginginfo/alzheimers.htm>
- 4) Corsi, A. K., Wightman, B. & Chalfie, M. A transparent window into biology: A primer on *Caenorhabditis elegans*. *Genetics* 200, 387–407 (2015).
- 5) Kamath R, Ahringer J. Genome-wide RNAi screening in *Caenorhabditis elegans*. *Methods.* 2003;30(4):313-321. [https://doi.org/10.1016/S1046-2023\(03\)00050-1](https://doi.org/10.1016/S1046-2023(03)00050-1)
- 6) Mondal, S., Hegarty, E., Martin, C. *et al.* Large-scale microfluidics providing high-resolution and high-throughput screening of *Caenorhabditis elegans* poly-glutamine aggregation model. *Nat Commun* 7, 13023 (2016). <https://doi.org/10.1038/ncomms13023>
- 7) Chung, K., Crane, M. M. & Lu, H. Automated on-chip rapid microscopy, phenotyping and sorting of *C. elegans*. *Nat. Methods* 5, 637–643 (2008).  
<https://doi.org/10.1038/nmeth.1227>
- 8) Hulme, S. E., Shevkoplyas, S. S., Apfeld, J., Fontana, W. & Whitesides, G. M. A microfabricated array of clamps for immobilizing and imaging *C. elegans*. *Lab. Chip* 7, 1515–1523 (2007). <https://doi.org/10.1039/B707861G>
- 9) Lee, H, Kim S, Coakley S, Mugno P, Hammarlund M, Hilliard M, Lu H. A multi-channel device for high-density target-selective stimulation and long-term monitoring of cells and

subcellular features in *C. elegans*. *Lab on a Chip*. 2014;23.

<https://doi.org/10.1039/C4LC00789A>

- 10) Caceres Ide, C., Valmas, N., Hilliard, M. A. & Lu, H. Laterally orienting *C. elegans* using geometry at microscale for high-throughput visual screens in neurodegeneration and neuronal development studies. *PLoS ONE* 7, e35037 (2012).

<https://doi.org/10.1371/journal.pone.0035037>

- 11) Wu, Y.; Wu, Z.; Butko, P.; Christen, Y.; Lambert, M. P.; Klein, W. L.; Link, C. D.; Luo, Y., Amyloid-beta-induced pathological behaviors are suppressed by Ginkgo biloba extract EGb 761 and ginkgolides in transgenic *Caenorhabditis elegans*. *J Neurosci* 2006, 26 (50), 13102–13.

- 12) Link, C. D. (1995). Expression of human  $\beta$ -amyloid peptide in transgenic *Caenorhabditis elegans*. *Proceedings of the National Academy of Sciences of the United States of America*, 92(20), 9368–9372. <https://doi.org/10.1073/pnas.92.20.9368>

- 13) Gallrein, C., Iburg, M., Michelberger, T., Kocak, A., Puchkov, D., Liu, F., Mariscal, S., Nayak, T., Schierle, G., Kirstein, J. (2021). Novel amyloid-beta pathology *C. elegans* model reveals distinct neurons as seeds of pathogenicity. *Progress in Neurobiology*, 198. <https://doi.org/10.1016/j.pneurobio.2020.101907>.

- 14) Deepak K, Choi S, Washicosky K, Eimer W, Tucker S, Ghofrani J, Lefkowitz A, McColl G, Goldstein L, Tanzi R, Moir R. ,Amyloid- $\beta$  peptide protects against microbial infection in mouse and worm models of Alzheimer's disease. *Sci. Transl. Med.* 2016; 8(340):340ra72. <https://doi.org/10.1126/scitranslmed.aaf1059>

- 15) Ramos-Cejudo J, Wisniewski T, Marmar C, Zetterberg H, Blennow K, de Leon MJ, Fossati S. Traumatic Brain Injury and Alzheimer's Disease: The Cerebrovascular Link.

EBioMedicine. 2018 Feb;28:21-30. doi: 10.1016/j.ebiom.2018.01.021. Epub 2018 Jan 31. PMID: 29396300; PMCID: PMC5835563.

- 16) Elonheimo HM, Andersen HR, Katsonouri A, Tolonen H. Environmental Substances Associated with Alzheimer's Disease—A Scoping Review. *International Journal of Environmental Research and Public Health*. 2021; 18(22):11839. <https://doi.org/10.3390/ijerph182211839>
- 17) Hartmann, T. (1999). Intracellular biology of Alzheimer's disease amyloid beta peptide. In *European Archives of Psychiatry and Clinical Neuroscience* (Vol. 249, Issue 6, pp. 291–298). Springer Verlag. <https://doi.org/10.1007/s004060050102>
- 18) Ferreira, I. L., Bajouco, L. M., Mota, S. I., Auberson, Y. P., Oliveira, C. R., & Rego, A. C. (2012). Amyloid beta peptide 1-42 disturbs intracellular calcium homeostasis through activation of GluN2B-containing N-methyl-d-aspartate receptors in cortical cultures. *Cell Calcium*, 51(2), 95–106. <https://doi.org/10.1016/j.ceca.2011.11.008>
- 19) Bayer, T. A., & Wirths, O. (2010). Intracellular accumulation of amyloid-beta - A predictor for synaptic dysfunction and neuron loss in Alzheimer's disease. *Frontiers in Aging Neuroscience*, 2(MAR). <https://doi.org/10.3389/fnagi.2010.00008>
- 20) Rajasekhar, K., Chakrabarti, M., & Govindaraju, T. (2015). Function and toxicity of amyloid beta and recent therapeutic interventions targeting amyloid beta in Alzheimer's disease. In *Chemical Communications* (Vol. 51, Issue 70, pp. 13434–13450). Royal Society of Chemistry. <https://doi.org/10.1039/c5cc05264e>
- 21) Renner, M., Lacor, P. N., Velasco, P. T., Xu, J., Contractor, A., Klein, W. L., & Triller, A. (2010). Deleterious Effects of Amyloid  $\beta$  Oligomers Acting as an Extracellular Scaffold for mGluR5. *Neuron*, 66(5), 739–754. <https://doi.org/10.1016/j.neuron.2010.04.029>

- 22) Townsend, M., Shankar, G. M., Mehta, T., Walsh, D. M., & Selkoe, D. J. (2006). Effects of secreted oligomers of amyloid  $\beta$ -protein on hippocampal synaptic plasticity: A potent role for trimers. *Journal of Physiology*, 572(2), 477–492.  
<https://doi.org/10.1113/jphysiol.2005.103754>
- 23) Shoji, M., Golde, T. E., Ghiso, J., Cheung, T. T., Estus, S., Shaffer, L. M., Cai, X. D., McKay, D. M., Tintner, R., Frangione, B., & Younkin, S. G. (1992). Production of the Alzheimer amyloid  $\beta$  protein by normal proteolytic processing. *Science*, 258(5079), 126–129. <https://doi.org/10.1126/science.1439760>
- 24) Vardy, E. R. L. C., Catto, A. J., & Hooper, N. M. (2005). Proteolytic mechanisms in amyloid- $\beta$  metabolism: Therapeutic implications for Alzheimer's disease. In *Trends in Molecular Medicine* (Vol. 11, Issue 10, pp. 464–472). Elsevier.  
<https://doi.org/10.1016/j.molmed.2005.08.004>
- 25) Storey, E., & Cappai, R. (1999). The amyloid precursor protein of Alzheimer's disease and the A $\beta$  peptide. In *Neuropathology and Applied Neurobiology* (Vol. 25, Issue 2, pp. 81–97). *Neuropathol Appl Neurobiol.* <https://doi.org/10.1046/j.1365-2990.1999.00164.x>
- 26) Hutter H, Ng MP, Chen N. GExplore: a web server for integrated queries of protein domains, gene expression and mutant phenotypes. *BMC Genomics*. 2009 Nov 16;10:529.
- 27) SignalP 5.0 improves signal peptide predictions using deep neural networks. José Juan Almagro Armenteros, Konstantinos D. Tsirigos, Casper Kaae Sønderby, Thomas Nordahl Petersen, Ole Winther, Søren Brunak, Gunnar von Heijne and Henrik Nielsen. *Nature Biotechnology*, 37, 420-423, doi:10.1038/s41587-019-0036-z (2019)
- 28) Link, C. D., Taft, A., Kapulkin, V., Duke, K., Kim, S., Fei, Q., Wood, D. E., & Sahagan, B. G. (2003). Gene expression analysis in a transgenic *Caenorhabditis elegans*

Alzheimer's disease model. *Neurobiology of Aging*, 24(3), 397–413.

[https://doi.org/10.1016/S0197-4580\(02\)00224-5](https://doi.org/10.1016/S0197-4580(02)00224-5)

29) Wiese, M., Antebi, A., & Zheng, H. (2010). Intracellular Trafficking and Synaptic Function of APL-1 in *Caenorhabditis elegans*. *PLoS ONE*, 5(9), e12790.

<https://doi.org/10.1371/journal.pone.0012790>

30) Daigle, I., & Li, C. (1993). *apl-1*, a *Caenorhabditis elegans* gene encoding a protein related to the human  $\beta$ -amyloid protein precursor. *Proceedings of the National Academy of Sciences of the United States of America*, 90(24), 12045–12049.

<https://doi.org/10.1073/pnas.90.24.12045>

31) Link, C. D. (2006). *C. elegans* models of age-associated neurodegenerative diseases: Lessons from transgenic worm models of Alzheimer's disease. *Experimental Gerontology*, 41(10), 1007–1013.

<https://doi.org/10.1016/j.exger.2006.06.059>

32) Link, C. D., Johnson, C. J., Fonte, V., Paupard, M. C., Hall, D. H., Styren, S., Mathis, C. A., & Klunk, W. E. (2001). Visualization of fibrillar amyloid deposits in living, transgenic *Caenorhabditis elegans* animals using the sensitive amyloid dye, X-34.

*Neurobiology of Aging*, 22(2), 217–226. [https://doi.org/10.1016/S0197-4580\(00\)00237-2](https://doi.org/10.1016/S0197-4580(00)00237-2)

33) Styren, S. D., Hamilton, R. L., Styren, G. C., & Klunk, W. E. (2000). X-34, a fluorescent derivative of Congo red: A novel histochemical stain for Alzheimer's disease pathology.

*Journal of Histochemistry and Cytochemistry*, 48(9), 1223–1232.

<https://doi.org/10.1177/002215540004800906>

34) Pastore, A., Raimondi, F., Rajendran, L. et al. Why does the A $\beta$  peptide of Alzheimer share structural similarity with antimicrobial peptides?. *Commun Biol* 3, 135 (2020).

<https://doi.org/10.1038/s42003-020-0865-9>

- 35) Drake J, Link C, Butterfield A. Oxidative stress precedes fibrillar deposition of Alzheimer's disease amyloid  $\beta$ -peptide (1–42) in a transgenic *Caenorhabditis elegans* model. *Neurobiology of Aging*. 2003; 24(3):415-420. [https://doi.org/10.1016/S0197-4580\(02\)00225-7](https://doi.org/10.1016/S0197-4580(02)00225-7).
- 36) Tissenbaum H. Chapter One - DAF-16: FOXO in the Context of *C. elegans*. *Current Topics in Developmental Biology*, Academic Press. 2018;127:1-21. <https://doi.org/10.1016/bs.ctdb.2017.11.007>
- 37) Kyriakou E, Taouktsi E, Syntichaki P. The Thermal Stress Coping Network of the Nematode *Caenorhabditis elegans*. *International Journal of Molecular Sciences*. 2022; 23(23):14907. <https://doi.org/10.3390/ijms232314907>
- 38) Powell-Coffman J. Hypoxia signaling and resistance in *C. elegans*. *Trends in Endocrinology and Metabolism*. 2010;21(7):435-440. <https://doi.org/10.1016/j.tem.2010.02.006>
- 39) Blackwell K, Steinbaugh M, Hourihan J, Ewald C, Isik M. SKN-1/Nrf, stress responses, and aging in *Caenorhabditis elegans*. *Free Radical Biology and Medicine*. 2015; 88:290-301. <https://doi.org/10.1016/j.freeradbiomed.2015.06.008>.
- 40) Calderwood S, Murshid A. Molecular Chaperone Accumulation in Cancer and Decrease in Alzheimer's Disease: The Potential Roles of HSF1. *Frontiers in Neuroscience*. 2017; 11. <https://doi.org/10.3389/fnins.2017.00192>
- 41) Du S, Zheng H. Role of FoxO transcription factors in aging and age-related metabolic and neurodegenerative diseases. *Cell Biosci*. 2021; 11:188. <https://doi.org/10.1186/s13578-021-00700-7>

- 42) Hassan H, Chen R. Hypoxia in Alzheimer's disease: effects of hypoxia inducible factors. *Neural Regen Res.* 2021;16(2):310-311. <https://doi.org/10.4103/1673-5374.290898>
- 43) Yuan J, Zhang S, Zhang Y. Nrfl is paved as a new strategic avenue to prevent and treat cancer, neurodegenerative and other diseases. *Toxicology and Applied Pharmacology.* 2018;360:273-283. <https://doi.org/10.1016/j.taap.2018.09.037>
- 44) Mielke MM, Ransom JE, Mandrekar J, Turcano P, Savica R, Brown AW. Traumatic Brain Injury and Risk of Alzheimer's Disease and Related Dementias in the Population. *J Alzheimers Dis.* 2022;88(3):1049-1059. doi: 10.3233/JAD-220159. PMID: 35723103; PMCID: PMC9378485.
- 45) Li L, Liang J, Fu H. An update on the association between traumatic brain injury and Alzheimer's disease: Focus on Tau pathology and synaptic dysfunction. *Neuroscience and Biobehavioral Reviews.* 2021;120:372-386. <https://doi.org/10.1016/j.neubiorev.2020.10.020>
- 46) [Johnson, V., Stewart, W. & Smith, D. Traumatic brain injury and amyloid- \$\beta\$  pathology: a link to Alzheimer's disease?. \*Nat Rev Neurosci\* \*\*11\*\*, 361–370 \(2010\).](#) <https://doi.org/10.1038/nrn2808>
- 47) [Edwards G, Moreno-Gonzalez I, Soto C. Amyloid-beta and tau pathology following repetitive mild traumatic brain injury. \*Biochemical and Biophysical Research Communivations.\* 2017;483\(4\):1137-1142. <https://doi.org/10.1016/j.bbrc.2016.07.123>](#)
- 48) Zanier E, Barzago M, Vegliante G, Romeo M, Restelli E, Bertani I, Natale C, Colnaghi L, Colombo L, Russo L, Micotti E, Fioriti L, Chiesa R, Diomedede L. *C. elegans* detects toxicity of traumatic brain injury generated tau. *Neurobiology of Disease.* 2021;153:105330. <https://doi.org/10.1016/j.nbd.2021.105330>

- 49) Diomedede, L., Zanier, E.R., Moro, F. *et al.* A $\beta$ 1-6<sub>A2V</sub>(D) peptide, effective on A $\beta$  aggregation, inhibits tau misfolding and protects the brain after traumatic brain injury. *Mol Psychiatry* **28**, 2433–2444 (2023). <https://doi.org/10.1038/s41380-023-02101-3>
- 50) Yang Y, Wang M, Yang P, Wang Z, Huang L, Xu J, Wang W, Yu M, Bu L, Fei J, Huang F. The A $\beta$  Containing Brain Extracts Having Different Effects in Alzheimer's Disease Transgenic *Caenorhabditis elegans* and Mice. *Frontiers in Aging Neuroscience*. 2018;10. <https://doi.org/10.3389/fnagi.2018.00208>
- 51) Miansari, M., Mehta, M.D., Schilling, J.M. *et al.* Inducing Mild Traumatic Brain Injury in *C. elegans* via Cavitation-Free Surface Acoustic Wave-Driven Ultrasonic Irradiation. *Sci Rep* **9**, 12775 (2019). <https://doi.org/10.1038/s41598-019-47295-1>
- 52) Huang LK, Kuan YC, Lin HW, Hu CJ. Clinical trials of new drugs for Alzheimer disease: a 2020-2023 update. *J Biomed Sci*. 2023 Oct 2;30(1):83. doi: 10.1186/s12929-023-00976-6. PMID: 37784171; PMCID: PMC10544555.